© 2017. Published by The Company of Biologists Ltd | Development (2017) 144, 2428-2444 doi:10.1242/dev.146050

RESEARCH ARTICLE

Dynamic regulation of VEGF-inducible genes by an ERK/ERG/p300 transcriptional network

Jason E. Fish[1,2,3,*,‡], Manuel Cantu Gutierrez[4,5,6,*], Lan T. Dang[1,2,3,*], Nadiya Khyzha[1,2,3], Zhiqi Chen[1,2,3], Shawn Veitch[1,2,3], Henry S. Cheng[1,2,3], Melvin Khor[1,2,3], Lina Antounians[7,8], Makon-Sébastien Njock[1,2,3], Emilie Boudreau[1,2,3], Alexander M. Herman[4,5], Alexander M. Rhyner[4,5], Oscar E. Ruiz[9], George T. Eisenhoffer[6,9,10], Alejandra Medina-Rivera[7,11], Michael D. Wilson[3,7,8] and Joshua D. Wythe[4,5,6,‡]

ABSTRACT

The transcriptional pathways activated downstream of vascular endothelial growth factor (VEGF) signaling during angiogenesis remain incompletely characterized. By assessing the signals responsible for induction of the Notch ligand delta-like 4 (DLL4) in endothelial cells, we find that activation of the MAPK/ERK pathway mirrors the rapid and dynamic induction of *DLL4* transcription and that this pathway is required for *DLL4* expression. Furthermore, VEGF/ERK signaling induces phosphorylation and activation of the ETS transcription factor ERG, a prerequisite for *DLL4* induction. Transcription of *DLL4* coincides with dynamic ERG-dependent recruitment of the transcriptional co-activator p300. Genome-wide gene expression profiling identified a network of VEGF-responsive and ERG-dependent genes, and ERG chromatin immunoprecipitation (ChIP)-seq revealed the presence of conserved ERG-bound putative enhancer elements near these target genes. Functional experiments performed *in vitro* and *in vivo* confirm that this network of genes requires ERK, ERG and p300 activity. Finally, genome-editing and transgenic approaches demonstrate that a highly conserved ERG-bound enhancer located upstream of *HLX* (which encodes a transcription factor implicated in sprouting angiogenesis) is required for its VEGF-mediated induction. Collectively, these findings elucidate a novel transcriptional pathway contributing to VEGF-dependent angiogenesis.

KEY WORDS: Endothelial cell, Transcription, Enhancer, Angiogenesis, Genome editing, ETS factor, Zebrafish, Mouse, Human

INTRODUCTION

The growth of new blood vessels is requisite for tissue repair and homeostasis and contributes to the pathogenesis of several diseases, including cancer and diabetic retinopathy. A comprehensive understanding of the signaling pathways and downstream transcriptional networks that control angiogenesis could be leveraged to identify novel therapeutic targets to either promote or inhibit vascular growth. The central mechanism responsible for the majority of vascular growth is angiogenesis. Angiogenesis is a highly coordinated process that requires the interaction of several intracellular and intercellular signaling pathways that ultimately converge on a network of transcriptional pathways to elicit cellular behaviors (Herbert and Stainier, 2011). Vascular endothelial growth factor (VEGF), one of the central drivers of angiogenesis, is required for blood vessel development during embryogenesis (Carmeliet et al., 1996; Ferrara et al., 1996) and contributes to vascular homeostasis, as well as physiological and pathological postnatal vascular growth (Kim et al., 1993; Lee et al., 2007). VEGF activates a number of signal transduction pathways in endothelial cells (ECs) that modulate cytoskeletal dynamics and gene expression (Olsson et al., 2006), resulting in a suite of angiogenic cell behaviors, including directed, polarized cell migration. Although some of the transcriptional networks involved in VEGF signaling have been identified (Herbert and Stainier, 2011), much remains to be discovered regarding the mechanisms by which VEGF coordinates new vessel growth.

ECs receiving a threshold of VEGF stimulation initiate a signal transduction pathway that culminates in the transcription of the Notch ligand delta-like 4 (DLL4) (Lobov et al., 2007), as well as a network of other angiogenic genes (Liu et al., 2008). Phenotypic changes occur in the VEGF receiving cell, endowing it with 'tip' cell characteristics, including acquisition of numerous filopodial projections, increased migratory behavior, and elevated VEGF receptor 2 (VEGFR2; also known as KDR) expression (Blanco and Gerhardt, 2013). DLL4 on the surface of a tip cell binds to, and activates, Notch receptors on adjacent stalk cells. Notch activity in stalk cells induces the transcription of Notch-dependent genes, such as those encoding members of the basic helix-loop-helix transcription factor families HEY and HES, and suppresses filopodia formation and cell migration, while also dampening VEGFR2 expression. Importantly, tip and stalk cell phenotypes are dynamic, and in time a stalk cell can become a tip cell, and vice versa (Jakobsson et al., 2010). Coordinating these dynamic cellular behaviors is essential for an effective angiogenic response. The molecular mechanisms responsible for the maintenance and conversion between these phenotypes are only partially understood, and include oscillations in *DLL4* induction in the tip cell (Lobov et al., 2007; Ubezio et al., 2016), as well as tight control of Notch signal duration in neighboring stalk cells (Guarani et al., 2011). How VEGF-regulated transcriptional programs control the dynamic expression of *DLL4* and other angiogenic genes during sprouting angiogenesis remains poorly understood.

[1]Toronto General Hospital Research Institute, University Health Network, Toronto M5G 2C4, Canada. [2]Department of Laboratory Medicine and Pathobiology, University of Toronto, Toronto M5S 1A8, Canada. [3]Heart and Stroke Richard Lewar Centre of Excellence in Cardiovascular Research, Toronto M5S 3H2, Canada. [4]Cardiovascular Research Institute, Baylor College of Medicine, Houston, TX 77030, USA. [5]Department of Molecular Physiology and Biophysics, Baylor College of Medicine, Houston, TX 77030, USA. [6]Graduate Program in Developmental Biology, Baylor College of Medicine, Houston, TX 77030, USA. [7]Genetics and Genome Biology, Hospital for Sick Children, Toronto M5G 0A4, Canada. [8]Department of Molecular Genetics, University of Toronto, Toronto M5S 1A8, Canada. [9]Department of Genetics, University of Texas MD Anderson Cancer Center, Houston, TX 77030, USA. [10]Graduate School of Biomedical Sciences, University of Texas, MD Anderson Cancer Center, Houston, TX 77030, USA. [11]Laboratorio Internacional de Investigación sobre el Genoma Humano, Universidad Nacional Autónoma de México, Querétaro 76230, México.
*These authors contributed equally to this work

[‡]Authors for correspondence (wythe@bcm.edu; jason.fish@utoronto.ca)

J.D.W., 0000-0002-3225-2937

Received 24 October 2016; Accepted 15 May 2017

Development (2017) 144, 2428-2444 doi:10.1242/dev.146050

We previously identified a highly conserved enhancer element located within intron 3 of murine *Dll4* that directs expression in arteries and angiogenic vessels (Wythe et al., 2013). Activity of this enhancer in arteries is VEGF responsive, and this is at least in part dependent on ETS transcription factors, including ETS-related gene (ERG) (Wythe et al., 2013). The ETS family of transcription factors play crucial roles in multiple stages of vascular development, including angiogenesis (Randi et al., 2009). More than a dozen ETS factors are expressed in ECs, and several of these [e.g. ETV2, TEL (ETV6), ETS1, ETS2, FLI1, ERG] have been implicated in vascular growth (Liu and Patient, 2008; Pham et al., 2007). ETS factors bind to a consensus 5′-GGA(A/T)-3′ sequence in the genome through a highly conserved ∼85 amino acid ETS domain (Sharrocks, 2001). Several of the family members also contain additional functional domains, such as the pointed (PNT) domain, a docking site for the serine/threonine kinase extracellular regulated kinase-2 (ERK2; MAPK1), which phosphorylates ETS1 and ETS2 in response to mitogen-activated protein kinase (MAPK) activation (Seidel and Graves, 2002). Phosphorylation of ETS1 and ETS2 enhances their activity through the recruitment of the transcriptional co-activator proteins p300 (EP300) and Creb-binding protein (CBP; CREBBP) (Foulds et al., 2004). Modulation of ETS factor activity by signal transduction pathways is not unique to ERK2, as other MAPK signaling pathways, such as p38 (MAPK14) and JNK (MAPK8) have been documented (Wasylyk et al., 1998; Yordy and Muise-Helmericks, 2000).

The specificity of MAPK pathways for particular ETS family members has recently been explored in prostate cancer cells *in vitro*. Interestingly, of the three MAPKs analyzed (p38, JNK and ERK2), only ERK2 phosphorylates ERG (yet multiple MAPK members act on ETS1/2) (Selvaraj et al., 2015). ERK2 primarily phosphorylates three residues on ERG: S96 (amino terminal to the PNT domain), S215 and S276 (both carboxy terminal to the PNT domain). Crucially, mutation of S215 to alanine, an amino acid refractory to phosphorylation (a so-called 'phospho mutant'), abolishes ERG function in prostate cancer cells (Selvaraj et al., 2015). Although several studies have implicated ERG as a mediator of EC survival, proliferation, motility and vascular integrity (Birdsey et al., 2008, 2012, 2015; Liu and Patient, 2008; Yuan et al., 2011), whether ERG acts as a hub, integrating signals downstream of VEGF to control these diverse EC behaviors is not known.

Here, we explore the signaling and transcriptional pathways activated downstream of VEGF signaling in ECs. We find that the dynamic induction of MAPK/ERK activity controls *DLL4* transcription in human ECs and that MAPK/ERK is required for angiogenesis in zebrafish *in vivo*. Furthermore, we demonstrate that MAPK/ERK activity leads to phosphorylation of ERG, and that ERG is required for the induction of *DLL4* and a network of other angiogenic genes in human, mouse and zebrafish ECs. Mechanistically, we show that ERG recruits p300 to enhancer elements to coordinate angiogenic gene expression. These findings provide new insight into the molecular mechanisms of VEGF-mediated angiogenesis, and suggest that MAPK/ERK activation of ERG/p300 might represent a novel therapeutic target for modulating vascular growth.

RESULTS

Dynamic MAPK/ERK signaling regulates gene induction in response to VEGF stimulation

Dll4 is dynamically expressed in tip cells during sprouting angiogenesis (Hellström et al., 2007; Jakobsson et al., 2010; Suchting et al., 2007; Ubezio et al., 2016). We first delineated the kinetics of VEGF-dependent *DLL4* transcription *in vitro*. We assayed *DLL4* unspliced pre-mRNA (as a surrogate of transcription) and mature mRNA transcript levels in VEGF-stimulated serum- and growth factor-starved human microvascular ECs (MVECs) or human umbilical vein ECs (HUVECs). In both cell types, *DLL4* transcription responded dynamically to VEGF stimulation, peaking at 15-30 min (15-30′) post addition of VEGF, and returning to baseline levels by 2 h (Fig. S1A; Fig. 1A). The expression of spliced *DLL4* mRNA was also transient and dynamic, with expression peaking at 1 h and returning to near baseline levels by 2 h (Fig. S1A; Fig. 1A).

As VEGF engagement of its principal angiogenic receptor, VEGFR2, can activate multiple downstream signaling pathways, we employed a panel of pharmacological cell signaling inhibitors to define the pathway(s) responsible for the rapid and transient induction of *DLL4* transcription. Inhibition of the MAPK/ERK signaling pathway [using inhibitors of either MEK or protein kinase C (PKC)] abrogated *DLL4* induction in response to VEGF (Fig. S1B; Fig. 1B). Immunofluorescent staining of VEGF-stimulated HUVECs revealed the presence of phosphorylated ERK (pERK) in both the nucleus and cytoplasm 15-30′ after treatment, with levels returning to baseline after 1 h (Fig. 1C). Measurement of pERK by western blotting mirrored the rapid and dynamic MAPK/ERK activation observed in immunofluorescence experiments, as pERK levels returned to near baseline levels by 1 h after stimulation (Fig. 1D). The kinetics of MAPK/ERK activation therefore parallels that of *DLL4* transcription in response to VEGF treatment.

Several VEGF/MAPK/ERK-responsive genes have been characterized, including the immediate early gene early growth response 3 (*EGR3*) (Liu et al., 2008) and the ERK phosphatase dual specificity phosphatase 5 (*DUSP5*) (Bellou et al., 2009; Kucharska et al., 2009). The transcriptional induction of *EGR3* and *DUSP5* (as measured by qRT-PCR analysis of unspliced pre-mRNA) largely mirrored that of MAPK/ERK activation and *DLL4* transcription (Fig. 1E). As expected, the induction of *DLL4*, *EGR3* and *DUSP5* mRNA was completely inhibited in the presence of the highly selective small molecule MEK inhibitor U0126 (Fig. 1F). In addition, the induction of these genes by VEGF stimulation was attenuated in HUVECs in which *ERK1* (*MAPK3*) and *ERK2* (*MAPK1*) were knocked down by siRNA (Fig. S1C). To determine whether MAPK/ERK activity in the absence of VEGF signaling was sufficient to induce expression of these genes, we treated serum-starved HUVECs with a PKC activator (and therefore an activator of MEK/ERK signaling), phorbol-ester myristate acetate (PMA) (Franklin et al., 1994; Schultz et al., 1997). PMA treatment markedly elevated *DLL4*, *EGR3* and *DUSP5* mRNA levels, and this response was blocked by pre-treatment with U0126, demonstrating that the MEK/ERK pathway is necessary and sufficient to activate transcription of a subset of angiogenic genes (Fig. 1G,H).

We further assessed the physiological relevance of MAPK/ERK signaling during sprouting angiogenesis *in vivo*. In agreement with recent reports (Costa et al., 2016; Shin et al., 2016), pERK was enriched in angiogenic sprouts (i.e. intersomitic vessels) in developing zebrafish embryos, indicative of active MAPK/ERK signaling (Fig. 2A; Fig. S2A). Importantly, inhibition of MAPK/ERK signaling using the MEK inhibitor SL327 completely abrogated the pERK signal throughout the embryo, including in the sprouting vessels (Fig. 2A; Fig. S2A). Inhibition of MEK signaling had a functional effect on angiogenesis, as sprout length (Fig. 2B) and the number of ECs per sprout (Fig. S2B) were decreased, as demonstrated previously (Shin et al., 2016). At this dose, SL327 did not cause developmental delay or necrosis (Fig. S2C). Inhibition of MAPK/ERK signaling diminished the

Development (2017) 144, 2428-2444 doi:10.1242/dev.146050

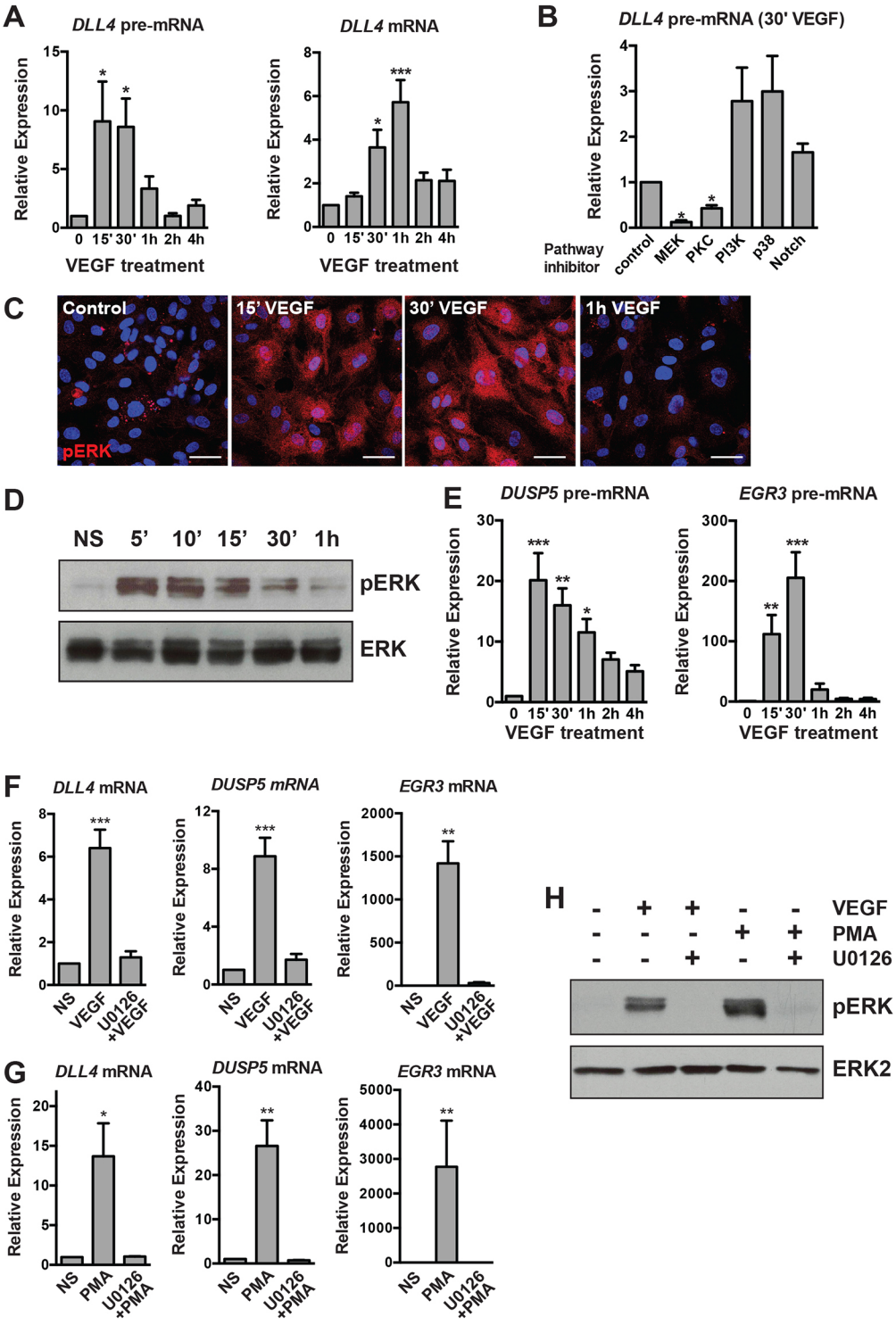

Fig. 1. Transcriptional activation of *DLL4* and other angiogenic genes in response to VEGF stimulation requires active MAPK/ERK signaling. (A) Kinetics of *DLL4* transcriptional activation (as measured by qRT-PCR of unspliced *DLL4* pre-mRNA) and expression of mature *DLL4* mRNA in HUVECs treated with VEGF (n=7). (B) Inhibition of the MAPK pathway (by PKC and MEK inhibitors) ablates induction of *DLL4* pre-mRNA (measured 30′ after VEGF treatment by qRT-PCR), whereas Notch inhibition has no effect (n=3). Expression is relative to vehicle-treated, VEGF-stimulated cells. (C) Kinetics of MAPK/ERK activation as detected by pERK (red) immunofluorescence in HUVECs. Blue, DAPI staining. Scale bars: 40 µm. Representative experiment of three. (D) Kinetics of pERK in VEGF-stimulated cells assessed by western blot. Total ERK is included as a loading control. Representative experiment of two. (E) Kinetics of *DLL4* pre-mRNA induction are similar to known MAPK/ERK-dependent genes (*EGR3*, *DUSP5*) (n=3). (F) Induction of *DLL4*, *DUSP5* and *EGR3* by VEGF is abrogated in cells pre-treated with the MEK inhibitor U0126 (n=5). (G) Induction of *DLL4*, *DUSP5* and *EGR3* by PMA is abrogated in cells pre-treated with the MEK inhibitor U0126 (n=4). (H) Western blot demonstrating the efficacy of U0126 pre-treatment of VEGF- or PMA-treated cells. pERK is not induced in U0126 pre-treated cells (n=1). NS, non-stimulated.

expression of *dll4* mRNA, as determined by qRT-PCR (Fig. 2C). Furthermore, time-lapse microscopy using a Notch biosensor revealed that attenuation of MEK activity reduced Notch signaling within the developing vasculature *in vivo*, and these results were confirmed by static confocal microscopy of a conventional Notch reporter (Fig. 2D,E; Fig. S3; Movies 1 and 2).

ERG activity is controlled by VEGF/MAPK/ERK signaling

To determine whether ERG is required for the dynamic induction of *DLL4* downstream of VEGF, we knocked down *ERG* using siRNA in HUVECs. *ERG* knockdown reduced the basal levels of *DLL4* and completely abrogated the induction of *DLL4* in response to VEGF stimulation (Fig. 3A,B). Furthermore, activation of MAPK/ERK with PMA stimulation failed to elevate *DLL4* transcription in *ERG* knockdown cells, confirming that ERG functions downstream of VEGF and MAPK/ERK (Fig. 3C).

To explore further the relationship between ETS factors and MAPK activity, we tested whether MAPK/ERK signaling modulates ETS factor activity by creating a luciferase reporter construct under the control of a concatemer (eight tandem copies) of

Development (2017) 144, 2428-2444 doi:10.1242/dev.146050

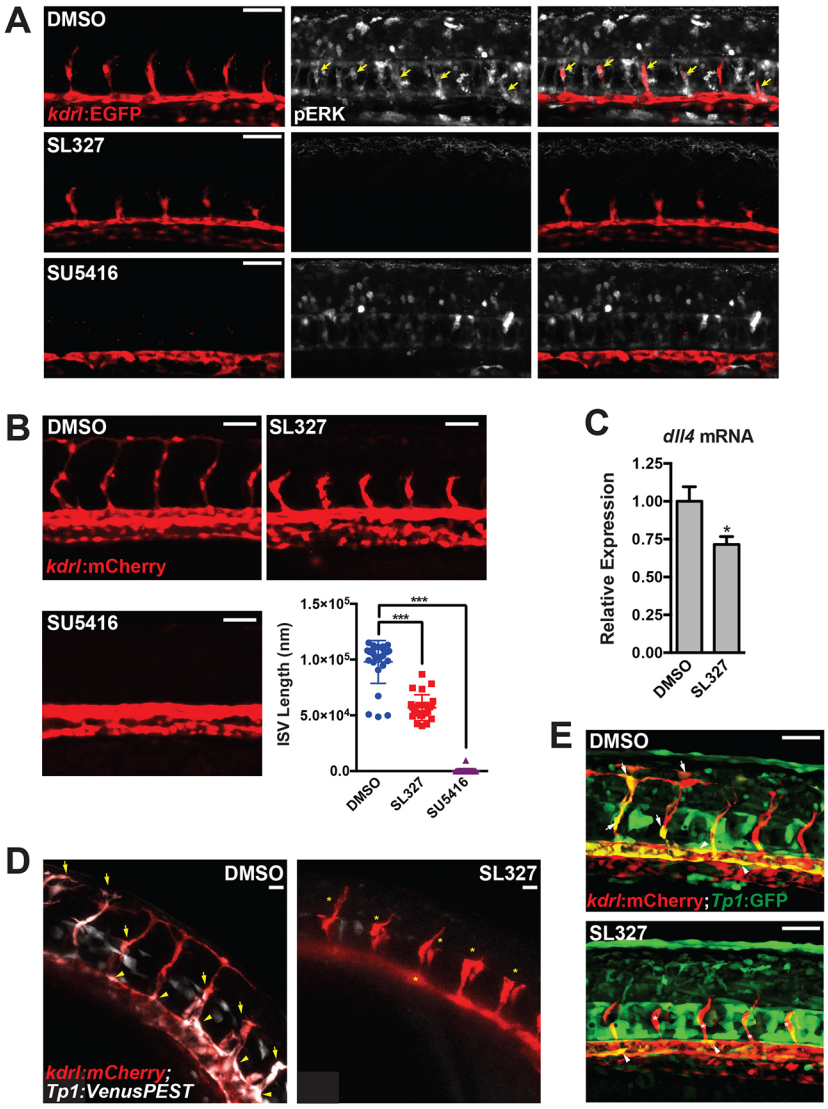

Fig. 2. Active MAPK/ERK signaling regulates sprouting angiogenesis in zebrafish. (A) pERK staining (white) in embryos treated with vehicle (i.e. DMSO), MEK (i.e. SL327) or VEGFR2 (i.e. SU5416) inhibitors [treated from 18-20 hours post-fertilization (hpf) to ~24 hpf]. See Fig. S2A for additional images and quantification. Yellow arrows indicate pERK-positive sprouting endothelial cells. (B) Inhibition of MEK activity by SL327 inhibits ISV sprout length. Inhibition of VEGFR2 signaling with SU5416 is included as a positive control. Quantification of ISV length at 28 hpf is shown. (C) *dll4* expression in SL327-treated embryos at 28 hpf (treatment initiated at 18-20 hpf) as assessed by qRT-PCR (n=6 individual embryos). (D) Notch activity is reduced in the vasculature of SL327-treated *Tg*(*kdrl*:mCherry); *Tg*(*Tp1bglob*:Venus-PEST) embryos. Still images from time-lapse microscopy of a representative experiment are shown. Arrows indicate Notch signaling-positive ISVs, arrowheads indicate Notch signaling-positive endothelial cells in the dorsal aorta, asterisks indicate Notch-negative ISVs. See Fig. S3 (for additional still images) and Movies 1 and 2. (E) Similar experiment to that shown in D, but with *Tg*(*kdrl*:mCherry); *Tg*(*Tp1bglob*:EGFP) embryos. Scale bars: 50 µm (A,B,E); 20 µm (D).

the ETS-DNA binding site within the intron 3 enhancer of murine *Dll4* [identified by Wythe et al. (2013)]. ETS reporter activity in bovine aortic ECs (BAECs) was attenuated by both MEK and PKC inhibition (Fig. 3D). This suggests that ETS factor transactivation is controlled by MAPK/ERK signaling.

Selvaraj et al. recently demonstrated that ERK2 preferentially bound and phosphorylated ERG at serines 96 (S96), 215 (S215) and 276 (S276), and that S215 phosphorylation was required for ERG activity in prostate cancer cells (Selvaraj et al., 2015). We found that S215 was dynamically phosphorylated in ECs in response to VEGF stimulation, with peak phosphorylation occurring at 15-30′, which coincides with increased MAPK/ERK activity following VEGF treatment (Fig. 3E). Pretreatment with a MEK inhibitor abolished S215 phosphorylation (Fig. 3F). To determine the functional importance of ERK-mediated phosphorylation of ERG, we eliminated endogenous ERG using an siRNA directed to the 3′ UTR of *ERG* and then reintroduced wild-type or phospho-mutant ERG. Expression of wild-type ERG restored *DLL4* transcription, whereas expression of ERG containing a mutation of one phosphorylation site (S215A) had less activity, and ERG containing mutations in all three ERK-phosphorylated residues (S96A, S215A, S276A) failed to rescue *DLL4* transcription (Fig. 3G). This suggests that ERK phosphorylation is functionally important in dictating ERG activity.

To test further the functional importance of ERG phosphorylation, transplantation experiments were performed in zebrafish. Wild-type or mutant (S96A, S215A, S276A) *ERG* mRNA was injected into *kdrl*:nls-EGFP donor embryos, followed by transplantation of these cells into *kdrl*:mCherry recipient hosts at sphere stage. The location of the donor cells within the trunk vasculature was scored at 28-30 hours post-fertilization (hpf) to determine whether expression of mutant ERG affects the ability of these cells to contribute to angiogenesis. There appeared to be no overt phenotypic consequence following mosaic overexpression of wild-type or mutant ERG. However, the percentage of ERG mutant-expressing cells contributing to intersegmental vessels (ISVs) (but not other vascular structures) was significantly reduced compared with wild-type ERG-expressing cells (Fig. 3H).

ERG coordinates dynamic co-activator recruitment to the *DLL4* intronic enhancer

p300 is recruited to VEGF-dependent enhancers and is required for regulating the expression of many angiogenic genes (Zhang et al., 2013). As the earliest time-point previously examined was 1 h post-

Development (2017) 144, 2428-2444 doi:10.1242/dev.146050

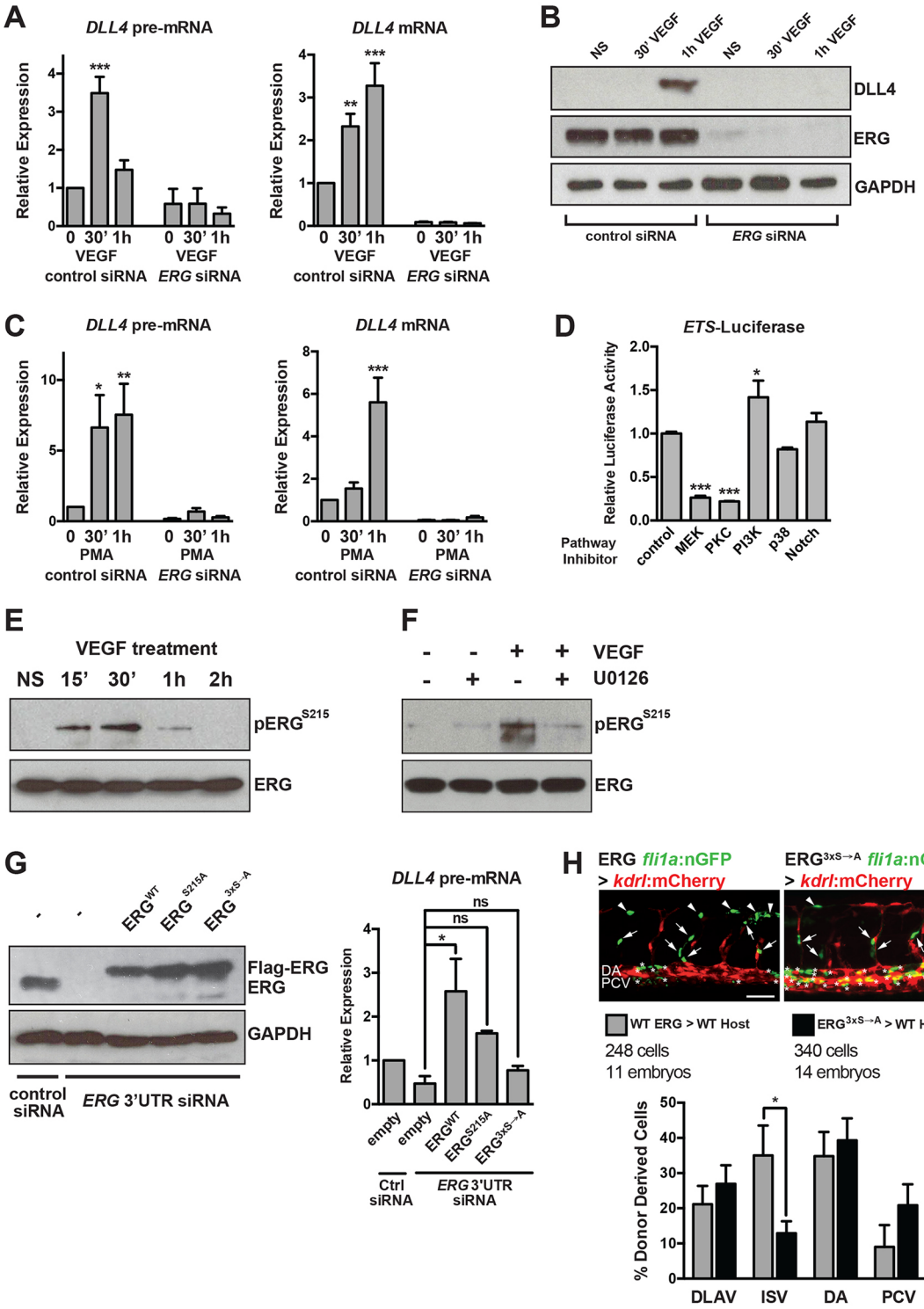

Fig. 3. VEGF/MAPK signaling stimulates ERG transcriptional activity to induce *DLL4* expression. (A) VEGF induction of *DLL4* transcription (as assessed by qRT-PCR measurement of *DLL4* pre-mRNA) and mature *DLL4* mRNA expression in HUVECs requires ERG (n=4). (B) VEGF induction of DLL4 protein expression requires ERG. Representative experiment of three. (C) Induction of *DLL4* transcription by PMA, an activator of MAPK/ERK signaling, requires ERG (n=4). (D) ETS activity (as assessed by activity of an 8× concatamer of an ETS element driving luciferase expression) in BAECs is suppressed by MEK or PKC inhibition. Triplicate determinations from a representative experiment of three. (E) ERG is phosphorylated at S215 in response to VEGF stimulation (15-30′) in HUVECs. Representative experiment of two. (F) VEGF-induced phosphorylation of ERG requires MEK activity. Representative experiment of two. (G) ERG was knocked down using siRNAs directed to the 3′ UTR, followed by overexpression of Flag-tagged wild-type (WT) or mutant (S215A or S96A;S215A;S276A, indicated as 3xS→A) ERG. ERG western blot indicates restoration of expression using electroporated constructs (a representative experiment of three is shown). *DLL4* expression as assessed by qRT-PCR of pre-mRNA after 1 h of VEGF treatment (n=3). (H) Representative images of transplanted cells from *Tg(fli1a*:nls-GFP) embryos injected with wild-type or mutant *ERG* mRNA into *Tg(kdrl*:mCherry*)* embryos. Arrows and asterisks indicate endothelial cells that are donor derived. Quantification of cellular position is shown below (n=248 cells from 11 embryos for wild type and n=340 cells from 14 embryos for mutant). Scale bar: 50 µm. DA, dorsal aorta (asterisks); DLAV, dorsal longitudinal anastomotic vessel (arrowheads); ISV, intersomitic vessel (arrows); NS, non-stimulated; PCV, posterior cardinal vein.

Development (2017) 144, 2428-2444 doi:10.1242/dev.146050

VEGF treatment, we sought to define the dynamic nature of p300 recruitment to the *DLL4* enhancer by ChIP assays in VEGF-stimulated HUVECs. ERG recruitment was modestly enhanced by VEGF treatment (Fig. 4A), but there is high basal ERG occupancy at this enhancer (Wythe et al., 2013). Strikingly, p300 was transiently recruited to the intronic *DLL4* enhancer 15-30′ after VEGF stimulation, mirroring the robust and transient increase in MEK/ERK activity and ERG phosphorylation (Fig. 4A). Of note, p300 recruitment did not coincide with increased acetylation of K27 of histone H3 (H3K27ac), although acetylation is already high at this region in ECs (Wythe et al., 2013). Importantly, we found that p300 recruitment to the intronic *DLL4* enhancer required ERG (Fig. 4B). In addition, co-immunoprecipitation in ECs demonstrated that ERG and p300 physically interacted following VEGF stimulation (Fig. 4C), and that this interaction was lost in cells expressing a phospho-mutant ERG (S96A, S215A, S276A) protein (Fig. 4D). To determine the functional importance of p300 in *DLL4* induction, we utilized a small molecule inhibitor of p300 and CBP histone acetyltransferase activity, c646 (Bowers et al., 2010). Inhibition of p300/CBP activity in HUVECs *in vitro* did not affect basal levels of *DLL4*, but completely blocked VEGF induction of *DLL4* mRNA (Fig. 4E). Furthermore, inhibition of p300/CBP in zebrafish suppressed elongation of intersomitic vessels (Fig. 4F), but did not result in other gross developmental defects (Fig. S2C).

ERG regulates a network of constitutive and VEGF-inducible genes

To determine the extent of the genetic network regulated by ERG, we transfected HUVECs with control or *ERG* siRNAs and performed microarray analysis of gene expression in serum-starved and VEGF-stimulated cells. We focused on transcripts induced at early stages of VEGF stimulation (i.e. within 1 h) to identify genes directly regulated by VEGF/ERK/ERG. Knockdown of *ERG* resulted in the downregulation of 202 genes, including *CLDN5*, *RASIP1* and *ARHGAP28* in serum-starved cells (Fig. S4A), consistent with previous studies (Birdsey et al., 2012; Yuan et al., 2012), and the upregulation of 68 genes. Gene ontology (GO) analysis revealed that the most frequent functional categories altered following loss of ERG were: response to wounding, inflammation, cell migration, cell motility and cell adhesion (Fig. S4B). VEGF treatment increased the expression of 160 genes and downregulated only four genes (Fig. S5A). Analysis of the genes modulated by VEGF revealed GO terms associated with transcriptional regulation and gene expression, cell proliferation and vascular development

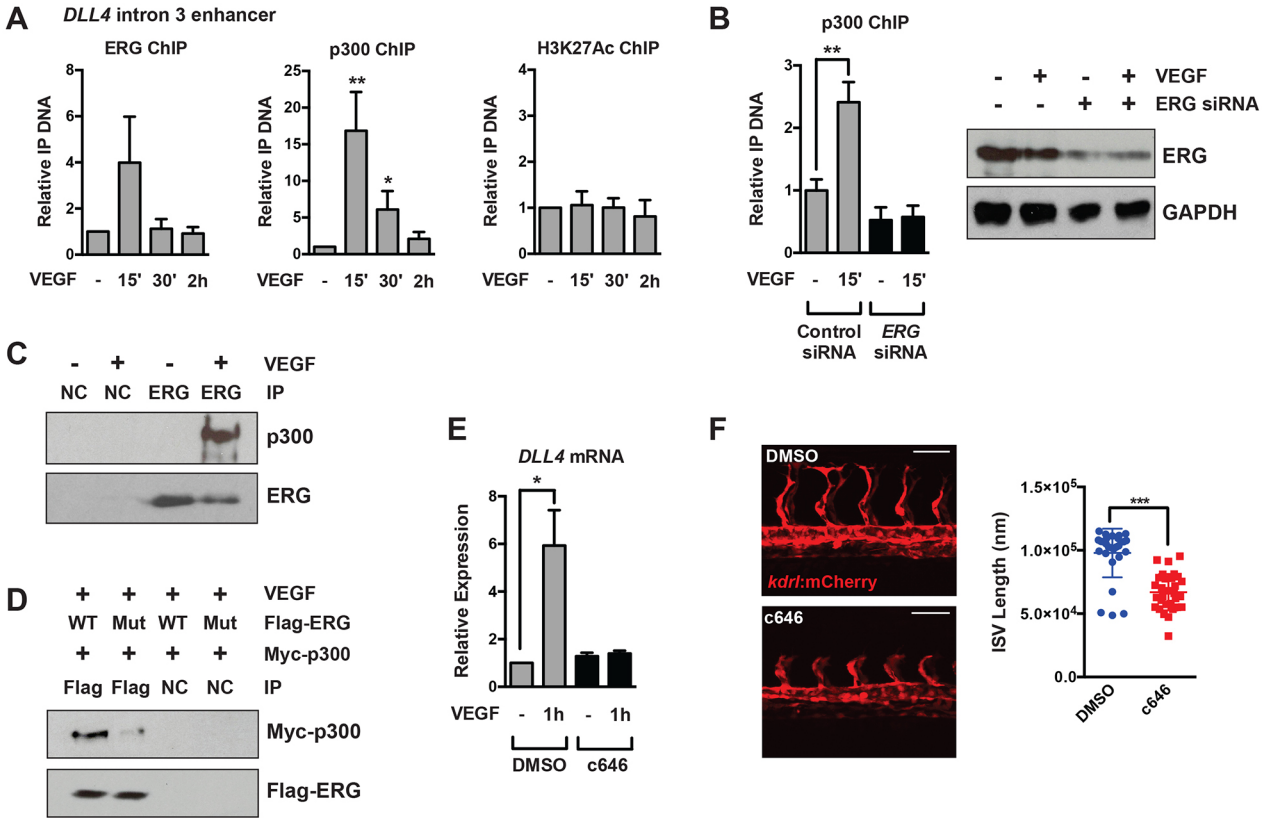

Fig. 4. p300 is dynamically recruited to the *DLL4* enhancer and regulates sprouting angiogenesis. (A) Recruitment of p300 to the *DLL4* enhancer located in intron 3 15-30′ after VEGF stimulation, as assessed by ChIP (n=5 for ERG and p300 ChIP, n=3 for H3K27ac ChIP). (B) p300 recruitment in response to VEGF stimulation requires ERG. Shown is a representative experiment of two with triplicate determinations. The extent of ERG knockdown as assessed by western blot is shown to the right. (C) Endogenous p300 and ERG physically interact by co-immunoprecipitation in HUVECs stimulated with VEGF. Shown is a representative experiment of three. (D) Exogenous Myc-p300 interacts with wild-type Flag-ERG in BAECs, but does not interact with phospho-mutant (S96A;S215A;S276A) Flag-ERG by co-immunoprecipitation. Shown is a representative experiment of three. (E) p300 activity is required for *DLL4* mRNA induction in HUVECs in response to VEGF stimulation (n=5). c646 is a potent inhibitor of p300/CBP activity. (F) Inhibition of p300 activity suppresses ISV elongation in zebrafish. Quantification is shown to the right. Note: Quantification of the DMSO control is the same as that shown in Fig. 2B, as both inhibitors were used in the same experiment. Scale bars: 50 µm. NC, negative control (V5 antibody).

Development (2017) 144, 2428-2444 doi:10.1242/dev.146050

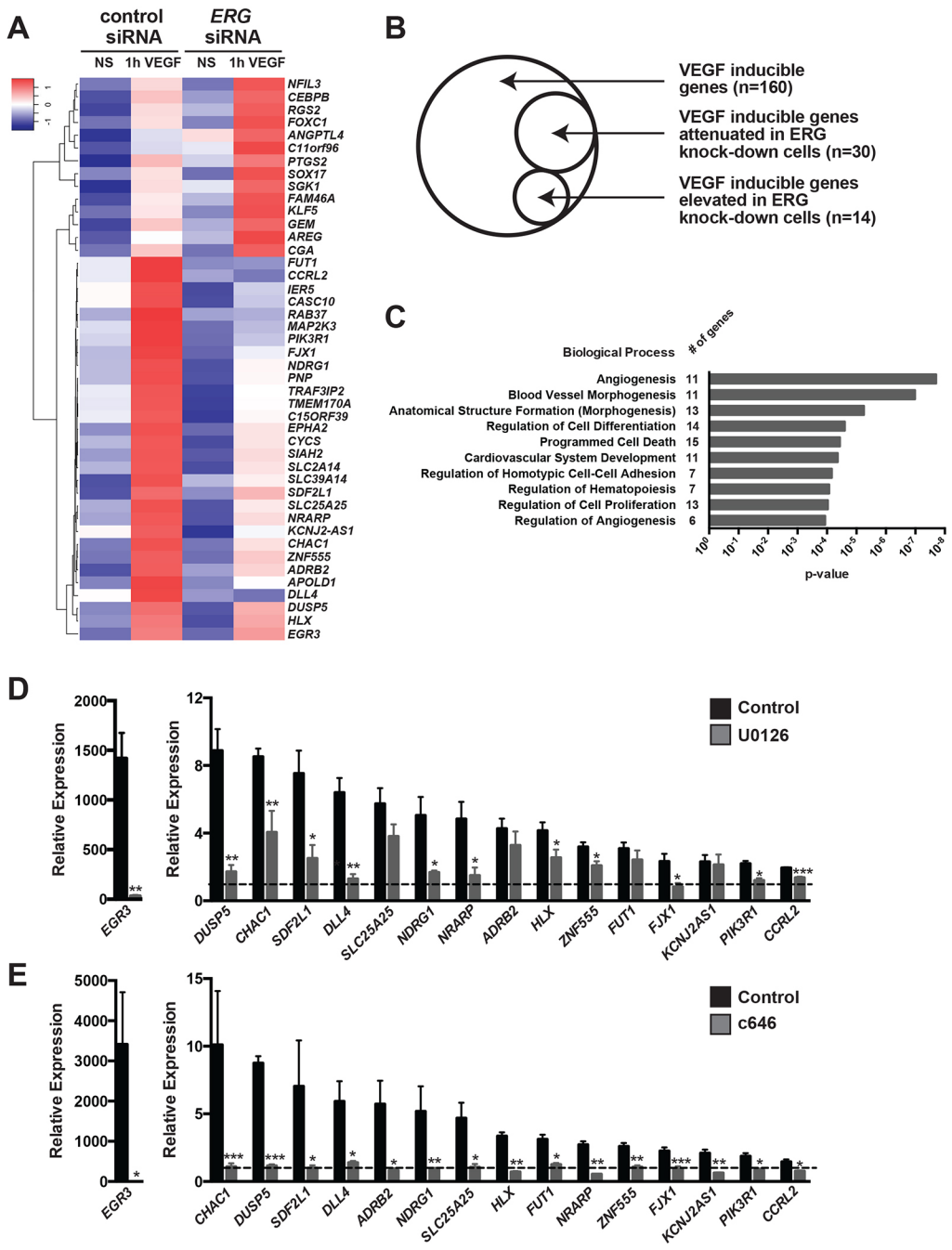

Fig. 5. A network of VEGF-inducible genes are ERK/ERG/p300 dependent. (A) Hierarchical clustering of microarray analysis identified a group of 30 VEGF-inducible genes that are suppressed in *ERG* knockdown cells, and a group of 14 VEGF-inducible genes that were further induced in *ERG* knockdown cells (HUVECs). NS, non-stimulated. (B) Venn diagram depicting the number of VEGF-inducible genes and the subset that are ERG dependent. See Fig. S5 for further details on VEGF-regulated transcripts. (C) Gene Ontology (GO) analysis of ERG/VEGF-dependent genes. Selected representative GO terms are displayed with their associated *P*-value. The number of genes in each GO category is indicated. The GO terms depicted are: Angiogenesis (GO:0001525), Blood vessel morphogenesis (GO:0048514), Anatomical structure formation (morphogenesis) (GO:0048646), Regulation of cell differentiation (GO:0045595), Programmed cell death (GO:0012501), Cardiovascular system development (GO:0072358), Regulation of homotypic cell-cell adhesion (GO:0034110), Regulation of hematopoiesis (GO:1903706), Regulation of cell proliferation (GO:0042127), Regulation of angiogenesis (GO:0045765). (D) qRT-PCR analysis of the MEK dependency of the VEGF induction of a subset of the genes identified by microarray. HUVECs were pre-treated with DMSO or U0126 (MEK inhibitor) prior to VEGF stimulation. Expression is relative to non-VEGF-stimulated cells (dashed line). Genes are arranged in decreasing order of VEGF induction. The induction of 12 out of 16 genes was found to be MEK dependent (n=4-5). (E) qRT-PCR analysis of the p300 dependency of the VEGF induction of a subset of the genes identified by microarray. HUVECs were pre-treated with DMSO or c646 (p300/CBP inhibitor) prior to VEGF stimulation. Expression is relative to non-VEGF-stimulated cells (dashed line). Genes are arranged in decreasing order of VEGF induction. All 16 VEGF-induced genes were found to be p300 dependent (n=4-5).

(Fig. S5B). Of the VEGF-induced genes, 30 (representing ~19% of all VEGF-inducible genes) were attenuated in *ERG* knockdown cells, and 14 genes (~9% of all VEGF-inducible genes) were further elevated in *ERG* knockdown cells (Fig. 5A,B). GO analysis revealed that these genes (e.g. *NRARP*, *HLX*, *DUSP5*, *EGR3* and *PIK3R1*; Bellou et al., 2009; Herbert et al., 2012; Liu et al., 2008;

Development (2017) 144, 2428-2444 doi:10.1242/dev.146050

Nicoli et al., 2012; Phng et al., 2009) are implicated in angiogenesis, blood vessel morphogenesis and development, homotypic cell-cell adhesion, cell proliferation and differentiation (Fig. 5C).

Examining the kinetics of a subset of the ERG-dependent, VEGF-induced genes revealed that their transcription is increased transiently by VEGF stimulation, with peak transcription occurring between 15′ and 1 h (Fig. S6). To query the requirement of MAPK/ERK signaling and p300 activity in this response, we measured the induction of these genes in the presence of MEK or p300/CBP inhibitors. We found that 12 of 16 (75%) were MEK dependent, and all required p300/CBP activity (Fig. 5D,E).

To probe the relevance of this pathway *in vivo*, we assessed the expression of several of the identified genes by *in situ* hybridization in zebrafish embryos treated with inhibitors of VEGF, MEK or p300/CBP. Importantly, *dll4*, *hlx1* and *dusp5* were regulated by this pathway within ISVs (Fig. 6A,B). In addition, *flt4*, which is regulated by MAPK/ERK signaling during sprouting angiogenesis (Shin et al., 2016), was also dependent on p300/CBP and MEK (Fig. 6A,B). To induce ectopic activation of the MAPK/ERK pathway in a VEGF-independent manner, *kdrl:*GFP zebrafish embryos were exposed to PMA for 2 h (until 24 hpf). PMA treatment induced the phosphorylation of ERK1/2 in a MEK-dependent manner (Fig. 6C) and led to the induction of *dll4*, *hlx1*, *dusp5* and *egr3* expression in the endothelium, as determined by qRT-PCR from fluorescence-activated cell sorting (FACS)-isolated ECs (Fig. 6D). Importantly, pre-treatment of the embryos with c646 inhibited the PMA-induced induction of *dll4*, *hlx1* and *egr3*, whereas *dusp5* was refractory to c646 inhibition (Fig. 6E).

To assess further the role of ERG in angiogenesis *in vivo*, we generated a novel *Erg* knockout/*lacZ* knock-in mouse line. Deletion of *Erg* resulted in embryonic lethality by embryonic day (E) 11.5-E12.5, similar to previous reports (Birdsey et al., 2015; Vijayaraj et al., 2012) (Fig. S7A-F). Following loss of ERG protein (Fig. 7A-B′), we observed major defects in vascular integrity and angiogenesis during embryogenesis, within both the cranial and the trunk vasculature (Fig. 7C-F). Conditional deletion of *Erg* (Erg^{iECKO}) using an EC-specific CreERT2 driver [*Cdh5(PAC)-CreERT2*] (Wang et al., 2010) led to defects in physiological angiogenesis, as determined by examination of angiogenesis within the postnatal retina (Fig. 7G-J; Fig. S7G-K). These data, combined with the embryonic lethality, hemorrhage and reduced angiogenesis all demonstrate a requirement for ERG in physiological angiogenesis.

To determine whether the candidate genes identified by our *in vitro* screen are downstream of Erg *in vivo*, we isolated ECs from wild-type or *Erg* mutant mouse embryos and performed qRT-PCR for several of the ERG- or VEGF/ERG-dependent genes (Fig. 7K,L). We found that several ERG-dependent, VEGF-independent genes identified in our screen (e.g. *Rasip1*, *Sox18*) or by others [e.g. *Cdh5* (Birdsey et al., 2008; Gory et al., 1998) and *Cldn5* (Yuan et al., 2012)] were downregulated in *Erg* loss-of-function embryos (Fig. 7K). Similarly, we observed a significant reduction in a typical VEGF-induced, ERG-dependent transcript, *Dll4*, in agreement with previous results (Wythe et al., 2013) (Fig. 7L). Additional candidates in this category, which showed robust sensitivity to MAPK and P300 activity *in vitro*, were substantially downregulated *in vivo* (e.g. *Fjx1*, *Pik3r1*, *Sdf2l1*, *Nrarp*). Collectively, these findings demonstrate that a VEGF/MAPK/ERG/p300 cascade is a crucial regulator of angiogenesis *in vitro* and *in vivo*.

We next sought to identify the enhancers/promoters that ERG might directly act upon to regulate this gene network. We previously found that conserved orthologous transcription factor binding can reveal functional enhancers (Ballester et al., 2014). To identify evolutionarily conserved, epigenetically modified enhancers for further functional analyses, we performed ERG ChIP-seq experiments in both human (HUVECs) and bovine (BAECs) ECs cultured in complete media (i.e. containing VEGF) (Fig. 8). We identified 31,175 ERG ChIP-seq peaks in HUVECs and 34,773 peaks in BAECs, and found that 8337 of the human peaks were conserved in cow (Tables S3 and S4). We also performed H3K27ac ChIP-seq and found that 94% of conserved ERG peaks overlapped H3K27ac-enriched regions, supporting their association with active enhancers. We found that the *DLL4* locus contains multiple conserved ERG-bound enhancers, including regions ∼12 kb upstream of the transcriptional start site (TSS) and within intron 3 (Fig. 8A), both of which were previously shown to have arterial-specific activity *in vivo* (Sacilotto et al., 2013; Wythe et al., 2013). We also identified an ERG-bound enhancer, conserved in cows and humans, ∼3.0 kb upstream of the gene H2.0-like homeobox (*HLX*) (Fig. 8B; Fig. S8). HLX, a homeobox transcription factor, expression of which is induced by VEGF *in vitro* (Schweighofer et al., 2009), has been implicated in controlling angiogenic sprouting of human cells *in vitro* (Prahst et al., 2014; Testori et al., 2011), and in ISV formation in zebrafish (Herbert et al., 2012), as well as yolk sac vascular remodeling in the mouse (Prahst et al., 2014). Further analysis of our ChIP-seq data revealed that the majority of ERG/VEGF-regulated genes (25 of 44) had an ERG ChIP-seq peak within 10 kb of the TSS, and ERG binding was conserved in cow for 16 of these genes (Fig. 8C). This is suggestive of direct regulation of these genes by ERG. Furthermore, ERG binding was significantly enriched near ERG- and ERG/VEGF-regulated genes (Fig. 8D).

HLX transcription is transiently induced in response to VEGF stimulation, similar to *DLL4* (Fig. 9A). We found that p300 was dynamically recruited to this evolutionarily conserved non-coding region (Fig. 9B) in an ERG-dependent manner (Fig. 9C). We cloned this conserved H3K27ac- and ERG-enriched −3 kb 5′ putative regulatory region (*HLX-3a*, 1565 bp fragment) upstream of a minimal promoter (SV40) driving a luciferase reporter, and found that it was VEGF responsive, and that the basal and VEGF-induced activity of this enhancer required ETS DNA-binding sequences (Fig. 9D). Furthermore, inhibition of MEK activity abrogated the VEGF responsiveness of this regulatory region (Fig. 9E). Although the full *HLX-3a* regulatory region failed to drive endothelial expression *in vivo* (data not shown; n=75), refinement of the element to the region bound by ERG (which was highly conserved across vertebrates; Fig. S8) and the 3′ acetylated region (*HLX-3b*, 435 bp fragment) drove robust EGFP reporter activity in the vasculature of the embryonic zebrafish (Fig. 9F). EGFP reporter expression was preferentially observed in the ECs of the ISVs (which form by angiogenesis) compared with the axial vessels (which form by vasculogenesis), and reporter activity was ETS element dependent (Fig. 9F). To test further the functional importance of this enhancer, we utilized clustered regularly interspaced short palindromic repeats/Cas9 (CRISPR/Cas9) genome editing to delete a portion (1201 bp; see Fig. 8B for schematic) of the H3K27ac-enriched, ERG-bound region upstream of *HLX* in TeloHAECs, an immortalized human aortic EC line. Several clonal lines (Δ*HLX15*, Δ*HLX17* and Δ*HLX21*) heterozygous for deletion of this region were generated and confirmed by PCR and DNA sequencing (data not shown). Comparison was made with a clonal line generated following transfection of scrambled control gRNAs (Scr3). Although the basal expression of *HLX* appeared to be unaffected in the deletion lines, the VEGF-

Development (2017) 144, 2428-2444 doi:10.1242/dev.146050

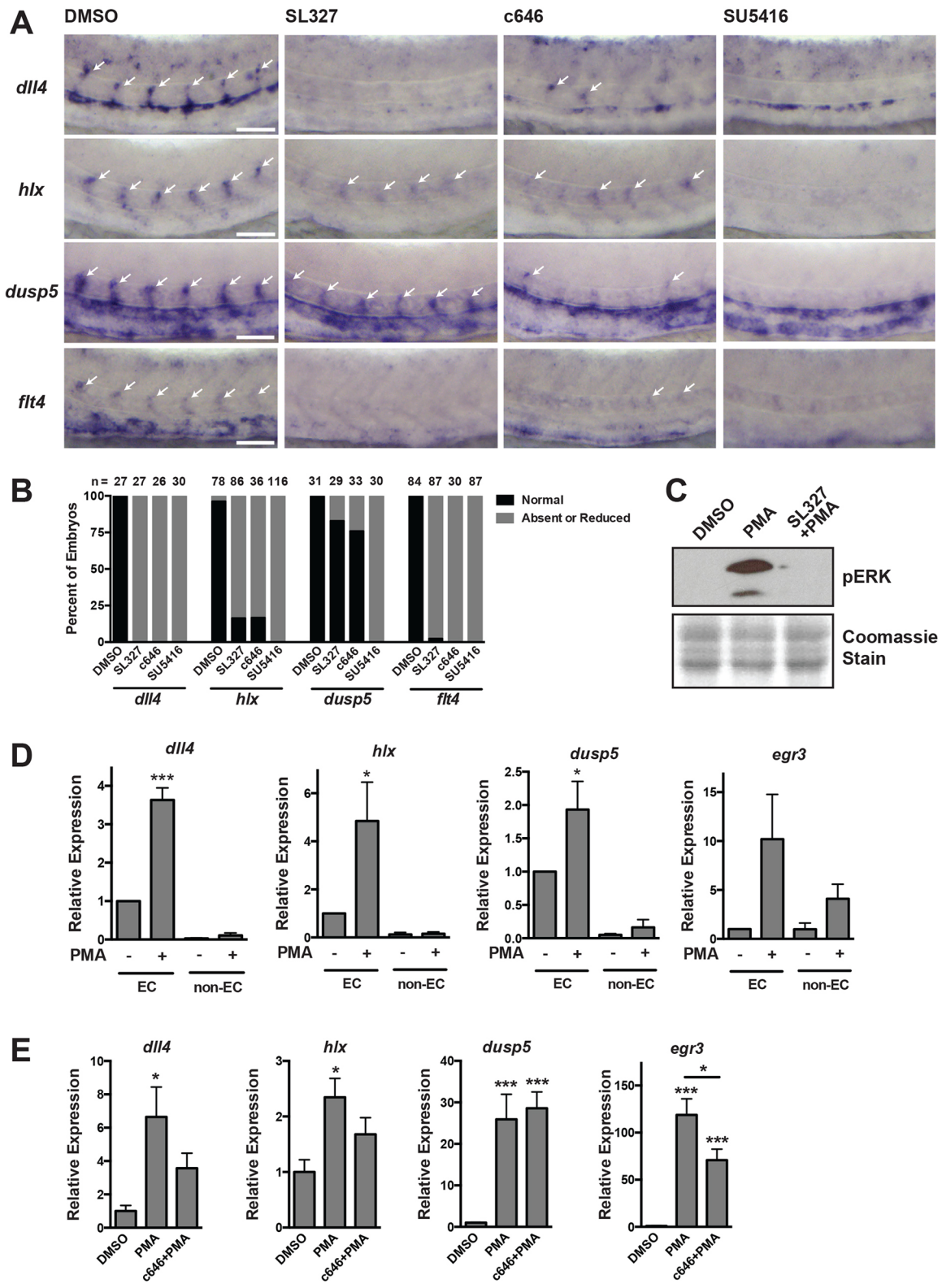

Fig. 6. Regulation of VEGF/ERK/ERG/p300-dependent genes *in vivo*. (A) *In situ* hybridization using probes for *dll4*, *hlx1*, *dusp5* and *flt4* at 26 hpf. Embryos were treated with inhibitors of MEK (SL327), p300/CBP (c646) or VEGF (SU5416) starting at the 20-somite stage. Expression of each of these genes is MEK, p300 and VEGF dependent. Arrows indicate ISVs expressing the indicated genes. Representative images are shown. (B) Quantification of *in situ* hybridization experiments. The number of embryos analyzed is indicated. (C) pERK western blot in embryos pre-treated with SL327 for 1 h, followed by addition of PMA for 2 h. Coomassie staining was used to assess loading. Representative experiment of two. (D) qRT-PCR analysis of endothelial or non-endothelial cells isolated from *kdrl*:GFP embryos exposed to PMA for 2 h (starting at 24 hpf). All of these genes are induced in the endothelium in response to ectopic MEK activation (n=3). (E) qRT-PCR of whole individual embryos that were exposed to DMSO or c646 for 1 h, prior to stimulation with PMA for 2 h at 24 hpf. The induction of *dll4*, *hlx* and *egr3* by PMA is p300 dependent (n=6).

Development (2017) 144, 2428-2444 doi:10.1242/dev.146050

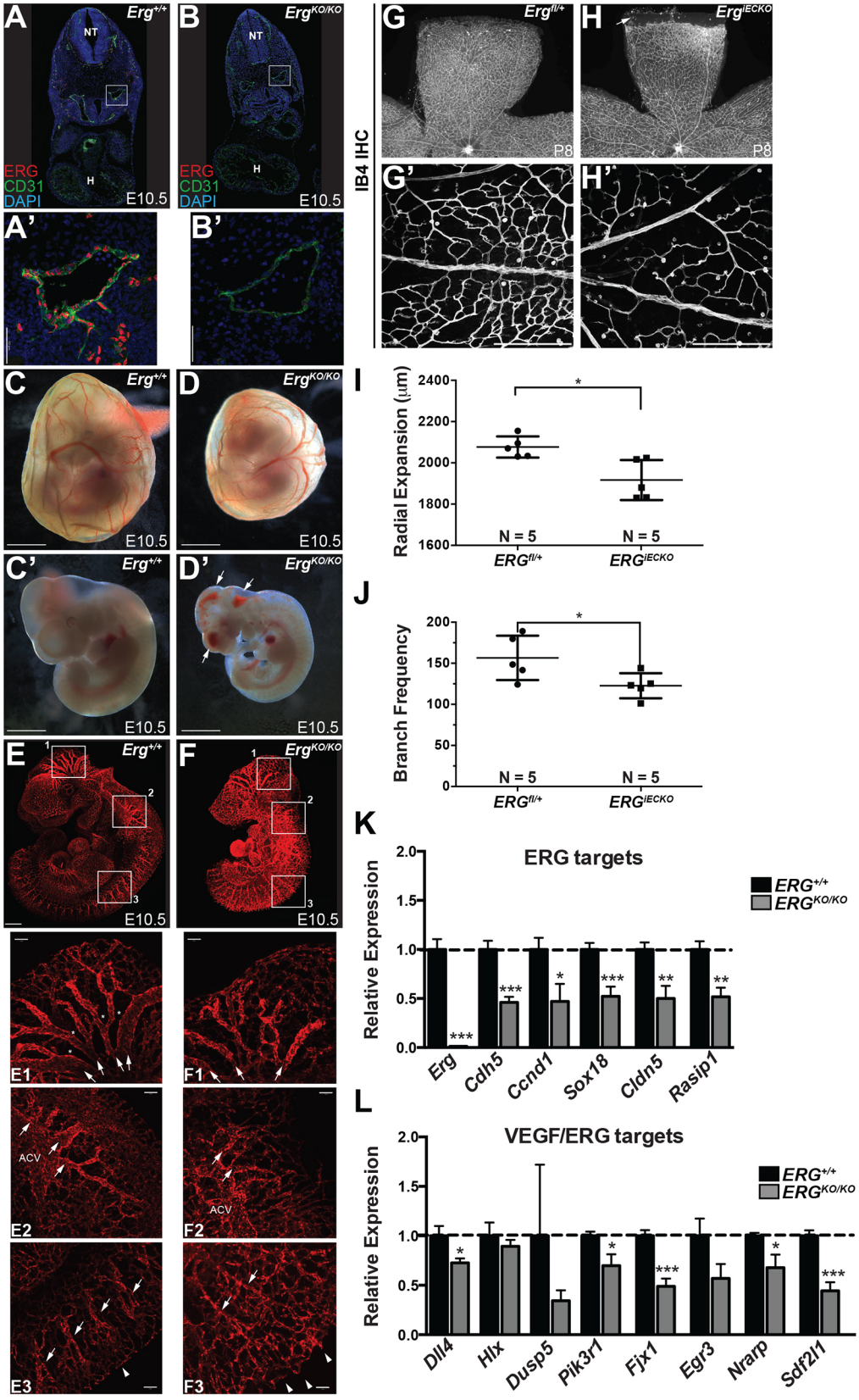

Fig. 7. ERG loss of function alters angiogenesis *in vivo*. (A-B′) Confocal microscopy following staining for ERG and CD31 on mouse embryo cryosections. Magnified views (A′,B′) of the dorsal aorta (boxed areas) reveal loss of ERG, and decreased CD31 (PECAM1), in $Erg^{KO/KO}$ embryos compared with wild-type littermate controls. Nuclei are stained with DAPI (blue). H, heart; NT, neural tube. (C-D′) Representative whole-mount bright-field images of E10.5 $Erg^{+/+}$ (C,C′) and $Erg^{KO/KO}$ (D,D′) yolk sacs and embryos. Arrows indicate hemorrhage. (E,F) Representative light-sheet microscopy images of endomucin-stained blood vessels in E10.5 $Erg^{+/+}$ (E) and $Erg^{KO/KO}$ (F) embryos. Boxed areas 1, 2 and 3 are shown below the whole-mount images at a higher magnification. Arrows in box 1 denote remodeled, larger caliber vessels, which are smaller in $Erg^{KO/KO}$ animals, and asterisks denote remodeled areas devoid of vessels, which are reduced in $Erg^{KO/KO}$ embryos compared with $Erg^{+/+}$. In box 2, the anterior cardinal vein (ACV), although present in the knockouts, showed a decreased diameter and the major large caliber vessels sprouting from it (denoted by arrows) were also smaller and more tortuous. In box 3, the remodeled ISVs are denoted by arrows, and the sprouting front (dorsal-most edge) is denoted by arrowheads. The vascular front appears less uniform in knockouts and the ISVs appear less organized compared with wild-type littermates. (G-H′) Representative images of the total retinal vasculature (G,H) and magnified view of the proximal region (G′,H′) stained with IB4 in $Erg^{fl/+}$ (G,G′) and Erg^{iECKO} (H,H′) retinas at P8 following tamoxifen administration at P1 and P3. The arrow in H indicates an avascular area in Erg^{iECKO} retina. (I) Quantification of radial expansion of the $IB4^+$ vasculature within the P8 retina (n=5 for both genotypes). (J) Vascular density as determined by quantification of $IB4^+$ branches in the proximal retinal vascular plexus at P8 (n=5 for each genotype). (K,L) ECs were isolated by FACS from $Erg^{+/+}$ or $Erg^{KO/KO}$ embryos at E10.5. qRT-PCR was performed on the indicated VEGF-independent, ERG-dependent (K) and VEGF-responsive, ERG-dependent (L) genes [n=14 ($Erg^{+/+}$) and 9 ($Erg^{KO/KO}$)]. Scale bars: 50 μm (A′,B′); 1000 μm (C-D′); 500 μm (E,F); 100 μm (E1-3,F1-3,G′,H′).

dependent induction of *HLX* appeared to be diminished (Fig. 9G). In contrast, *DLL4* induction was unaffected. Furthermore, knockdown of *ERG* appeared to attenuate the induction of *HLX* to a greater extent in the control line compared with the deletion lines, implying that ERG acts through the deleted enhancer region. Collectively, these findings demonstrate the requirement of a highly conserved ERG-bound regulatory element in the VEGF responsiveness of the angiogenic gene *HLX*.

Development (2017) 144, 2428-2444 doi:10.1242/dev.146050

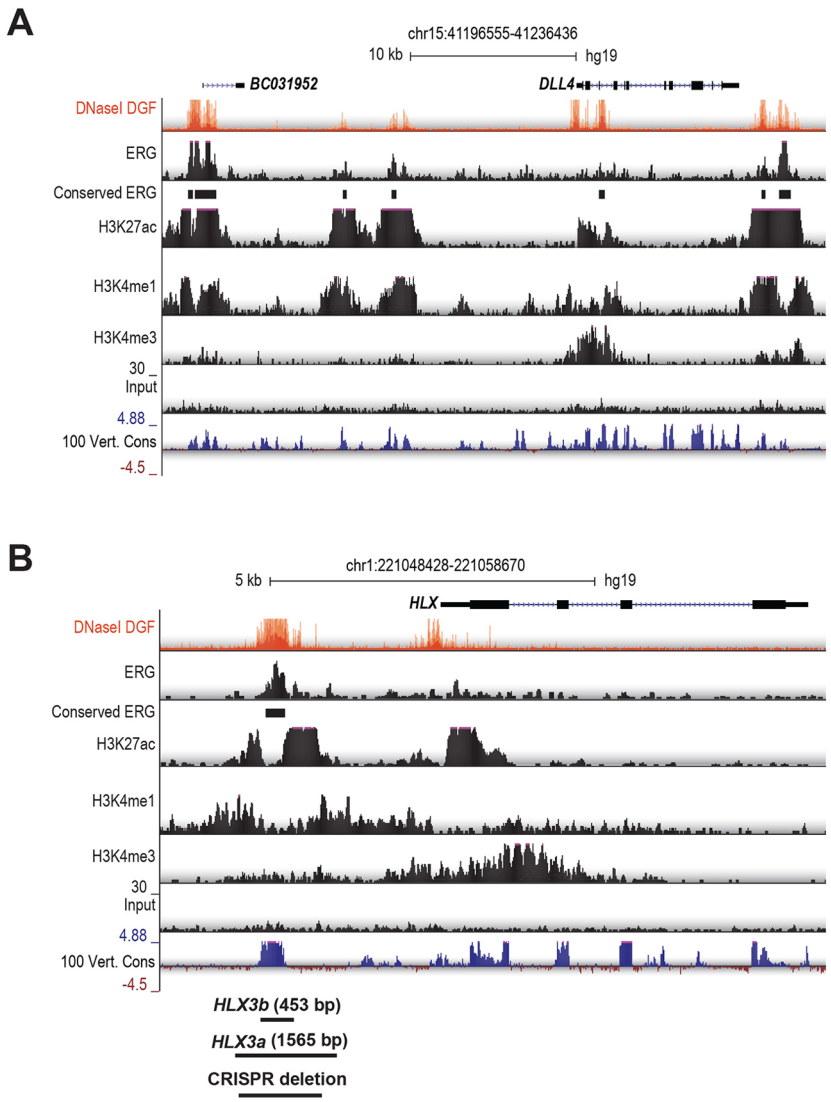

C

Gene	ERG-binding (within 10 kb) in HUVEC	Conserved Binding in Cow
FUT1	+	+
CCRL2	+	-
IER5	-	-
CASC10	-	-
RAB37	+	-
MAP2K3	+	-
PIK3R1	+	+
FJX1	+	-
NDRG1	-	-
PNP	+	-
TRAF3IP2	+	+
TMEM170A	-	-
C15ORF39	-	-
EPHA2	+	+
CYCS	+	-
SIAH2	-	-
SLC2A14	-	-
SLC39A14	+	+
SDF2L1	+	+
SLC25A25	+	+
NRARP	+	+
KCNJ2-AS1	-	-
CHAC1	-	-
ZNF555	+	-
ADRB2	-	-
APOLD1	+	+
DLL4	+	+
DUSP5	+	+
HLX	+	+
EGR3	-	-
C11ORF96	+	+
FAM46A	-	-
GEM	+	-
AREG	-	-
PTGS2	-	-
RGS2	-	-
ANGPTL4	+	+
KLF5	-	-
CGA	-	-
FOXC1	+	-
SGK1	+	+
NFIL3	-	-
SOX17	+	+
CEBPB	-	-

D

	Total # of Genes in Genome	# of Genes with ERG Binding in HUVEC	# Regulated by ERG or ERG/VEGF	# Regulated by ERG/VEGF with ERG Binding	Enrichment	Adjusted p-value
ERG-dependent (total)	55778	13902	267	126	1.9	4.77E-15
ERG- and VEGF-dependent (total)	55778	13902	44	25	2.3	9.87E-06
ERG-dependent (conserved)	55778	5544	267	47	1.8	1.27E-04
ERG- and VEGF-dependent (conserved)	55778	5544	44	16	3.7	2.49E-06

Fig. 8. Identification of ERG-bound enhancers. (A) Visualization of ChIP-seq assessing ERG binding, enhancer modifications (H3K27ac, H3K4me1, DNaseI hypersensitivity) and promoter modifications (H3K3me3) in HUVECs at the *DLL4* locus. *y*-axis denotes reads per million (RPM) sequences. Conservation of ERG binding in BAECs is indicated, as is sequence conservation across 100 vertebrate species (*y*-axis denotes the magnitude of the conservation score). (B) Visualization of ChIP-seq data and sequence conservation surrounding the human *HLX* locus, a VEGF- and ERG-regulated gene, revealing a putative enhancer located ~3 kb upstream of the transcriptional start site (TSS). The locations of the *HLX-3a* and *HLX-3b* fragments used in subsequent functional analyses are indicated, as is the region deleted by CRISPR/Cas9-mediated genome editing. (C) The presence of ERG-bound regions within 10 kb of the TSS of ERG/VEGF-dependent genes in HUVECs is indicated. Binding that is conserved in cow (i.e. in BAECs) is indicated. Genes that are induced by ERG are shown in green, whereas those repressed by ERG are shown in red. (D) Analysis of the enrichment of ERG-bound enhancers nearby ERG- and ERG/VEGF-dependent genes, compared with all genes in the genome.

DISCUSSION

Dynamic control of gene expression and the resultant cellular outputs in tip cells and adjacent stalk cells are central to the growth of nascent angiogenic sprouts (Blanco and Gerhardt, 2013; Lobov et al., 2007). The pathways that regulate the temporal VEGF-dependent expression of *DLL4* in tip cells are of particular importance

Development (2017) 144, 2428-2444 doi:10.1242/dev.146050

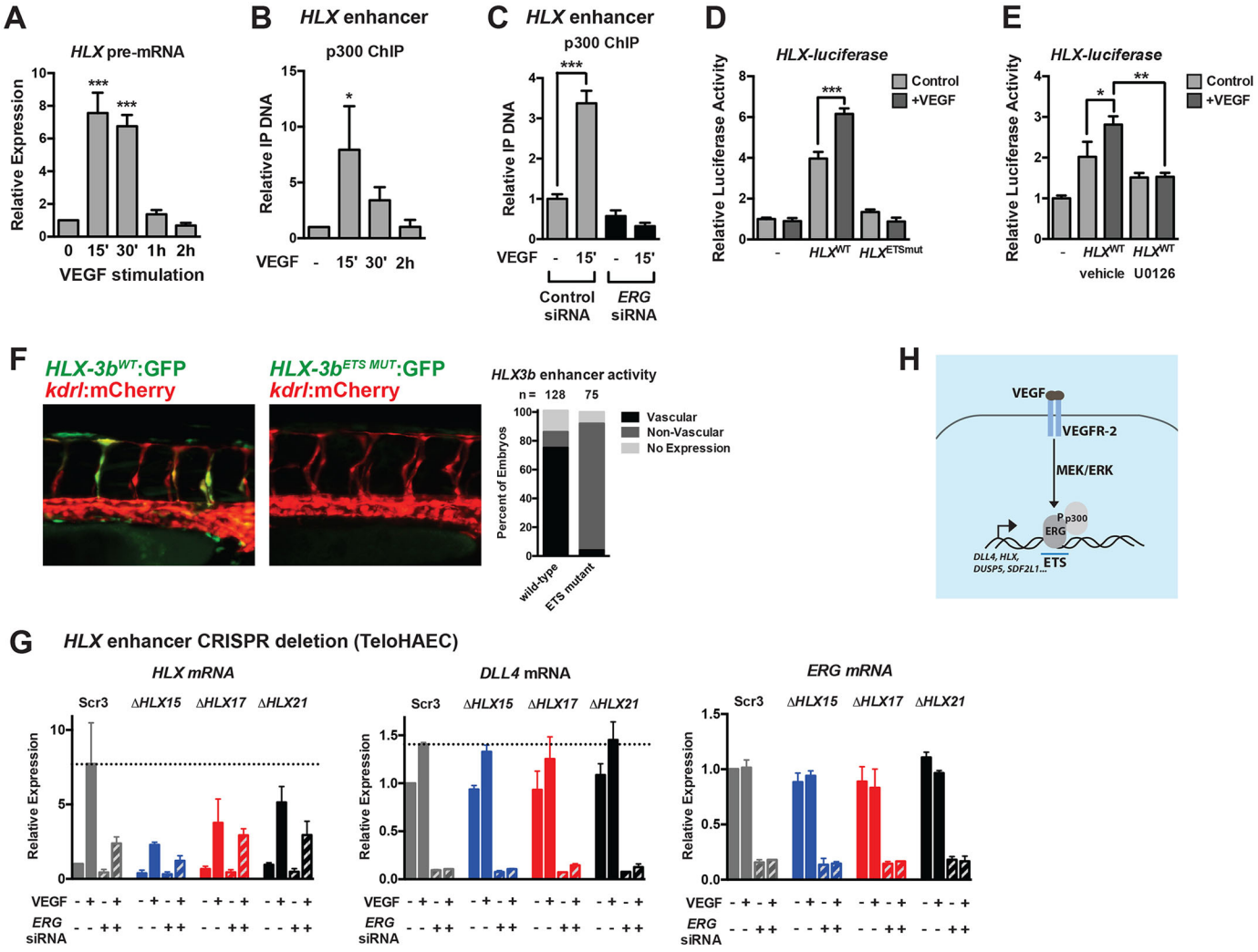

Fig. 9. A conserved enhancer upstream of *HLX* is regulated by ETS factors and is required for VEGF induction. (A) Transcription of *HLX* (as assessed by qRT-PCR of *HLX* pre-mRNA) reveals dynamic transcription, peaking at 15-30′ post-VEGF stimulation in HUVECs (*n*=3). (B) p300 is transiently recruited to a putative *HLX* enhancer element during VEGF stimulation, as assessed by ChIP assay (*n*=3). (C) p300 ChIP was performed in control and *ERG* knockdown cells. Shown are triplicate measures of a representative experiment of two. (D) Luciferase analysis of the *HLX* enhancer (*HLX-3a*), demonstrating that it is regulated by VEGF and ETS factors. ETS-binding sites were mutated in the *HLX* enhancer (HLX^{ETSmut}, see Materials and Methods). A representative experiment (of three) with triplicate determinations is shown. (E) Luciferase analysis of the *HLX* enhancer (*HLX-3a*), demonstrating that it is regulated by MAPK/ERK activity. A representative experiment (of two) with triplicate determinations is shown. (F) The human *HLX* enhancer (*HLX-3b*) is functional in ISVs in zebrafish during sprouting angiogenesis. Activity is lost when the ETS sites in the enhancer are mutated. Shown are representative images of embryos at 42 hpf. Quantification of enhancer activity is shown to the right. (G) CRISPR/Cas9-mediated deletion of a highly conserved enhancer upstream of *HLX* inhibits VEGF-mediated induction. Shown are a clonal scrambled-control line (Scr3) and three heterozygous deletion lines (Δ*HLX15*, Δ*HLX17*, Δ*HLX21*). Induction of *DLL4* is included as a control. Knockdown of *ERG* affects the induction of *HLX* in the control line to a greater extent than in the deletion lines. *n*=2. (H) Schematic of the VEGF/MEK/ERK/ERG/p300 transcriptional pathway identified in this study.

considering the central role of this ligand, and its receptor, Notch, in directing tip and stalk cell behaviors (Hellström et al., 2007; Jakobsson et al., 2010; Suchting et al., 2007; Ubezio et al., 2016). Here, we identify one potential mechanism for the transient VEGF-dependent induction of *DLL4* transcription. VEGF stimulation initiates a rapid and transient burst of MAPK/ERK activity, with similar kinetics to VEGF induction of *DLL4* transcription. Downstream target proteins modulated by ERK kinase activity are also dynamically modified, as illustrated by the transient phosphorylation of ERG at serine 215. Additionally, we find that the co-activator p300 is recruited to angiogenic enhancers in an ERG-dependent manner, with kinetics mirroring ERG phosphorylation. This VEGF/ERK/ERG/p300 transcriptional pathway also dynamically regulates a network of genes shown to positively (e.g. *HLX*, *FJX1*, *EGR3*, *APOLD1*, *ADRB2*, *EPHA2*, *FUT1*, *MAP2K3*, *NDRG1*) and negatively (e.g. *DUSP5*, *NRARP*) regulate angiogenesis (Fig. 9H) (Al-Greene et al., 2013; Bellou et al., 2009; Herbert et al., 2012; Iaccarino et al., 2005; Liu et al., 2008; Mirza et al., 2013; Moehler et al., 2008; Phng et al., 2009; Pin et al., 2012; Prahst et al., 2014; Toffoli et al., 2009; Zhou et al., 2011).

The ETS family of transcription factors has previously been implicated as signal-dependent effectors (Wasylyk et al., 1998), but how ETS factors act downstream of VEGF has not been explored in detail. Interestingly, we find that *DLL4* induction by VEGF signaling requires MAPK/ERK signaling, as well as ERG expression. Previous studies in cancer cells revealed that phosphorylation of ERG at S96, S215 and S276 is mediated by ERK2 (Selvaraj et al., 2015). We find that VEGF signaling leads to dynamic ERK-dependent

Development (2017) 144, 2428-2444 doi:10.1242/dev.146050

phosphorylation of ERG at S215, and that S96, S215 and S276 are required for maximal ERG activity. The ability of ERG to drive expression of VEGF target genes appears to be p300 dependent, as VEGF initiates a physical interaction between ERG and p300, and ERG is required for p300 recruitment to *DLL4* and *HLX* enhancer elements. Furthermore, p300/CBP inhibition abolishes VEGF/ERG-dependent gene expression. Mutation of ERK-phosphorylated residues in ERG prevents its interaction with p300, suggesting a role for ERG phosphorylation in recruitment of p300 to target genes. Furthermore, the termination of p300 recruitment temporally coincides with loss of ERG phosphorylation, implying a functional role for these phosphorylation events. It will be of interest to determine whether all DNA-localized ERG, or only those molecules involved in VEGF signaling output, become phosphorylated in response to VEGF signaling. It will also be of interest to determine how diverse activators of MAPK/ERK signaling, which have distinct effects on angiogenesis (e.g. ANG1/TIE2 (ANGPT1/TEK) signaling), might differentially activate ERG. Answering these questions will be vital for the development of targeted therapeutics to suppress angiogenesis. Because ERG regulates vascular integrity (presumably in cells lacking active ERK), it is possible that ERG functions to maintain vascular stability in an ERK-independent manner, suggesting the possibility of selectively blocking angiogenesis through targeting ERG phosphorylation, while maintaining vascular stability. Furthermore, ERG is known to function as an oncogenic fusion protein (e.g. TMPRSS2-ERG) in prostate cancer (Adamo and Ladomery, 2016). Of note, the amino terminus of ERG (included in many of these fusion proteins) appears to contain the same serine residues phosphorylated by ERK2. It will be of interest to determine how upstream signaling pathways (e.g. activated RAS/MAPK/ERK) influence ERG transcriptional activity in cancer. Perhaps targeting ERG phosphorylation could be of interest to quell ERG oncogenic activity.

Previous studies identified a role for another ETS factor, TEL (ETV6), in the repression, rather than the activation, of *DLL4* (Roukens et al., 2010). In this case, TEL bound to the *DLL4* promoter under basal conditions to recruit a co-repressor protein, CTBP. Addition of VEGF led to the rapid disassembly of this repressive complex. The kinetics of this repressive TEL/CTBP complex disassembly are comparable to the assembly of the activating ERG/p300 complex that we report here, suggesting that TEL and ERG dynamically control co-activator/co-repressor recruitment. Recently, VEGF has also been shown to stimulate dynamic exchange of co-repressors for co-activators bound to MEF2 transcription factors (Sacilotto et al., 2016), suggesting that several families of transcription factors may coordinate VEGF-dependent sprouting angiogenesis. Indeed, ETS proteins interact with multiple transcription factor families (Carrère et al., 1998; De Val et al., 2008). Of note, we have identified a number of transcription factor binding motifs that are enriched under ERG ChIP-seq peaks in the vicinity of ERG- and ERG/VEGF-dependent genes that might functionally interact with ERG to control gene expression (Table S3). Although a subset of VEGF inducible genes are regulated by ERG, it is equally important to note that many VEGF-dependent genes are ERG independent. This could be attributable to redundancy of ETS factors, but could also imply that additional transcriptional pathways responsible for angiogenic gene regulation remain to be uncovered.

In summary, our study has identified a VEGF/MAPK/ERK/ERG/p300 network that is required for the induction of a subset of VEGF-inducible genes in ECs, allowing us to propose a model for how transient activation of an angiogenic program might be regulated to orchestrate sprouting (Fig. 9H).

MATERIALS AND METHODS

Zebrafish experiments

Zebrafish protocols were approved by the Animal Care Committee at the University Health Network, the University of Texas MD Anderson Cancer Center and Baylor College of Medicine. The following transgenic lines were utilized: *Tg(kdrl:mCherry)*^{ci5} (Proulx et al., 2010), *Tg(kdrl:GFP)*^{s843} (Jin et al., 2005), *Tg(fli1a:nls-EGFP)*^{y7} (Roman et al., 2002), *Tg(TP1bglob:EGFP)*^{um14} (Parsons et al., 2009) and *Tg(TP1bglob:VenusPEST)*^{S940} (Ninov et al., 2012).

Inhibitor treatments

Embryos were dechorionated, then treated from 18-20 hpf until 26-28 hpf (unless noted otherwise) with the following inhibitors: SU5416 (VEGFR2 inhibitor, 5 µM, LC Laboratories), SL327 (MEK inhibitor, 30 µM, Sigma) or c646 (p300 inhibitor, 3 µM, Sigma), with all inhibitors prepared as 1000× stocks in DMSO, and embryos treated in E3 supplemented with PTU to prevent pigmentation. PMA (Bioshop) was used at a concentration of 1 µM. DMSO (0.1%) was used as a vehicle control. Of note, repeated freeze thaw of c646 stocks diminished efficacy and higher doses of c646 produced serious developmental delay and growth defects (data not shown).

Imaging

See supplementary Materials and Methods for details regarding confocal imaging.

pERK immunofluorescence

Treated *Tg(kdrl:GFP)*^{s843} embryos were processed following the protocol of Inoue and Wittbrodt (2011), with the modifications suggested in Le Guen et al. (2014) (see supplementary Materials and Methods for details).

Time-lapse microscopy

Tg(TP1bglob:VenusPEST); Tg(kdrl:mCherry) animals at 18-20 somites were mounted in 1% low-melt agarose on a four-compartment glass-bottom cell culture dish (Cellview, #627975), treated with PTU and tricaine in E3, along with the same concentration indicated above for either DMSO (vehicle control) or SL327 (MEK inhibitor) (see supplementary Materials and Methods for details).

Isolation of ECs by FACS

Embryos were washed with PBS (without calcium/magnesium) and 1 ml of pre-warmed 0.25% Trypsin was added to the embryos. Embryos were incubated at 28°C and gently pipetted up and down every 5 min until digestion was complete. After digestion, 100 µl of fetal bovine serum (FBS; 100%) was added to stop digestion. The cells were spun at 1100 rpm (300 ***g***) for 5 min at 4°C and the supernatant was removed and the cell pellet was re-suspended in 500 µl of FACS solution (450 µl PBS+50 µl 10% bovine serum albumin). Sytox Red (0.5 µl) was added and the samples were incubated at room temperature for 15 min and then passed through a cell sieve. FACS was performed by the UHN Flow Cytometry Facility using a low differential pressure (20 psi). Cells were sorted directly into RLT buffer (Qiagen) for RNA extraction using the RNeasy Micro Kit (Qiagen).

In situ hybridization

Experiments were performed as described previously (Wythe et al., 2011). Riboprobes, with the exception of *flt4*, were amplified by PCR with primers containing SP6 and T7 overhangs and sense and digoxigenin-labeled antisense probes were synthesized from the PCR template. The *hlx1* template was provided by Dr Saulius Sumanas (Cincinnati Children's Medical Center, OH, USA), *dll4* in pGEM-T was from Dr Jiandong Liu (University of North Carolina, NC, USA), *dusp5* was from GE Dharmacon (Clone ID: 4199935), and *flt4* was from Dr Jeffrey Essner (Iowa State University, IA, USA) (digested with *Eco*RI, transcribed with T7). See supplementary Materials and Methods for primers used.

Enhancer transgenesis

pTol2 enhancer injections were performed as previously published (Wythe et al., 2013). Briefly, an injection mixture consisting of 100 ng of DNA, 125 ng of Tol2 transposase mRNA (Kawakami et al., 2004), 1 µl 0.8% Phenol Red/0.1 M KCl, pH 7.0, and ddH_2O in 10 µl total volume was

Development (2017) 144, 2428-2444 doi:10.1242/dev.146050

combined and 1 nl injected directly into the cell of one-cell stage *Tg(kdrl:mCherry)*^{ci5} zebrafish embryos. Embryos were then maintained at 28.5°C and scored at 42 hpf for enhancer activity within and outside of the vasculature (mCherry^{+}).

Transplantation experiments

Sense-strand-capped mRNA was transcribed using the mMessage mMachine kit (Ambion) from either a pCS2-3xFlag-ERG or pCS2-3xFlag-ERG-3xS→A template (see 'Cloning' in supplementary Materials and Methods for details). mRNA (5 µl of 125 ng/µl) was mixed with 1 µl of 2 mg/ml Alexa 647 10,000 MW, Anionic, Fixable Dextran (Life Technologies, D22914) as a lineage tracer, then 1 nl of this mixture was injected into one-cell stage *Tg(fli1a:nls-EGFP)*^{y7} donor embryos. Dividers were pulled 1-2 h later for *Tg(kdrl:mCherry)*^{ci5} host embryos. Animals were dechorionated on agarose dishes using pronase in E2 media supplemented with penicillin and streptomycin, as suggested by Westerfield (2007). When donor embryos reached approximately sphere stage to 30% epiboly (about 4 hpf), they were transferred to agarose wells (Adaptive Science Tools, PT-1) in E2 plus antibiotics, and 20-40 cells from the lateral margin were transferred from donor to host embryos (at a similar location). Embryos were reared at 28.5°C in 1.5% agarose dishes in E2 supplemented with antibiotics until their fixation in 4% paraformaldehyde (PFA) at 28-30 hpf. See supplementary Materials and Methods for details on imaging. The percentage contribution of donor-derived cells contributing to a location in the host trunk vasculature was quantified as the number of donor-derived cells within the structure divided by the total number of donor-derived cells within the entire vasculature in the region of interest.

Erg murine knockout experiments

Generation of *Erg* knockout mice was carried out by the KOMP consortium (project ID: 48771; *Erg*$^{tm1a(KOMP)Wtsi}$). Cryopreserved sperm were received and *in vitro* fertilization was performed at the Genetically Engineered Mouse (GEM) core at Baylor College of Medicine. In this *Erg*^{tm1a} allele, insertion of a splice acceptor-IRES-lacZ-stop, human beta actin promoter driving Neomycin between exon 5 and 6 acts as a null mutation (i.e. a gene trap) (Fig. S7A). For these studies, a global *Erg* null allele (*Erg*$^{lacZ\Delta NEO/+}$, *Erg*$^{KO/+}$ or *Erg*^{tm1b}) was generated by Cre-mediated removal of the *hBact::Neo* cassette by crossing *Erg*$^{tm1a/+}$ male mice to females harboring a *Tg(ACTB::Cre)* (MGI#2176050) (Lewandoski et al., 1997) driver (see Fig. S7A). To generate a conditional allele (*Erg*$^{flox/+}$ or *Erg*^{tm1c}), an *Erg*$^{tm1a/+}$ male was crossed to a *Tg(ATCB::FlpE)* female (MGI#2448985) (Rodríguez et al., 2000) for Flp-mediated removal of the FRT-flanked promoterless *lacZ* gene trap. The resulting animals, with two *loxP* sites flanking exon 6, were incrossed to generate *Erg*$^{flox/flox}$ animals for postnatal studies (see below). For further details regarding PCR genotyping, see Table S1.

Immunohistochemistry

Timed matings between heterozygous mutant animals (*Erg*$^{KO/+}$) mice were conducted, and noon of the day a vaginal plug was detected was considered day 0.5. Embryos were collected at E10.5, and the yolk sac was used for PCR genotyping of the embryos. Embryos were fixed overnight in 4% PFA then subjected to whole-mount IHC using an endomucin antibody (eBioscience, V.7C7) (1:200); biotinylated goat anti-rat secondary antibody (Vector, BA-9401) (1:250), ABC Elite Kit (Vector Labs, PK-6100) and Alexa 488 Tyramide (Thermo Fisher Scientific, T20948) and imaged by light-sheet microscopy, as previously published (Wang et al., 2016). For frozen sections, embryos were fixed in fresh 4% PFA at 4°C for 20 min, washed in PBS, cryoprotected in 30% sucrose overnight at 4°C, equilibrated in optimal cutting temperature compound (Sakura, #25608) in peel-away molds (Electron Microscopy Sciences, #701081), solidified on dry ice, then stored overnight at −80°C. For additional detail, see supplementary Materials and Methods.

X-gal staining

Whole-mount embryos were processed as detailed previously (Wythe et al., 2013). See supplementary Materials and Methods for further details.

Analysis of FACS-isolated ECs

Embryos were collected at E10.5 (their yolk sac was removed for PCR genotyping) and dissociated to single cells by a 20-min incubation at 37°C in collagenase type I (1 mg/ml) (ThermoFisher Scientific, #17100017). See supplementary Materials and Methods for details. Next, 25,000 live ECs per embryo were collected into 350 µl RLT Buffer (Qiagen) for downstream processing. Total RNA was isolated from sorted cells using the RNAeasy Mini Kit (Qiagen, #74104). RNA was eluted in 30 µl RNAse-free H_2O, and 20 µl of purified RNA was reverse transcribed to cDNA with 5 µl of SuperScript VILO Master Mix (Thermo Fisher Scientific, #11755050). The resulting cDNA was diluted 1:10 with RNAse-free dH_2O, and 4 µl was used for each qPCR reaction (15 µl total reaction volume). qPCR reactions were performed in technical triplicate using iTaq Universal SYBR Green Supermix (Bio-Rad, #1725124) and run on a ViiA 7 Real-Time PCR System (Applied Biosystems). Relative abundance of mRNA transcripts was calculated by normalization to *Gapdh* using the ΔΔCt method (Livak and Schmittgen, 2001). All embryonic RNA samples used for analysis had a deviation no greater than two Cts (range 16-18) for *Gapdh*. For a list of all primers used, see Table S2.

Analysis of retinal vasculature

Erg$^{flox/flox}$ (aka *Erg*$^{tm1c/tm1c}$) females were crossed to *Erg*$^{KO/+}$ (aka *Erg*$^{tm1a/+}$); *Cdh5(PAC)CreERT2* (Wang et al., 2010) males and 30 µl of tamoxifen was administered by subcutaneous injection at a concentration of 10 mg/ml (≈30 µg total per mouse) to their progeny at postnatal days (P) 1 and 3. See supplementary Materials and Methods for details regarding quantification of vascular branching and radial expansion in the retina.

Cell culture

The following cells were utilized for experiments: human umbilical vein endothelial cells (HUVECs, ScienCell), telomerase-immortalized aortic endothelial cells (TeloHAECs, ATCC), dermal microvascular endothelial cells (MVECs, Life Technologies) and bovine aortic endothelial cells (BAECs, Lonza). Cells were cultured according to manufacturer's recommendations. ECs were serum-starved in basal EC media (ScienCell) containing 0.1% FBS and no growth factors for at least 6 h (typically overnight) prior to stimulation with VEGF or PMA. Pathway inhibitors were added 1 h prior to stimulation with VEGF-165 (50 ng/ml, recombinant human protein, R&D Systems or Thermo Fisher Scientific), except for c646, which was added 20 min prior to stimulation. The following inhibitors were used: U0126 (MEK inhibitor, 20 µM, InvivoGen), GF109203X (PKC inhibitor, 5 µM, Tocris Bioscience), LY294002 (PI3K inhibitor, 10 µM, Cell Signaling), SB203580 (p38 inhibitor, 10 µM, Tocris Bioscience), DAPT (γ-secretase inhibitor, 38.5 µM, Sigma) and c646 (p300/CBP inhibitor, 5 µM, Sigma). All drugs were dissolved in DMSO, and comparison was made with vehicle (i.e. DMSO, 0.1%) treated controls. PMA was from BioShop and was used at a concentration of 100 nM.

siRNA experiments

HUVECs were transfected at 30-50% confluency with 40 nM siRNA (Silencer Select, Thermo) targeting the coding region of *ERG* (assay ID: s4813), *ERK1* (*MAPK3*) (assay ID: S230180) or *ERK2* (*MAPK1*) (assay ID: S11138) using RNAiMax (Invitrogen), and cellular assays were performed 48-72 h later. Western blotting and qRT-PCR were used to assess ERG, ERK1 and ERK2 knockdown. Comparison was made with cells transfected with 40 nM Silencer Select negative control #1. For ERG rescue experiments, an independent siRNA recognizing the 3′ untranslated region of *ERG* (40 nM, Silencer Select, custom synthesis) was utilized. After 48-72 h, cells were electroporated using the P5 Primary Cell 4D Nucleofector kit and a Lonza 4D Nucleofector; ∼0.5×10^6 cells were electroporated with 2.5 µg of pCS2 control or pCS2-Flag-ERG expression constructs (wild type and phospho-mutants; see 'Cloning' in supplementary Materials and Methods), and 0.2 µg of pmaxGFP (to assess electroporation efficiency). After 18 h, cells were serum-starved for 6 h prior to VEGF stimulation (1 h) and harvested for RNA/protein analyses.

Cloning

For details regarding cloning of ETS concatamer reporter constructs, *HLX* enhancer reporter constructs and wild-type and mutant ERG expression constructs, please see the supplementary Materials and Methods.

Development (2017) 144, 2428-2444 doi:10.1242/dev.146050

Luciferase experiments

For luciferase assays, BAECs (80% confluent) were transfected with 0.5 µg of luciferase construct (ETS reporter, *HLX* enhancer, see 'Cloning' in supplementary Materials and Methods) and 0.1 µg of pRenilla construct using Lipofectamine 2000 (Invitrogen) (2 µl per 1 µg of plasmid) in 12-well dishes. Cells were treated with cellular signaling pathway inhibitors for 18 h (as above). In some experiments, VEGF (50 ng/ml) was added to OptiMEM medium for 18 h. After 24 h, dual luciferase (*Renilla* and firefly) was measured using a GloMax20/20 Luminometer (Promega).

Western blotting and co-immunoprecipitation

Western blotting was performed as before (Fish et al., 2011) using the following antibodies: anti-pERK1/2 (Thr202/Tyr204, rabbit polyclonal, Cell Signaling, #9101; 1:1000), anti-ERK2 (mouse monoclonal, Santa Cruz, D-2; 1:500), anti-ERK1/2 (rabbit monoclonal, Cell Signaling, clone 137F5; 1:500), anti-DLL4 (rabbit polyclonal, Cell Signaling, #2589; 1:1000), anti-GAPDH (mouse monoclonal, Santa Cruz, #0411; 1:500), anti-ERG (rabbit polyclonal, Santa Cruz, C-20 or mouse monoclonal antibody, BioCare Medical, 9FY; 1:1000), anti-pERG^{S215} [rabbit polyclonal, a kind gift from Peter Hollenhorst, Indiana University, IN, USA (Selvaraj et al., 2015); 1:500], anti-p300 (rabbit polyclonal, Santa Cruz, C-20; 1:200). All antibodies have been previously validated. See supplementary Materials and Methods for details regarding pERG western blots and co-immunoprecipitation experiments.

Immunofluorescence on cultured cells

HUVECs were plated on Permanox eight-well chamber slides. Following stimulation with VEGF, cells were fixed with 4% PFA followed by permeabilization with 0.25% Triton X-100. Staining with anti-pERK (rabbit polyclonal, Cell Signaling, #9101, 1:500) was performed overnight at 4°C, followed by addition of a secondary antibody (anti-rabbit Alexa Fluor647, Cell Signaling #4414). Slides were mounted using Vectashield mounting medium with DAPI (Vector Labs H-1200) and imaged using an Olympus FV1000 confocal microscope.

RNA isolation, reverse transcription and quantitative PCR

RNA was isolated from cells and zebrafish using Trizol and reverse transcription was performed using a high-capacity cDNA reverse transcription kit (Applied Biosystems). qRT-PCR was performed using a Roche Lightcycler 480 with LC 480 SYBR Green I Master Mix (Roche). Data were normalized to TATA-box binding protein (*TBP*) or *Gapdh* using the ΔΔCt method. For further details regarding primer sequences, see Table S2.

Gene expression array

HUVECs were transfected with control or *ERG* siRNA and after 48 h the cells were serum-starved overnight and cells were then left unstimulated or were treated with 50 ng/ml VEGF for 1 h. RNA was isolated from four independent experiments using Trizol and analyzed on Agilent microarray, performed at the Princess Margaret Genomics Centre. See supplementary Materials and Methods for details regarding microarray processing and analysis.

Gene ontology analysis

Differentially expressed genes were submitted to the Database for Annotation, Visualization and Integrated Discovery (DAVID) bioinformatics resource (https://david-d.ncifcrf.gov/home.jsp) to be classified into gene ontology (GO) annotation groups (Ashburner et al., 2000; Huang et al., 2009). Fisher's exact test was applied to identify significant GO categories. Select representative GO categories are included in figures.

ChIP-qPCR experiments

ChIP was performed as before (Wythe et al., 2013), using the Imprint ChIP kit (Sigma) or the Magna ChIP A/G kit (Millipore). HUVECs were serum-starved overnight prior to stimulation with 50 ng/ml VEGF for 15′, 30′ or 2 h. Following fixation and shearing of chromatin, immunoprecipitation was performed overnight at 4°C using 1 µg (or 1 µl) of antibodies to ERG (rabbit polyclonal, Santa Cruz, C-20), p300 (rabbit polyclonal, Santa Cruz, C-20) or H3K27ac (rabbit polyclonal, Abcam, ab4729). Mouse IgG (Sigma) was used as a non-specific background control. qPCR was performed using primers that amplified the *DLL4* intron 3 enhancer or an enhancer upstream of *HLX* (see Table S2 for primer sequences). IP DNA was calculated by subtracting the IgG value from the specific antibody value and dividing by a diluted input sample. In some experiments, control or *ERG* siRNAs were transfected into HUVECs 48 h prior to stimulation with VEGF (15′), followed by p300 ChIP.

ChIP-seq experiments and analysis

Primary HUVECs and BAEC cells were grown in supplier-recommended EC Growth Media (ScienCell) and cultured at 37°C in a 5%-CO_2 humidified incubator. Approximately 20 million cells were used for the ERG and ∼3 million cells for the H3K27ac ChIPs. ChIP experiments were conducted as previously described (Ballester et al., 2014). Antibodies used for ChIP were mouse anti-H3K27ac (Millipore, 05-1334 monoclonal) and rabbit anti-ERG 1/2/3 (Santa Cruz Biotechnology, sc353 polyclonal). Two replicates were performed. See supplementary Materials and Methods for details regarding processing and analysis of ChIP-seq experiments.

CRISPR/Cas9-mediated *HLX* enhancer deletion

The *HLX* enhancer region to be targeted for deletion was defined by H3K27ac ChIP-seq enhancer marks (∼1200 bp). The MIT CRISPR/Cas9 design tool (http://crispr.mit.edu/) was used to generate gRNAs targeting the 5′ and 3′ boundaries of the *HLX* enhancer. Two scrambled sequence gRNAs were used as controls. For further details, see the supplementary Materials and Methods.

Statistical analyses

Unless otherwise stated, all experiments were performed a minimum of three times and data represent the mean±s.e.m. Statistical analyses were performed using a Student's *t*-test (for two groups) or ANOVA (for more than two groups), followed by the Newman–Keuls post-hoc test. $P<0.05$ was considered statistically significant. In all figures, $*P<0.05$, $**P<0.01$ and $***P<0.001$.

Acknowledgements

The authors thank the Optical Imaging and Vital Microscopy (OIVM) Core at BCM for support with imaging and data processing; Dr Neil I. Bower (The University of Queensland, Dr Benjamin M. Hogan laboratory) for advice and suggestions regarding pERK staining; Dr Peter Hollenhorst for providing an antibody to phosphorylated ERG and for advice on ERG immunoprecipitation; Dr Jiandong Liu and Ms Nicole Fleming (UNC Chapel Hill) for suggestions on transplantation experiments; and Mrs Karen Berman de Ruiz for excellent mouse husbandry care and colony management.

Competing interests

The authors declare no competing or financial interests.

Author contributions

Conceptualization: J.E.F., J.D.W.; Methodology: J.E.F., M.C.G., L.T.D., L.A., G.T.E., M.D.W., J.D.W.; Software: L.A., A.M.-R., M.D.W.; Validation: J.E.F., M.C.G., N.K., Z.C., S.V., H.S.C., M.K., L.A., M.-S.N., E.B., O.E.R., A.M.-R., M.D.W., J.D.W.; Formal analysis: J.E.F., M.C.G., L.T.D., N.K., Z.C., S.V., H.S.C., M.K., L.A., M.-S.N., E.B., A.M.H., A.M.R., O.E.R., A.M.-R., M.D.W., J.D.W.; Investigation: J.E.F., M.C.G., L.T.D., N.K., Z.C., S.V., H.S.C., M.K., L.A., M.-S.N., E.B., A.M.H., A.M.R., O.E.R., G.T.E., A.M.-R., M.D.W., J.D.W.; Resources: J.E.F., G.T.E., M.D.W., J.D.W.; Data curation: J.E.F., M.C.G., L.T.D., L.A., A.M.-R., M.D.W., J.D.W.; Writing - original draft: J.E.F., J.D.W.; Writing - review & editing: J.E.F., M.C.G., O.E.R., G.T.E., A.M.-R., M.D.W., J.D.W.; Visualization: J.E.F., M.C.G., E.B., A.M.H., A.M.R., O.E.R., G.T.E., J.D.W.; Supervision: J.E.F., G.T.E., M.D.W., J.D.W.; Project administration: J.E.F., G.T.E., J.D.W.; Funding acquisition: J.E.F., G.T.E., M.D.W., J.D.W.

Funding

J.E.F. was funded by an operating grant from the Canadian Institutes of Health Research (CIHR) (MOP-119506), and a Leaders Opportunity Fund/Canada Foundation for Innovation equipment grant (26422). J.E.F. and M.D.W. were supported by Early Researcher Awards from the Ontario Ministry of Research and Innovation, Canada Research Chairs from CIHR, and a Team Project Award from the University of Toronto's Medicine by Design initiative, which receives funding from

the Canada First Research Excellence Fund. L.T.D. was supported by a post-doctoral fellowship from the Toronto General Hospital Research Institute, N.K. was supported by a Canada Graduate Studentship from the Natural Sciences and Engineering Research Council of Canada. M.S.N. was supported by a Vascular Network Scholar Award (CIHR funded). H.S.C. was supported by an Ontario Graduate Student award. ChIP-seq and bioinformatics work was supported by the Natural Sciences and Engineering Research Council of Canada (NSERC) (436194-2013 to M.D.W.). L.A. was supported by an Alexander Graham Bell Canada Graduate Scholarship; and A.M.-R. was supported by a CONACYT fellowship (203853) and a CIHR STAGE fellowship. A.M.-R.'s laboratory is supported by a CONACYT grant (269449) and a Programa de Apoyo a Proyectos de investigación e innovación tecnológica - Universidad Nacional Autónoma de México (PAPIIT-UNAM) grant (IA206517). G.T.E. was supported by a Cancer Prevention and Research Institute of Texas (CPRIT) First-Time Tenure-Track Faculty Recruitment Award (RR140077). This project was supported by the Cytometry and Cell Sorting Core at Baylor College of Medicine with funding from the National Institutes of Health (CA125123 and RR024574). A.M.H. was supported by a Molecular Physiology of the Cardiovascular System Training Grant, The National Institutes of Health (T32HL07676). J.D.W. was supported by institutional startup funds from the CVRI at Baylor College of Medicine, the Caroline Wiess Law Fund, the Curtis Hankamer Basic Research Fund, and the ARCO Foundation Young Teacher-Investigator Award. Work within the Wythe lab is supported by the American Heart Association (16GRNT31330023). Deposited in PMC for release after 12 months.

Data availability

All microarray and ChIP-seq data have been made publicly available. Microarray data were submitted to ArrayExpress (accession number: E-MTAB-5207). ERG and H3K27ac ChIP-seq data from HUVEC and ERG ChIP-seq data from BAEC were submitted to ArrayExpress (accession number: E-MTAB-5148). We also utilized HUVEC H3K4me3 ChIP-seq data (pooled signal from biological replicates, ENCODE accession numbers: ENCFF000BTS, ENCFF000BTL) and HUVEC H3K4me1 ChIP-seq data (pooled signal from biological replicates, ENCODE accession numbers: ENCFF000BTD, ENCFF000BSY, ENCFF000BSX) from the Encyclopedia of DNA Elements Consortium (ENCODE Project Consortium, 2012). Vertebrate conservation across 100 genomes was extracted from UCSC Genome Browser.

Supplementary information

Supplementary information available online at
http://dev.biologists.org/lookup/doi/10.1242/dev.146050.supplemental

References

Adamo, P. and Ladomery, M. R. (2016). The oncogene ERG: a key factor in prostate cancer. *Oncogene* **35**, 403-414.

Al-Greene, N. T., Means, A. L., Lu, P., Jiang, A., Schmidt, C. R., Chakravarthy, A. B., Merchant, N. B., Washington, M. K., Zhang, B., Shyr, Y. et al. (2013). Four jointed box 1 promotes angiogenesis and is associated with poor patient survival in colorectal carcinoma. *PLoS ONE* **8**, e69660.

Ashburner, M., Ball, C. A., Blake, J. A., Botstein, D., Butler, H., Cherry, J. M., Davis, A. P., Dolinski, K., Dwight, S. S., Eppig, J. T. et al. (2000). Gene ontology: tool for the unification of biology. The Gene Ontology Consortium. *Nat. Genet.* **25**, 25-29.

Ballester, B., Medina-Rivera, A., Schmidt, D., Gonzàlez-Porta, M., Carlucci, M., Chen, X., Chessman, K., Faure, A. J., Funnell, A. P., Goncalves, A. et al. (2014). Multi-species, multi-transcription factor binding highlights conserved control of tissue-specific biological pathways. *Elife* **3**, e02626.

Bellou, S., Hink, M. A., Bagli, E., Panopoulou, E., Bastiaens, P. I. H., Murphy, C. and Fotsis, T. (2009). VEGF autoregulates its proliferative and migratory ERK1/2 and p38 cascades by enhancing the expression of DUSP1 and DUSP5 phosphatases in endothelial cells. *Am. J. Physiol. Cell Physiol.* **297**, C1477-C1489.

Birdsey, G. M., Dryden, N. H., Amsellem, V., Gebhardt, F., Sahnan, K., Haskard, D. O., Dejana, E., Mason, J. C. and Randi, A. M. (2008). Transcription factor Erg regulates angiogenesis and endothelial apoptosis through VE-cadherin. *Blood* **111**, 3498-3506.

Birdsey, G. M., Dryden, N. H., Shah, A. V., Hannah, R., Hall, M. D., Haskard, D. O., Parsons, M., Mason, J. C., Zvelebil, M., Gottgens, B. et al. (2012). The transcription factor Erg regulates expression of histone deacetylase 6 and multiple pathways involved in endothelial cell migration and angiogenesis. *Blood* **119**, 894-903.

Birdsey, G. M., Shah, A. V., Dufton, N., Reynolds, L. E., Osuna Almagro, L., Yang, Y., Aspalter, I. M., Khan, S. T., Mason, J. C., Dejana, E. et al. (2015). The endothelial transcription factor ERG promotes vascular stability and growth through Wnt/beta-catenin signaling. *Dev. Cell* **32**, 82-96.

Blanco, R. and Gerhardt, H. (2013). VEGF and Notch in tip and stalk cell selection. *Cold Spring Harb. Perspect. Med.* **3**, a006569.

Bowers, E. M., Yan, G., Mukherjee, C., Orry, A., Wang, L., Holbert, M. A., Crump, N. T., Hazzalin, C. A., Liszczak, G., Yuan, H. et al. (2010). Virtual ligand screening of the p300/CBP histone acetyltransferase: identification of a selective small molecule inhibitor. *Chem. Biol.* **17**, 471-482.

Carmeliet, P., Ferreira, V., Breier, G., Pollefeyt, S., Kieckens, L., Gertsenstein, M., Fahrig, M., Vandenhoeck, A., Harpal, K., Eberhardt, C. et al. (1996). Abnormal blood vessel development and lethality in embryos lacking a single VEGF allele. *Nature* **380**, 435-439.

Carrère, S., Verger, A., Flourens, A., Stehelin, D. and Duterque-Coquillaud, M. (1998). Erg proteins, transcription factors of the Ets family, form homo, heterodimers and ternary complexes via two distinct domains. *Oncogene* **16**, 3261-3268.

Costa, G., Harrington, K. I., Lovegrove, H. E., Page, D. J., Chakravartula, S., Bentley, K. and Herbert, S. P. (2016). Asymmetric division coordinates collective cell migration in angiogenesis. *Nat. Cell Biol.* **18**, 1292-1301.

De Val, S., Chi, N. C., Meadows, S. M., Minovitsky, S., Anderson, J. P., Harris, I. S., Ehlers, M. L., Agarwal, P., Visel, A., Xu, S.-M. et al. (2008). Combinatorial regulation of endothelial gene expression by ets and forkhead transcription factors. *Cell* **135**, 1053-1064.

ENCODE Project Consortium. (2012). An integrated encyclopedia of DNA elements in the human genome. *Nature* **489**, 57-74.

Ferrara, N., Carver-Moore, K., Chen, H., Dowd, M., Lu, L., O'Shea, K. S., Powell-Braxton, L., Hillan, K. J. and Moore, M. W. (1996). Heterozygous embryonic lethality induced by targeted inactivation of the VEGF gene. *Nature* **380**, 439-442.

Fish, J. E., Wythe, J. D., Xiao, T., Bruneau, B. G., Stainier, D. Y. R., Srivastava, D. and Woo, S. (2011). A Slit/miR-218/Robo regulatory loop is required during heart tube formation in zebrafish. *Development* **138**, 1409-1419.

Foulds, C. E., Nelson, M. L., Blaszczak, A. G. and Graves, B. J. (2004). Ras/mitogen-activated protein kinase signaling activates Ets-1 and Ets-2 by CBP/p300 recruitment. *Mol. Cell. Biol.* **24**, 10954-10964.

Franklin, R. A., Tordai, A., Patel, H., Gardner, A. M., Johnson, G. L. and Gelfand, E. W. (1994). Ligation of the T cell receptor complex results in activation of the Ras/Raf-1/MEK/MAPK cascade in human T lymphocytes. *J. Clin. Invest.* **93**, 2134-2140.

Gory, S., Dalmon, J., Prandini, M. H., Kortulewski, T., de Launoit, Y. and Huber, P. (1998). Requirement of a GT box (Sp1 site) and two Ets binding sites for vascular endothelial cadherin gene transcription. *J. Biol. Chem.* **273**, 6750-6755.

Guarani, V., Deflorian, G., Franco, C. A., Krüger, M., Phng, L.-K., Bentley, K., Toussaint, L., Dequiedt, F., Mostoslavsky, R., Schmidt, M. H. H. et al. (2011). Acetylation-dependent regulation of endothelial Notch signalling by the SIRT1 deacetylase. *Nature* **473**, 234-238.

Hellström, M., Phng, L.-K., Hofmann, J. J., Wallgard, E., Coultas, L., Lindblom, P., Alva, J., Nilsson, A.-K., Karlsson, L., Gaiano, N. et al. (2007). Dll4 signalling through Notch1 regulates formation of tip cells during angiogenesis. *Nature* **445**, 776-780.

Herbert, S. P. and Stainier, D. Y. R. (2011). Molecular control of endothelial cell behaviour during blood vessel morphogenesis. *Nat. Rev. Mol. Cell Biol.* **12**, 551-564.

Herbert, S. P., Cheung, J. Y. M. and Stainier, D. Y. R. (2012). Determination of endothelial stalk versus tip cell potential during angiogenesis by H2.0-like homeobox-1. *Curr. Biol.* **22**, 1789-1794.

Huang, D. W., Sherman, B. T. and Lempicki, R. A. (2009). Systematic and integrative analysis of large gene lists using DAVID bioinformatics resources. *Nat. Protoc.* **4**, 44-57.

Iaccarino, G., Ciccarelli, M., Sorriento, D., Galasso, G., Campanile, A., Santulli, G., Cipolletta, E., Cerullo, V., Cimini, V., Altobelli, G. G. et al. (2005). Ischemic neoangiogenesis enhanced by beta2-adrenergic receptor overexpression: a novel role for the endothelial adrenergic system. *Circ. Res.* **97**, 1182-1189.

Inoue, D. and Wittbrodt, J. (2011). One for all–a highly efficient and versatile method for fluorescent immunostaining in fish embryos. *PLoS ONE* **6**, e19713.

Jakobsson, L., Franco, C. A., Bentley, K., Collins, R. T., Ponsioen, B., Aspalter, I. M., Rosewell, I., Busse, M., Thurston, G., Medvinsky, A. et al. (2010). Endothelial cells dynamically compete for the tip cell position during angiogenic sprouting. *Nat. Cell Biol.* **12**, 943-953.

Jin, S.-W., Beis, D., Mitchell, T., Chen, J. N. and Stainier, D. Y. (2005). Cellular and molecular analyses of vascular tube and lumen formation in zebrafish. *Development* **132**, 5199-5209.

Kawakami, K., Takeda, H., Kawakami, N., Kobayashi, M., Matsuda, N. and Mishina, M. (2004). A transposon-mediated gene trap approach identifies developmentally regulated genes in zebrafish. *Dev. Cell* **7**, 133-144.

Kim, K. J., Li, B., Winer, J., Armanini, M., Gillett, N., Phillips, H. S. and Ferrara, N. (1993). Inhibition of vascular endothelial growth factor-induced angiogenesis suppresses tumour growth in vivo. *Nature* **362**, 841-844.

Kucharska, A., Rushworth, L. K., Staples, C., Morrice, N. A. and Keyse, S. M. (2009). Regulation of the inducible nuclear dual-specificity phosphatase DUSP5 by ERK MAPK. *Cell. Signal.* **21**, 1794-1805.

Le Guen, L., Karpanen, T., Schulte, D., Harris, N. C., Koltowska, K., Roukens, G., Bower, N. I., van Impel, A., Stacker, S. A., Achen, M. G. et al. (2014). Ccbe1

regulates Vegfc-mediated induction of Vegfr3 signaling during embryonic lymphangiogenesis. *Development* **141**, 1239-1249.
Lee, S., Chen, T. T., Barber, C. L., Jordan, M. C., Murdock, J., Desai, S., Ferrara, N., Nagy, A., Roos, K. P. and Iruela-Arispe, M. L. (2007). Autocrine VEGF signaling is required for vascular homeostasis. *Cell* **130**, 691-703.
Lewandoski, M., Meyers, E. N. and Martin, G. R. (1997). Analysis of Fgf8 gene function in vertebrate development. *Cold Spring Harb. Symp. Quant. Biol.* **62**, 159-168.
Liu, F. and Patient, R. (2008). Genome-wide analysis of the zebrafish ETS family identifies three genes required for hemangioblast differentiation or angiogenesis. *Circ. Res.* **103**, 1147-1154.
Liu, D., Evans, I., Britton, G. and Zachary, I. (2008). The zinc-finger transcription factor, early growth response 3, mediates VEGF-induced angiogenesis. *Oncogene* **27**, 2989-2998.
Livak, K. J. and Schmittgen, T. D. (2001). Analysis of relative gene expression data using real-time quantitative PCR and the 2(-Delta Delta C(T)) Method. *Methods* **25**, 402-408.
Lobov, I. B., Renard, R. A., Papadopoulos, N., Gale, N. W., Thurston, G., Yancopoulos, G. D. and Wiegand, S. J. (2007). Delta-like ligand 4 (Dll4) is induced by VEGF as a negative regulator of angiogenic sprouting. *Proc. Natl. Acad. Sci. USA* **104**, 3219-3224.
Mirza, M. A., Capozzi, L. A., Xu, Y., McCullough, L. D. and Liu, F. (2013). Knockout of vascular early response gene worsens chronic stroke outcomes in neonatal mice. *Brain Res. Bull.* **98**, 111-121.
Moehler, T. M., Sauer, S., Witzel, M., Andrulis, M., Garcia-Vallejo, J. J., Grobholz, R., Willhauck-Fleckenstein, M., Greiner, A., Goldschmidt, H. and Schwartz-Albiez, R. (2008). Involvement of alpha 1-2-fucosyltransferase I (FUT1) and surface-expressed Lewis(y) (CD174) in first endothelial cell-cell contacts during angiogenesis. *J. Cell. Physiol.* **215**, 27-36.
Nicoli, S., Knyphausen, C.-P., Zhu, L. J., Lakshmanan, A. and Lawson, N. D. (2012). miR-221 is required for endothelial tip cell behaviors during vascular development. *Dev. Cell* **22**, 418-429.
Ninov, N., Borius, M. and Stainier, D. Y. R. (2012). Different levels of Notch signaling regulate quiescence, renewal and differentiation in pancreatic endocrine progenitors. *Development* **139**, 1557-1567.
Olsson, A.-K., Dimberg, A., Kreuger, J. and Claesson-Welsh, L. (2006). VEGF receptor signalling - in control of vascular function. *Nat. Rev. Mol. Cell Biol.* **7**, 359-371.
Parsons, M. J., Pisharath, H., Yusuff, S., Moore, J. C., Siekmann, A. F., Lawson, N. and Leach, S. D. (2009). Notch-responsive cells initiate the secondary transition in larval zebrafish pancreas. *Mech. Dev.* **126**, 898-912.
Pham, V. N., Lawson, N. D., Mugford, J. W., Dye, L., Castranova, D., Lo, B. and Weinstein, B. M. (2007). Combinatorial function of ETS transcription factors in the developing vasculature. *Dev. Biol.* **303**, 772-783.
Phng, L.-K., Potente, M., Leslie, J. D., Babbage, J., Nyqvist, D., Lobov, I., Ondr, J. K., Rao, S., Lang, R. A., Thurston, G. et al. (2009). Nrarp coordinates endothelial Notch and Wnt signaling to control vessel density in angiogenesis. *Dev. Cell* **16**, 70-82.
Pin, A.-L., Houle, F., Guillonneau, M., Paquet, E. R., Simard, M. J. and Huot, J. (2012). miR-20a represses endothelial cell migration by targeting MKK3 and inhibiting p38 MAP kinase activation in response to VEGF. *Angiogenesis* **15**, 593-608.
Prahst, C., Kasaai, B., Moraes, F., Jahnsen, E. D., Larrivee, B., Villegas, D., Pardanaud, L., Pibouin-Fragner, L., Zhang, F., Zaun, H. C. et al. (2014). The H2.0-like homeobox transcription factor modulates yolk sac vascular remodeling in mouse embryos. *Arterioscler. Thromb. Vasc. Biol.* **34**, 1468-1476.
Proulx, K., Lu, A. and Sumanas, S. (2010). Cranial vasculature in zebrafish forms by angioblast cluster-derived angiogenesis. *Dev. Biol.* **348**, 34-46.
Randi, A. M., Sperone, A., Dryden, N. H. and Birdsey, G. M. (2009). Regulation of angiogenesis by ETS transcription factors. *Biochem. Soc. Trans.* **37**, 1248-1253.
Rodríguez, C. I., Buchholz, F., Galloway, J., Sequerra, R., Kasper, J., Ayala, R., Stewart, A. F. and Dymecki, S. M. (2000). High-efficiency deleter mice show that FLPe is an alternative to Cre-loxP. *Nat. Genet.* **25**, 139-140.
Roman, B. L., Pham, V. N., Lawson, N. D., Kulik, M., Childs, S., Lekven, A. C., Garrity, D. M., Moon, R. T., Fishman, M. C., Lechleider, R. J. et al. (2002). Disruption of acvrl1 increases endothelial cell number in zebrafish cranial vessels. *Development* **129**, 3009-3019.
Roukens, M. G., Alloul-Ramdhani, M., Baan, B., Kobayashi, K., Peterson-Maduro, J., van Dam, H., Schulte-Merker, S. and Baker, D. A. (2010). Control of endothelial sprouting by a Tel-CtBP complex. *Nat. Cell Biol.* **12**, 933-942.
Sacilotto, N., Monteiro, R., Fritzsche, M., Becker, P. W., Sanchez-Del-Campo, L., Liu, K., Pinheiro, P., Ratnayaka, I., Davies, B., Goding, C. R. et al. (2013). Analysis of Dll4 regulation reveals a combinatorial role for Sox and Notch in arterial development. *Proc. Natl. Acad. Sci. USA* **110**, 11893-11898.
Sacilotto, N., Chouliaras, K. M., Nikitenko, L. L., Lu, Y. W., Fritzsche, M., Wallace, M. D., Nornes, S., García-Moreno, F., Payne, S., Bridges, E. et al. (2016). MEF2 transcription factors are key regulators of sprouting angiogenesis. *Genes Dev.* **30**, 2297-2309.
Schultz, H., Engel, K. and Gaestel, M. (1997). PMA-induced activation of the p42/44ERK- and p38RK-MAP kinase cascades in HL-60 cells is PKC dependent but not essential for differentiation to the macrophage-like phenotype. *J. Cell. Physiol.* **173**, 310-318.
Schweighofer, B., Testori, J., Sturtzel, C., Sattler, S., Mayer, H., Wagner, O., Bilban, M. and Hofer, E. (2009). The VEGF-induced transcriptional response comprises gene clusters at the crossroad of angiogenesis and inflammation. *Thromb. Haemost.* **102**, 544-554.
Seidel, J. J. and Graves, B. J. (2002). An ERK2 docking site in the Pointed domain distinguishes a subset of ETS transcription factors. *Genes Dev.* **16**, 127-137.
Selvaraj, N., Kedage, V. and Hollenhorst, P. C. (2015). Comparison of MAPK specificity across the ETS transcription factor family identifies a high-affinity ERK interaction required for ERG function in prostate cells. *Cell Commun. Signal.* **13**, 12.
Sharrocks, A. D. (2001). The ETS-domain transcription factor family. *Nat. Rev. Mol. Cell Biol.* **2**, 827-837.
Shin, M., Beane, T., Quillien, A., Male, I., Zhu, L. J. and Lawson, N. D. (2016). Vegfa signals through ERK to promote angiogenesis, but not artery differentiation. *Development.* **143**, 3796-3805.
Suchting, S., Freitas, C., le Noble, F., Benedito, R., Breant, C., Duarte, A. and Eichmann, A. (2007). The Notch ligand Delta-like 4 negatively regulates endothelial tip cell formation and vessel branching. *Proc. Natl. Acad. Sci. USA* **104**, 3225-3230.
Testori, J., Schweighofer, B., Helfrich, I., Sturtzel, C., Lipnik, K., Gesierich, S., Nasarre, P., Hofer-Warbinek, R., Bilban, M., Augustin, H. G. et al. (2011). The VEGF-regulated transcription factor HLX controls the expression of guidance cues and negatively regulates sprouting of endothelial cells. *Blood* **117**, 2735-2744.
Toffoli, S., Delaive, E., Dieu, M., Feron, O., Raes, M. and Michiels, C. (2009). NDRG1 and CRK-I/II are regulators of endothelial cell migration under Intermittent Hypoxia. *Angiogenesis* **12**, 339-354.
Ubezio, B., Blanco, R. A., Geudens, I., Stanchi, F., Mathivet, T., Jones, M. L., Ragab, A., Bentley, K. and Gerhardt, H. (2016). Synchronization of endothelial Dll4-Notch dynamics switch blood vessels from branching to expansion. *Elife* **5**, e12167.
Vijayaraj, P., Le Bras, A., Mitchell, N., Kondo, M., Juliao, S., Wasserman, M., Beeler, D., Spokes, K., Aird, W. C., Baldwin, H. S. et al. (2012). Erg is a crucial regulator of endocardial-mesenchymal transformation during cardiac valve morphogenesis. *Development* **139**, 3973-3985.
Wang, Y., Nakayama, M., Pitulescu, M. E., Schmidt, T. S., Bochenek, M. L., Sakakibara, A., Adams, S., Davy, A., Deutsch, U., Lüthi, U. et al. (2010). Ephrin-B2 controls VEGF-induced angiogenesis and lymphangiogenesis. *Nature* **465**, 483-486.
Wang, J., Xiao, Y., Hsu, C.-W., Martinez-Traverso, I. M., Zhang, M., Bai, Y., Ishii, M., Maxson, R. E., Olson, E. N., Dickinson, M. E. et al. (2016). Yap and Taz play a crucial role in neural crest-derived craniofacial development. *Development* **143**, 504-515.
Wasylyk, B., Hagman, J. and Gutierrez-Hartmann, A. (1998). Ets transcription factors: nuclear effectors of the Ras-MAP-kinase signaling pathway. *Trends Biochem. Sci.* **23**, 213-216.
Westerfield, M. (2007). *The Zebrafish Book. A guide for the Laboratory Use of Zebrafish (Danio rerio)*, 5th edn. Eugene: University of Oregon Press.
Wythe, J. D., Jurynec, M. J., Urness, L. D., Jones, C. A., Sabeh, M. K., Werdich, A. A., Sato, M., Yost, H. J., Grunwald, D. J., MacRae, C. A. et al. (2011). Hadp1, a newly identified pleckstrin homology domain protein, is required for cardiac contractility in zebrafish. *Dis. Model. Mech.* **4**, 607-621.
Wythe, J. D., Dang, L. T. H., Devine, W. P., Boudreau, E., Artap, S. T., He, D., Schachterle, W., Stainier, D. Y. R., Oettgen, P., Black, B. L. et al. (2013). ETS factors regulate Vegf-dependent arterial specification. *Dev. Cell* **26**, 45-58.
Yordy, J. S. and Muise-Helmericks, R. C. (2000). Signal transduction and the Ets family of transcription factors. *Oncogene* **19**, 6503-6513.
Yuan, L., Sacharidou, A., Stratman, A. N., Le Bras, A., Zwiers, P. J., Spokes, K., Bhasin, M., Shih, S.-C., Nagy, J. A., Molema, G. et al. (2011). RhoJ is an endothelial cell-restricted Rho GTPase that mediates vascular morphogenesis and is regulated by the transcription factor ERG. *Blood* **118**, 1145-1153.
Yuan, L., Le Bras, A., Sacharidou, A., Itagaki, K., Zhan, Y., Kondo, M., Carman, C. V., Davis, G. E., Aird, W. C. and Oettgen, P. (2012). ETS-related gene (ERG) controls endothelial cell permeability via transcriptional regulation of the claudin 5 (CLDN5) gene. *J. Biol. Chem.* **287**, 6582-6591.
Zhang, B., Day, D. S., Ho, J. W., Song, L., Cao, J., Christodoulou, D., Seidman, J. G., Crawford, G. E., Park, P. J. and Pu, W. T. (2013). A dynamic H3K27ac signature identifies VEGFA-stimulated endothelial enhancers and requires EP300 activity. *Genome Res.* **23**, 917-927.
Zhou, N., Zhao, W.-D., Liu, D.-X., Liang, Y., Fang, W.-G., Li, B. and Chen, Y.-H. (2011). Inactivation of EphA2 promotes tight junction formation and impairs angiogenesis in brain endothelial cells. *Microvasc. Res.* **82**, 113-121.

Supplementary Materials and Methods:

Zebrafish Experiments:

Imaging inhibitor-treated embryos − 28-30 hpf embryos were fixed overnight, then mounted in low melt agarose the following day, and somites 7-12 were imaged (20X objective, NA=0.8, laser power=20%, pinhole = 182 µm, 32 µm step size, 16 total slices) using a LSM780 microscope and ZenPro imaging software. Intersomitic vessel length was measured using the Distance Tracking function in ZenPro.

pERK immunostaining − Briefly, embryos were fixed in freshly made 4% PFA / PBS / 0.1% Tween-20 overnight at 4°C, then dehydrated to absolute methanol at 4°C. Endogenous peroxidase activity was quenched by incubation in 3% H_2O_2 / 97% methanol at 4°C for 1 h, then embryos were washed extensively in methanol and stored for at least 2 days at -20°C. Embryos were then rehydrated to PBS / 0.1% Tween-20 (PBST), and cryoprotected in PBST / 30% sucrose overnight at 4°C. The following day, embryos were equilibrated for 5 min in 150 mM Tris-HCl (pH 9.0) at room temperature (RT), then this was replaced with 70°C 150 mM Tris-HCl (pH 9.0) and the embryos were maintained at this temperature for 15 min for antigen retrieval. After cooling to RT, embryos were washed in PBST, rinsed multiple times in ddH_2O, then incubated in acetone at -20°C for 20 min. Embryos were then washed in PBST at RT, transferred to TBS / 0.1% Tween-20 / 0.1% Triton X-100 (TBSTx), then blocked (TBST / 0.8% Triton X-100 / 1% BSA / 10% goat serum) overnight at 4°C. The next day embryos were incubated with anti-phospho ERK antibody (phospho-p44/42 MAPK (Thr202/Tyr204) XP rabbit monoclonal antibody, Cell Signaling Technologies, #4370) (1:250) in TBST / 0.8% Triton X-100 / 1% BSA / 1% goat serum overnight at 4°C for 3 days. Embryos were then washed extensively in TBSTx, then washed in maleic acid buffer (150 mM maleic acid (pH 7.4) / 100 mM NaCl / 0.001% Tween-20) (MABT), then incubated in HRP-conjugated goat anti-rabbit IgG secondary antibody (Jackson ImmunoResearch, 111-035-144) (1:1,000) in 2% Blocking Reagent (Sigma,

11096176001) / MABT overnight at 4°C for 2 days. Embryos were washed in 2% blocking reagent / MABT at RT, washed in MABT, transferred to PBS, then incubated (upright, rocking) in 150 µL of Alexa-568 TSA reagent (Life Technologies, T20950) (1:50) for 3 h in the dark at RT. Embryos were washed extensively in TBSTx, then blocked in TBSTx / 10% goat serum / 1% BSA for 1 h at RT, and incubated with rat anti-GFP (Chromotek, 3h9) (1:500) overnight 4°C in TBST / 0.5% Triton X-100 / 1% goat serum / 1% BSA, washed in TBST / 0.5% Triton X-100, washed in TBSTx, then incubated with Alexa-488 conjugated goat anti-Rat IgG (Life Technologies, A11006) (1:250) overnight at 4°C. Embryos were then washed extensively, briefly post-fixed in 4% PFA, washed in PBS, then mounted in low-melt agarose for confocal analysis. Embryos without primary pERK antibody were always included as a negative control for tyramide amplification. Images were collected at a step size of 1.5 µm, for 43 total slices, using a Plan Apochromat 20X/0.8 objective, laser power=2.20% (488 nm), 5.50% (561 nm), pinhole=57 µm, on a LSM800 confocal laser scanning microscope using ZenBlack imaging software. Stacks were exported to ImageJ where individual cells were counted and the stack was compressed to a Maximum Intensity Projection (MIP). Vessels were imaged as above (for sprout length) and GFP^+ vessels with pERK staining were scored as positive.

Time-lapse confocal microscopy − 2 embryos were analyzed per experiment, and the movies shown are representative of these results (DMSO=6 embryos, SL327=6 embryos). Images were collected every 10 minutes, at a 5 µm step size, with a total stack size of 205 µm, using a Plan Apochromat 20X objective, laser power=20.8% (488), 56.4% (546), NA=0.8, WD=0.55 mm, pinhole=57 µm, on a LSM800 confocal laser scanning microscope using ZenBlack imaging software. Images were compressed to a maximum intensity projection (MIP), then stitched together as a movie in Zen and exported as an AVI (with no compression).

Imaging transplantation experiments: Embryos were embedded in low melt agarose, then imaged using a LSM 780 confocal microscope (Zeiss) with the following conditions: Plan-Apochromat 20x/0.8 M27 objective, 488 laser power at 4.5%, 594 laser power at 4.7%, 647 laser power at 5%. A total tack of 96 µm was collected, scanning every 2 µm (averaging set to 8). The pinhole was set to 126 µm (488), 55 µm (561), 113 µm (640). Stacks were exported to ImageJ where individual cells were counted and the stack was compressed to a Maximum Intensity Projection (MIP).

In situ hybridization primers −
JDW 436 (T7 *drhlx* FWD): 5'-
GCAAATTAATACGACTCACTATAGGGAGAGCGGTGGATAGCATGAAGAAAC

JDW 437 (SP6 *drhlx* REV): 5'-
TATGCGATTTAGGTGACACTATAGAACAGGTTGGAAAACACAGCTCTG
JDW 295 (SP6 *drdusp5* FWD): 5'-
TATGCGATTTAGGTGACACTATAGAACTTTGTCGCACTTGACGAGTA
JDW 296 (T7 *drdusp5* REV): 5'-
CGAAATTAATACGACTCACTATAGGGTTGGACTCAGTTTGAATGATGG
JDW 297 (SP6 *drdll4* FWD): 5'-
TATGCGATTTAGGTGACACTATAGAAGGACATCGTGTCCCAAGAGGA
JDW 298 (T7 *drdll4* REV): 5'-
CGAAATtaatacgactcactatagggCAATCCAAGAAGACCCGGGCA

Mouse experiments:

Immunohistochemistry on sections − For frozen sections, after equilibration at -20°C, 10 µm sections were collected on Superfrost Plus slides (Fisher, #12-550-15) using a Leica CM1850 cryotome. Sections were stored at -80°C until ready for processing. For IHC, slides were dried for 10 minutes at 42°C, washed 3X in PBS, permeabilized in 0.3% Triton-X100 / 1X PBS, washed in PBS, blocked in TNB (0.1 M Tris-HCl (pH 7.5) / 0.15 M NaCl / 0.5% Blocking Reagent (Roche, #10447200)) for 1 h at room temperature, then incubated with anti-ERG1/2/3 (Santa Cruz Biotechnology, SC-353) (1:200) overnight at 4°C. Tissue was washed in PBS, incubated with Alex 594 conjugated goat anti-rabbit (Life Technologies, A11034) (1:150) for 1.5 h at room temperature, washed in PBS, then stained for CD31 (BD Biosciences, #550274) for 2 h at room temperature, washed in PBS, incubated in Alexa 488 conjugated goat anti-rat (Life Technologies, A11006) (1:150) for 1.5 at room temperature, washed in PBS, counterstained in DAPI (300 nM) (Life Technologies, #D3571) for 10 min at room temperature, washed in PBS, coverslipped in aqueous mounting media (Vector Labs, #H-5501), cured, then sealed with nail polish. Images were acquired using a EC Plan-Neofluar 10x/0.30 M27 objective with laser power 6.5% (405 nm); 11% (488 nm); 6% (561 nm); or a 40x/1.4 oil DIC M27 objective with laser power 0.8% (405 nm); 4% (488 nm); 4% (561 nm) using a Zeiss LSM 780 confocal microscope. Confocal stacks of 12.25 µm were collected with a step size of 1.75 µm. Stacks were compressed to a maximum intensity projection using ZenBlue (Zeiss), and images were exported to Adobe Photoshop and Illustrator.

X-gal staining on sections − 10 µm cryosections (processed as detailed above) were dried for 10 min at room temperature, washed in PBS, post-fixed (2% PFA / 0.2% glutaraldehyde / 1X PBS / 0.02% sodium deoxycholate / 0.01% IGEPAL CA-630) for 5 min at room temperature, washed in

Permeabilization Buffer (1X PBS / 0.02% sodium deoxycholate / 0.01% IGEPAL CA-630) at room temperature, then incubated in Staining Buffer (1 mg/mL X-gal / 5 mM postassium ferricyanide / 5 potassium ferrocyanide / 2 mM $MgCl_2$ in Permeabilization Buffer) overnight at 37°C, washed in PBS, fixed, washed, then counter-stained with nuclear fast red (Vector Labs, #H-3404) for 10 min, washed in dH_2O, dehydrated to absolute ethanol, washed in xylene, and mounted in Entellan New (Electron Microscopy Sciences, #14800). Slides were imaged on a Zeiss Axio Zoom.V16 stereoscope using Zen Blue software. Images were exported in Adobe Photoshop.

Collecting ECs from mouse embryos by FACS − Following collagenase digestion, cells were washed and blocked in HBSS++ (HBSS without calcium, magnesium, or phenol red (Gibco, Cat#14175095) / 2% FBS (HyClone, Cat #SH30910.03) / 1% penicillin-streptomycin (Lonza, Cat #12001-324) / 1% 1M HEPES (Gibco, Cat #15630080). Cells were then incubated in HBSS++ with BV421 Rat anti-mouse CD31 (BD Biosciences, Cat #562939) (1:100) for 90 min at 4°C, washed in HBSS++, then stained in TO-PRO-3 Iodide (Life Technologies, Cat # T3605) (1:1,000) for 15 min at 4°C, all while rocking gently. Cells were then washed and filtered through a 35 μm cell strainer (Falcon, Cat#352235). The single cell suspension was sorted at the Cytometry and Cell Sorting Core (CCSC) (BCM) on a FACSAria II (BD Biosciences) using the following gating parameters: Sort set up to 85 μm, precision set to purity. Events were recorded until 25,000 live endothelial cells per embryo were collected into 350 μL of RLT Buffer (Qiagen) for downstream processing. Embryos with EC viability lower than 70% were not used for downstream analysis.

Analysis of retinal vasculature – Following administration of tamoxifen at P1 and P3, pups were euthanized at P8 by CO_2 asphyxiation, tail tissue was acquired for DNA genotyping, and eyes were enucleated and placed in 4% PFA at 4°C overnight. The following morning, retinas were isolated, then partially cut into 4 quadrants (i.e. leaflets) to allow for flat mounting. Isolated retinas were first blocked and permeabilized overnight with gentle shaking at 4°C in retina blocking buffer (1% BSA / 0.5% Triton-X100 / 1X PBS / pH 7.2). The following morning, retinas were washed 3 times for 5 minutes each wash in 1X PBS. Retinas were then equilibrated to room temperature in Pblec solution (1X PBS / 1 mM $CaCl_2$ / 1 mM $MgCl_2$ / 0.1 mM $MnCl_2$ / 1% Triton-X100 / pH 6.8) 3 times, for 20 minutes each time. Retinas were then incubated overnight with gentle shaking at 4°C with biotinylated *Griffonia simplicifolia* Isolectin B4 (Vector Labs, B-1205) at a concentration of 1:50 prepared in Pblec solution. Retinas were rinsed twice with 1X PBS, followed by 3X 10-minute washes in retina wash buffer (retina blocking buffer diluted 1:1 in

1X PBS), then incubated in DyLight 594 Streptavidin (Vector Labs, SA-5594) prepared in retina blocking buffer for 2 h at room temperature with gentle agitation. After incubation, retinas were rinsed twice with 1X PBS, followed by 3X 10-minute washes in retina wash buffer. Retinas were mounted on glass slides and coverslipped using Fluoromount-G mounting medium (SouthernBiotech, 0100-01). For P6 retinal harvests, pups were given a single, 50 µL dose (10 mg/mL) of tamoxifen (equivalent to 50 µg per mouse) by subcutaneous injection at P1, and harvested eyes were fixed in 4% PFA and then retinas were collected after 2 hours and processed identically as P8 retinas.

To quantify vascular branching in the retina, a single 20X image was taken from a middle point of the central plexus for each of the 4 quadrants per retina (i.e. 4 images per retina examined). All branch points were tallied using ImageJ software within each full 20X field of view and averaged across the 4 quadrants for a single averaged measurement of vascular branching per biological sample. This was performed from 1 retina per animal, from 5 different animals for both control ($ERG^{fl/+}$) and experimental (ERG^{iECKO}) groups at P8, and 3 animals for control ($ERG^{fl/+}$) and 2 animals for the experimental (ERG^{iECKO}) groups at P6. Data was graphed using GraphPad Prism software and shown as an average ± SEM. Comparisons were made using a two-way, unpaired Student's T-test for the P8 retinas. Images for both ages were obtained on a Leica TCS SPE confocal microscope with a 20X objective lens (1,024 x 1,024 pixels) at 15% power (561 nm).

Radial expansion of the retinal vasculature was quantified using the integrated length calculator function in the Zen Pro software suite (Zeiss). Images were taken on a Zeiss Axio Zoom.V16 fluorescent stereoscope at a 65X magnification. At this magnification, the entirety of a retinal quadrant to the optic nerve could be collected in one image. Images were taken for each quadrant (4 per retina), and a single line was drawn from the center of the optic nerve, through the center of the quadrant, to the vascular front. Total length was recorded for each of the 4 quadrants for a single retina and the average determined. This was performed for all retinas from both control and experimental groups. Radial expansion was graphed using GraphPad Prism software and shown as an average ± SEM. Comparisons were made using a two-way, unpaired Student's T-test for the P8 retina data.

To quantify sprouting within the P6 retina, a single 40X image (1,024 x 1,024 pixels) was acquired from each leaflet (i.e. 4 images per retina). Major sprouting vessels at the vascular front were tallied within each full 40X field of view and averaged across the four leaflets to yield a single measurement per animal. One retina per animal was analyzed, and for P6 3 control ($ERG^{fl/+}$) and 2 experimental (ERG^{iECKO}) animals were quantified. Data was graphed using

GraphPad Prism software and shown as an average ± SEM. Images were taken on a Leica TCS SPE confocal microscope using a 20X objective with a 2X zoom magnification at 22% laser power (561 nm).

Cloning:

ETS concatemer − Oligos containing the previously EMSA-validated ETS site B (site #2, GCGTTTCCTGCGGG) of the minimal 30 bp murine *Dll4* intron 3 arterial enhancer (F2-6) (Wythe et al., 2013) were synthesized as a multimer (8X), and the duplex was annealed and cloned into pDONR221 to generate JDW 295 (8X WT) and JDW 242 (8X MT, GCGTTTttTGCGGG) constructs. Subsequently, this was recombined into pGL3-Pro-DV (JDW 250/ETS WT; JDW 241/ETS MT).

HLX enhancers − Nucleotides of the gene regulatory element *HLX-3a*, spanning 1,565 bp on human chromosome 1, beginning approximately 3 kb upstream of the 5' UTR of *HLX*, were directly synthesized as a gene block (IDT) with all ETS sites intact, or all ETS sites mutated as follows: ETS A: TTCC>TTaa*;* ETS B: GGAA>aaAA*;* ETS C: TTCC>TTtt; ETS D: TTCC>TTtt; ETS E: GGAA>aaAA; ETS F: GGAA>ttAA; ETS G: GGAA>aaAA; ETS H: TTAA>TTtt; ETS I: GGAA>GGgg; ETS J: GGAA>aaAA; ELK1: TCCG>TttG; ETS K: TTCC>TTtt; ETS L: GGAA>ctct; ETS M: GGAA>aaAA; ETS N: GGAA>aaAA; ETS O: TTCC>ccCC; ETS P: GGAA>aaAA; ETS Q: GGAA>aaAA
Subsequently, primers containing flanking attB1/B2 sites and BamHI and NotI restriction sites (5' and 3', respectively) were designed to amplify the entire region (*HLX-3a*) or the smaller fragment (*HLX-3b*), from both wild-type and mutant templates, and were directly cloned into pDONR221 via a BP clonase reaction.

HLX Enhancer Activity Assays − Following sequence verification, *HLX-3a/3b* donor clones were recombined with a destination vector, pGL4.23[luc2 minP]-DV, for *in vitro* luciferase analysis. pGL4.23[luc2 minP]-DV was created by digesting the parental vector (pGL4.23[luc2 minP]) with NheI and inserting a PCR-amplified gateway RFA cassette via Cold Fusion (SBI). The RFA insert was amplified using the following primers, JDW 356 (FWD): 5'-ACTGGCCGGTACCTGAGCTCACAAGTTT GTACAAAAAAGC; JDW 357 (REV): 5'-CAGATCTTGATATCCTCGAGCCACTTTG TACAAGAAAGCT. For *in vivo* analyses, the *HLX* pDONR clones were recombined with a modified pTol2-E1b-EGFP destination vector. Briefly, to stabilize reporter activity, pT2KXIGQ-DV (Smith et al., 2013) (a kind gift of Nadav Ahituv, UCSF), which has a gateway RFA cassette inserted between XhoI and BglII, and is a variant of

pT2KXIGQ (Li et al., 2010), originally derived from pT2KXIG (Kawakami et al., 2004), was digested with ClaI and a WPRE element was amplified by PCR and placed downstream of EGFP, upstream of the poly(A), using Cold Fusion (SBI).
JDW 348 (FWD): 5'-GGTGGAGCTCGAATTAATTCATCGATTCAACCTCTGGATTACAA AATTTGTG; JDW 360 (REV): 5'-CTTATCATGTCTGGATCATCATCGATTCGAG GTCGAGGTCGACGGTAT. This construct was validated using a *myh6* (aka *cmlc2*) promoter (data not shown).

Wild-type and mutant ERG constructs − The ORF of human ERG was amplified by PCR, adding a 3X-FLAG sequence and a Gly-Gly-Ala-Gly-Gly flexible linker (Sabourin et al., 2007) at the amino terminus, with two stop sequences and an XbaI site at the carboxy terminus.
JDW 497 (FWD) (ERG homology is underlined, linker is in bold): GCCACCATGGACTAC AAAGACCATGACGGTGATTATAAAGATCATGATATCGATTACAAGGATGACGAT GACAAG**GGTGGTGCTGGTGGT**ATGGCCAGCACTATTAAGGAAGCC
JDW 498 (with an attB2 site):
CCCCACCACTTTGTACAAGAAAGCTGGGTCTAGATTATTAGTAGTAAGTGCCCAGATGAGA AGGC
Then an attB1 site was added at the 5' end by PCR, using the same REV primer as above:
JDW 499 (FWD):
GGGGACAAGTTTGTACAAAAAAGCAGGCTGCCACCATGGACTACAAAGACCATGAC GG
This PCR product was cloned via a BP reaction directly into pDONR221, and then used as the template for site directed mutagenesis. The primers are listed below:
JDW 500 (S215A FWD; TCT>GcC): gatgttgataaagccttacaaaacgccccacggttaatgcatgcta,
JDW 501 (S215A REV; TCT>GcC): tagcatgcattaaccgtggggcgttttgtaaggctttatcaacatc.
JDW 448 (S96A FWD; AGC>gGC): 5'-ggaagatggtgggcgccccagacaccgttg
JDW 449 (S96A REV; AGC>gGC): 5'- caacggtgtctggggcgcccaccatcttcc
JDW 450 (S276A FWD; TCT>gCT) 5'-gaaagctgctcaaccagctccttccacagtgcc
JDW 451 (S276A REV; TCT>gCT) 5'-ggcactgtggaaggagctggttgagcagctttc

All constructs were then recombined by a LR clonase reaction into pCS2-DEST (Addgene # 22423) (Villefranc et al., 2007) for *in vitro* validation by immunofluorescence and western blot (using by anti-Myc and anti-Flag antibodies).

pERG western blots and co-immunoprecipitation experiments:
For pERG western blots, ERG was immunoprecipitated from cell lysates (in RIPA buffer). 25 µL of Dynabeads M-280 sheep anti-mouse IgG was mixed overnight at 4°C with 5 µL of anti-ERG

antibody (BioCare) in 500 µl ChIP dilution buffer. 1 mg of cell lysate in RIPA was added to the mixture and rotated overnight at 4°C. The protein complexes bound to the beads were collected using a magnetic separator, and Western blotting was performed on SDS-PAGE gels. Blots were probed with anti-pERG^{S215} [provided by Dr. Peter Hollenhost, (Selvaraj et al., 2015)] and then stripped and reprobed with anti-ERG (BioCare). The specificity of this antibody was determined by performing western blots on wild-type and S215A mutant ERG. No signal was observed for S215A ERG. Similar procedures to those described above were used for co-immunoprecipitation experiments in HUVEC, except non-denaturing buffer was used (20 mM Tris-HCl (pH 8.0) / 137 mM NaCl / 1% NP-40 / 2 mM EDTA). Anti-V5 antibody (mouse monoclonal, Thermo Fisher Scientific) was used as a negative control for co-immunoprecipitation experiments. Blots were probed with anti-p300 (Santa Cruz Biotechnology) and anti-ERG (BioCare). Co-immunoprecipitation experiments were performed in BAECs to assess the interaction between Myc-p300 (a gift from Dr. Tso-Pang Yao, Addgene plasmid #30489) and either wild-type or mutant Flag-ERG (cloning described below). Briefly, BAECs on a 10 cm plate were transfected with 6 µg of Myc-p300 and 6 µg of Flag-ERG constructs using Lipofectamine 2000. After 48 h, cells were treated with VEGF (50 ng/mL) for 1 h. Flag-ERG was precipitated from two 10 cm plates of BAEC (~ 1 mg of total input protein per IP) overnight at 4°C using 5 µL of Flag antibody (Cat. #F1804, Sigma) and Dynabeads (Sacilotto et al.). V5 antibody was used as a negative control (as above). The samples were lysed in Non-denaturing lysis buffer (20 mM Tris HCl (pH 8) /137 mM NaCl / 1% Nonidet P-40 / 2 mM EDTA) and run on a 4% SDS-PAGE gel, transferred using a semi-dry blotter (15V, 1 h) and then blotted with anti-Flag (1:1,000) or anti-Myc antibody (Cat. #sc-4084) (1:500). The signals were detected using standard chemiluminescence.

Microarray processing and analysis:

Processing − Low Input Quick Amp Labeling Kit from Agilent (Cat#0006177230) was used to generate fluorescent cyanine 3-labeled complimentary RNA (cRNA) from total RNA (150 ng) for one-color processing. Labeled cRNA was purified using RNeasy Mini Kit (Qiagen, Cat# 74104). For microarray hybridization, 600 ng of cyanine 3-labeled cRNA was fragmented and hybridized on Agilent G3 Human 8x60K microarrays at 65°C for 17 hours at 20 rpm using the Agilent gene expression hybridization kit (part number 5188-5281). The hybridized microarrays were dissembled at room temperature in gene expression wash buffer 1 (part number 5188-5325), then washed in gene expression wash buffer 1 at room temperature for 1 minute. This was followed by a wash for 1 minute in gene expression wash buffer 2 (part number 5188-5326) at

37°C. The processed microarrays were scanned with an Agilent DNA microarray scanner (Scanner Model G2505B-C), and extracted with Agilent feature extraction software (version 10.7.3.1).

Analysis − Data was checked for overall quality using R (v2.15.3) with the Bioconductor framework and the Array Quality Metrics package installed. All samples passed quality control, but two outliers (1 sample from control siRNA, non-stimulated and 1 sample from ERG siRNA, VEGF stimulated) were identified from visualizing correlation coefficient data and were removed from subsequent analysis. Data was imported into GeneSpring v12.6.1 for analysis. During import, the data was normalized using the recommended Agilent spatial detrending method with a "per probe" median centered normalization. All data analysis and visualization were performed on log2 transformed data. Data was first filtered to remove probes that showed low signal and positive control probes were also eliminated from further analysis. Only probes that were above the 20th percentile of the distribution of intensities in 80% of any of the 4 groups were allowed to pass through this filtering. One-way ANOVA with a Benjamini-Hochberg FDR corrected $p<0.05$ was performed, revealing 498 significantly varying probes. A post-hoc Tukey's HSD test was used following the ANOVA to identify significant differences between groups. The probes that were significantly different between control siRNA and ERG siRNA in the presence of VEGF stimulation (n=357 probes) were cross-referenced with the list of VEGF regulated genes (control siRNA, no stimulation vs. control siRNA, 1 h VEGF stimulation, n=196 probes) to identify a group of 44 unique genes that were both ERG regulated and VEGF-dependent. Microarray data was submitted to ArrayExpress (accession number: E-MTAB-5207).

ChIP-seq experiments:

Processing − ChIP DNA was prepared for Illumina sequencing by blunt-end repair, dA-tailing, and ligation of Illumina adaptors using a NEBNext DNA library preparation kit (New England Biolabs, catalogue #E6040L). Total ChIP DNA (approximately 200-500 ng) and 220 ng of DNA input (WCE) was end repaired for 30 minutes at room temperature, and then purified using column purification with either DNA Clean and Concentrator (Zymogen, catalogue #D4014) or PCR purification columns (Qiagen, catalogue #28106) as recommended by the manufacturers' protocols. Blunt-end repaired DNA was dA-tailed for 40 minutes at 37°C, then column purified. dA-tailed DNA was ligated to Illumina adaptors (final concentration 6.67 nM) that have a T-overhang. USER enzyme was used to cleave the uracil hairpin of the Illumina adaptor, and adaptor-ligated DNA was column purified. The library was PCR amplified for 16-18 cycles using a universal primer and a barcoded primer (New England Biolabs, catalogue #E7335L). PCR-

amplified DNA was purified using PCR column purification and eluted in 20 µL of elution buffer for preparation of gel extraction, or 30 µL of TE for preparation of Pippin Prep size selection. Library samples were size selected from 200-350 bp using a 2% agarose dye-free automated size selection cassette from Pippin Prep (Sage Sciences, catalogue #CDF2010).

Analysis − Samples were submitted for quality control analysis to the Donnelley Sequencing Center (University of Toronto) or The Center for Applied Genomics (Hospital for Sick Children) for Bioanalyzer analysis and library quantification using KAPA Biosystems. Libraries were sequenced using Illumina HiSeq2500. The flowcells were prepared and processed by the sequencing facility according to the manufacturer's protocol, with 100-bp single-end sequencing for 75 cycles. ChIP-seq and input reads were aligned to hg19 [GRCh37] genome assembly with Burrow-Wheeler Aligner (BWA), using default parameters (Li and Durbin, 2009), and quality control indicators were measured according to the ENCODE Consortium guidelines (Landt et al., 2012). Peaks were called for each sample relative to the WCE input using MACS2 with a cutoff of false-discovery rate ($q \leq 0.05$) (Zhang et al., 2008). ChIP-seq data was submitted to ArrayExpress (accession number: E-MTAB-5148). We also utilized HUVEC H3K4me3 (pooled signal from biological replicates, ENCODE accession numbers: ENCFF000BTS, ENCFF000BTL) and HUVEC H3K4me1 (pooled signal from biological replicates, ENCODE accession numbers: ENCFF000BTD, ENCFF000BSY, ENCFF000BSX) from the Encyclopedia of DNA Elements Consortium (Consortium, 2012). Vertebrate conservation across 100 genomes was extracted from UCSC Genome Browser. Further details regarding quality control of ChIP-seq experiments can be found in the supplementary Materials and Methods (Table S4).

Motif analysis − Motif enrichment analysis was performed using the tool peak-motifs (Thomas-Chollier et al., 2012) from the Regulatory Sequence Analysis tools (Medina-Rivera et al., 2015) with parameters: -markov auto -disco oligos,positions -nmotifs 5 -minol 6 -maxol 7 -no_merge_lengths -2str -origin center . peak-motifs builds motifs using over-represented oligos present in the sequence set given as input, the tool is also able to compare the discovered motifs with any given set of known motifs in order to identify the putative transcription factors that could be binding the sequences, for this task we used the none redundant JASPAR motif collection for vertebrates (Castro-Mondragon et al., 2016; Mathelier et al., 2016). Secondary motif sets were discovered by using a control sequence set as background to eliminate motifs enriched in such control set and increase the signal of other motifs with less representation but that still can have biological and statistical significance. Further details regarding motif analysis of ERG target genes can be found in the supplementary Materials and Methods (Table S3).

CRISPR-mediated *HLX* enhancer deletion:

The gRNAs were ordered as standard DNA oligomers from Integrated DNA Technologies (IDT) (see below for sequences). The oligomers were then annealed, phosphorylated, and cloned into pSpCas9(BB)-2A-GFP (PX458) under control of the U6 promoter (Addgene Plasmid ID 48138). TeloHAECs were transfected with 6 µg of PX458 plasmid containing each 5' and 3' gDNA or two scrambled control gRNAs using Lipofectamine 2000 (2 µL/1 µg DNA, Invitrogen) in 100 mm dishes. After 48 h, TeloHAECs were FACS sorted to isolate GFP^+ cell populations. Following expansion of the GFP^+ cells, they were then seeded as single cell colonies in 96 well plates. Subsequently, the cells were cultured, expanded and genotyped. Genomic DNA was isolated from cell pellets after overnight incubation at 56°C in lysis buffer (100 mM NaCl / 10 mM Tris-HCl (pH 8) / 25 mM EDTA (pH 8) / 0.5% SDS / 0.2 mg/mL ProK) and phenol-chloroform extraction. For genotyping, PCR reactions were performed using Taq Polymerase (Invitrogen) as per manufacturer's instructions. A forward anchor primer was used along with a reverse primer nested either within the deletion region (wild type allele) or 3' of the deletion region (deletion allele). The PCR products were separated by gel electrophoresis and visualized using MiniBIS Pro (DNR Bio-Imaging Systems). Furthermore, the PCR products were gel extracted (QIAquick Gel Extraction Kit) and the deletion was confirmed by DNA sequencing.

Guide sequences for CRISPR experiments:

*HLX*_3'_gRNA_F	5'-CACCGTCCAAGGTTTGCGACGCTCC
*HLX*_3'_gRNA_R	5'-AAACGGAGCGTCGCAAACCTTGGAC
*HLX*_5'_gRNA_F	5'-CACCGATTGCATAAGCCCCTGATTC
*HLX*_5'_gRNA_R	5'-AAACGAATCAGGGGCTTATGCAATC
SCR_1_gRNA_F	5'-CACCGGCACTACCAGAGCTAACTCA
SCR_1_gRNA_R	5'-AAACTGAGTTAGCTCTGGTAGTGCC
SCR_2_gRNA_F	5'-CACCGACAACTTTACCGACCGCGCC
SCR_2_gRNA_R	5'-AAACGGCGCGGTCGGTAAAGTTGTC

Genotyping primers for HLX CRISPR experiments:

*HLX*_Enh_Anchor:	5'-TTGACCTGTGCTCAGTGTGG
*HLX*_Enh_WT:	5'-TATCGCATTGGCTGGGGTTT
*HLX*_Enh_Del:	5'-GAGGGTTCTGGTGAGCCTTC

Table S1: Primers used for murine genotyping

MGI #	Allele	Forward 5'-3'	Reverse 5'-3'	Band Size
NA	*Erg*$^{KO/+}$ WT allele	AATGCTCTGGTAAGGCACACAAGG	AGAGTCTCTGCACACAGAACTTCC	312 bp
NA	*Erg*$^{KO/+}$ lacZ allele	GCTACCATTACCAGTTGGTCTGGTGTC	AGAGTCTCTGCACACAGAACTTCC	644 bp
NA	*Erg*$^{fl/+}$ WT allele	AATGCTCTGGTAAGGCACACAAGG	AGAGTCTCTGCACACAGAACTTCC	312 bp
NA	*Erg*$^{fl/+}$ Flox allele	GAGATGGCGCAACGCAATTAATG	AGAGTCTCTGCACACAGAACTTCC	346 bp
3848982	Cdh5-PAC-CreERT2	TCCTGATGGTGCCTATCCTC	CCTGTTTTGCACGTTCACCG	548 bp

Table S2: Primers used for quantitative PCR: qPCR primers were designed using Primer3 (http://bioinfo.ut.ee/primer3/), selecting for an amplicon length of 80-140 bp, spanning at least one exon-exon boundary with an intervening intron greater than 400 bp to favor mRNA amplification, with an efficiency of greater than 80% as determined by qPCR dissociation (melting curve), with a single amplicon (confirmed by melt curve dissociation).

Gene	Forward Primer	Reverse Primer
Human Genes:		
ADRB2 mRNA	TCA CAC GGG GTA TTT TAG GC	CAA GGG GTT TTG GAG AAA CA
APOLD1 pre-mRNA	GCT GAC CGC GTG TCT ATG T	AGC AGC AGT CCC TGG AAG
CCRL2 mRNA	TGC CAG CTG ATG AGA CAT TC	ACC TCT GCT CCC TGA ACC TT
CHAC1 mRNA	GCA GCG ACA AGA TGC CTG	CTT CAG GGC CTT GCT TAC CT
CHAC1 pre-mRNA	GAC TTC GCC TAC AGC GAC A	AAG ATG GTG AGC ATC CAA CC
DLL4 mRNA	TGC GAG AAG AAA GTG GAC AG	ACA GTA GGT GCC CGT GAA TC
DLL4 pre-mRNA	TGC GAG AAG AAA GTG GAC AG	ACC CTC CCT CAC CAG AAG T
DUSP5 mRNA	ATG GAT CCC TGT GGA AGA CA	TCA CAG TGG ACC AGG ACC TT
DUSP5 pre-mRNA	CCA ACT CAC TCC CAC CAT CT	CGG AAC TGC TTG GTC TTC AT
EGR3 mRNA	AAG AGC AGG GGG TTG TGA AT	CCT CCT GGC AAA CTT CAT CT
EGR3 pre-mRNA	ACT CAC CCC TCC CCT CTC TC	GGA AGG AGC CGG AGT AAG AG
FJX mRNA (single exon)	CTT TCT GGA CAA TGA GGC GG	GCG GCT CGT TAT ACT TGT CC
FUT1 mRNA	TTG GTC TTT GTC TGC AGG TG	ACG GTA CCT GCC AGT TTG TC
HLX mRNA	GCC TGG AGA AAA GGT TTG AG	CTG GAA CCA CAC CTT CAC CT
HLX pre-mRNA	GGC CCT CTT GTC TTT CTT CC	CTT TCC TCT GCA GGT TGG AG
KCNJ2AS1 mRNA	AGC GGG AGG AAG GTC ATA AT	TTG CTG CAC ATC CTT CAG TC
NDRG1 mRNA	CTC GCT GAG GCC TTC AAG TA	GGG TGC CAT CCA GAG AAG T
NDRG1 pre-mRNA	TTG GTC TTG GAT TTG CTT CC	GAG ACA TGT CCC TGC TGT CA
NRARP mRNA (single exon)	CAT TGA AAT GGA GGC ACA GA	ACC CAC ACA CAG CTT CGA TA
PIK3R1 mRNA	TGT CCG GGA GAG CAG TAA AC	AGC CAT AGC CAG TTG CTG TT
PIK3R1 pre-mRNA	CAG ATG GCA AAG TGT GCT GT	GCC CAA TCC TTT CTG ACA CT
SLC25A25 mRNA	CTG TGG CAC CAT GTC CAG TA	GGT CCG CAG GAT ATG TTT GA
SLC25A25 pre-mRNA	AGG GCG AGC TCC AGG TAG	GCA CCC TTC CTC TGG ACA GT
SDF2L1 mRNA	AGG CTC ACG CAT GTG CTT AC	TGT CCA TAG GTC CAG GTC GT
SDF2L1 pre-mRNA	CAT GGT GTC ACC TTT TGC AG	CCA AAG GCA CTC ACC TCC TA
TBP mRNA	TCG GAG AGT TCT GGG ATT GT	CAC GAA GTG CAA TGG TCT TT
ZNF555 mRNA	GCA TCG AAG ATC AAA CCA CA	GAT GTG GAA TCT GGC TGA GG
Zebrafish genes:		
dll4 mRNA	GGA CAA ATG CAC CAG TAT GC	GTT TGC GCA GTC GTT AAT GT
tbp mRNA	TGG GTT TCC CTG CCA AAT TCT T	GGA AAT AAC TCC GGT TCA TAG CTG C
Murine genes:		
Cdh5 mRNA	TCAACGCATCTGTGCCAGAGA	CACGATTTGGTACAAGACAGTG
Erg mRNA	GGAGCTGTGCAAGATGACAA	TCAGATGTGGAAGGGGAGTC
Dll4 mRNA	ACAAGAATAGCGGCAGTGGT	GGATGTTGAGTGAGAAGGTTCC
Hlx mRNA	TTCAGCATCAATTCCAAGACACA	ACCTCTTCTCCAGGCCTTTTCT
Dusp5 mRNA	TGCACCACCCACCTACACTA	AGGACCTTGCCTCCTTCTTC
Ccdn1 mRNA	CCAACAACTTCCTCTCCTGCT	GACTCCAGAAGGGCTTCAATC

Pik3r1 mRNA	CAAAGCGGAGAACCTATTGC	CCGGTGGCAGTCTTGTTAAT
Fjx1 mRNA	CTCTACAGTCGCCACGAACC	AAATGTGTTTGGCGAGGAAG
Egr3 mRNA	GACTCGGTAGCCCATTACAATCAG	GTAGGTCACGGTCTTGTTGCC
Nrarp mRNA	TGGTGAAGCTGTTGGTCAAG	CTTGGCCTTGGTGATGAGAT
Sdf2l1 mRNA	TCATCACCCTCACCGTCTTCCC	AACCTGCACACGCACCACTTC
Rasip1 mRNA	CCGTCCCTACTTCCTTCTGCTC	ACGTGCTGCTCTCGTGTCAT
Cldn5 mRNA	GCAAGGTGTATGAATCTGTGCTGG	GCGCCGGTCAAGGTAACAAAG
Sox18 mRNA	AGGACGAGCGCAAGCGACTG	CGTGTTCAGCTCCTTCCACGCT
Gapdh mRNA	GATGGCAACAATCTCCACTTTGC	GCCGCATCTTCTTGTGCAGT
ChIP primers:		
DLL4 intron 3	GTT TCC TGC GGG TTA TTT TT	CTT TCC AAA GGA GCG GAA T
HLX enhancer	TTG AAA GGG GAA GTG CTA GG	GGC TCA AAC TCG GGA CTA AA

Table S3: Motif analysis of ERG target genes.

Primary motifs were discovered using peak-motifs in ERG peaks overlapping extended (10 kb) transcriptional start sites (TSSs) of the corresponding gene data sets. Motifs were annotated as belonging to a transcription factor (TF) by similarity to Jaspar vertebrates non-redundant annotate motifs.

Secondary motifs were discovered using peak-motifs in the ERG peaks overlapping extended TSSs for the specified data set using a control background corresponding to ERG peak regions overlapping extended TSS for genes with opposite expression pattern. Motifs were annotated as belonging to a TF by similarity to Jaspar vertebrates non-redundant motifs.
** Indicates data sets where the Secondary Motifs cotained one or more TFs not contained in the Primary Motifs set.*

Data Set	Num. Peaks	Primary Motifs
ERG target genes	221	Gabpa, ETV6, ELF5, ETS1, ERG, Gabpa, ELK4, ETS1, NFIC, SPIB, ETV6, NKX6-1, NKX6-2, BSX, Tcfl5, ZBTB33, TEAD4, EBF1, MZF1, ERF, SP1, SP2, KLF5, SPIC, FOSL1, JUNB, FOSL2, OTX2, Pitx1, Arid3b, FOXD2, ELK3
ERG-sensitive VEGF regulated genes	62	ELF5, ETS1, ERG, REL, RELA, Stat4, SP1, KLF5, SP2, EWSR1-FLI1, SPIB, BATF::JUN, MAFG::NFE2L1, Gfi1, Gfi1b, ETV2, POU5F1B, POU3F4, POU2F1, NKX2-8, NKX2-3, FOSL1, FOSL2, JUNB, JDP2, NFE2, HIC2, Hic1, MXF1

Data Set	Num. Peaks	Primary Motifs	Secondary Motifs	
ERG target genes (down-regulated following *ERG* knock-down)	187	Gabpa, ETV6, ELF5, ETS1, ERG, ELK4, NFIC, SPIB, TEAD4, EBF1, MZF1, ERF, SP1, SP2, KLF5	HOXD11 , NFATC2, REST, NHLH1, Ascl2, Myog, ZNF263, Zfx	*
ERG target genes (upregulated following *ERG* knock-down)	34	REL, RELA, SPIB, EWSR1-FLI1, ETV2; SP1, KLF5, SP2, TEAD4, POU3F4, TEAD3, Bcl6; Ahr::Arnt; ETS1, ELF5, ERF, FOSL2, FOSL1, JUNB, EWSR1-FLI1	SP2, LKF5, SP1 ; CREB, ATF7; NRF1 ; NKX6-1, mix-a, Alx4 ; USF2, PKNOX2, FOS::JUN ; Hic1, NFIX, NFIC ; JDP2(var.2), CREB1, ATF7	*
ERG-sensitive VEGF regulated genes (down-regulated following *ERG* knock-down)	50	ELF5, ETS1, ERG, RELA, REL, SPIB, KLF5, SP1, SP2, HOXC10, CDX1, HOXD11, ETV2, Nkx3-1, NKX2-3, NKX3-2, MZF1, JDP2, NFE2	ZBTB7C, ZNF354C, ZBTB7A, Nkx3-1, NKX3-2, NKX2-3, Nr2e1, Nkx3-1, NKX3-2, NKX2-3	*
ERG-sensitive VEGF regulated genes (upregulated following *ERG* knock-down)	12	EWSR1-FLI1, SP2, KLF5, SP1, ELF5, REL, SPIB, HOXA5,NFIC, SP1, Nr2e1	Nr2e1, FOXP3, FOXI1, FOXD, Nr2e1. Atf3	*

Table S4: Summary and quality control analysis of ChIP-seq experiments. A) Sequencing statistics and QC measurements for individual libraries. ENCODE practice (see *Landt et al.,* 2012 and https://genome.ucsc.edu/ENCODE/protocols/dataStandards/ChIP_DNase_FAIRE_DNAme_v2_2011.pdf for a detailed explanation of QC). Normalized strand-cross correlation (NSC) coefficient and the relative strand cross correlation (RSC) are a peak-calling independent means to assess data quality and NSC values above 1.05 and RSC above 0.8 indicate high quality transcription factor ChIP-seq data. PCR bottleneck coefficient (PBC) indicates PCR based artifacts. We observe a low PBC score in the WL375 library however this library is comparable to the better replicate WL379 and so we retained both experiments for analysis. B) Irreproducible discovery rate (IDR) analysis of ChIP-seq replicates. As a rule of thumb, ENCODE recommends that reproducible replicates possess Nt/Np and N1/N2 ratios within a factor of 2 ($0.5 \leq N \leq 2$). C) Summary of number peaks and conserved peaks in HUVEC and BAEC experiments.

A)

	Species	Factor	# Raw Reads	# Mapped Reads	# Unique Mapped Reads	% Unique Mapped	PBC	NRF	NSC	RSC	# Peaks
WL375	hsap	Erg	17155982	14662609	13425327	78	0.3	0.37	2.13	5.16	15104
WL379	hsap	Erg	21892688	19915133	18082059	83	0.93	0.92	1.14	1.11	22194
WL373	hsap	H3K27Ac	22680375	18749798	17255873	76	0.83	0.83	1.22	1.22	39183
WL377	hsap	H3K27Ac	29876586	28064462	26908616	90	0.82	0.8	2.25	1.15	54830
WL376	hsap	Input	27173361	20910309	19096572	70	0.93	0.93	1.03	0.74	NA
WL380	hsap	Input	22088949	20466251	18560981	84	0.97	0.96	1.03	0.58	NA
WL383	btau	Erg	27258172	25175440	17419369	64	0.95	0.94	1.05	0.21	24531
WL387	btau	Erg	26755810	25276242	18369459	69	0.92	0.92	1.16	0.80	23327
WL384	btau	Input	26864153	25540351	18730958	70	0.95	0.94	1.02	0.23	NA
WL388	btau	Input	21820116	20694192	16120267	74	0.81	0.81	1.02	0.17	NA

B)

Species	ChIP	Rep 1	Rep 2	Nt	Np	Nt / Np	N1	N2	N1 / N2	# Peaks from Merged Reps
btau	Erg	WL383	WL387	22169	17550	1.26	20965	25724	0.82	35183
hsap	Erg	WL375	WL379	7773	13275	0.59	27176	13711	1.98	31175
hsap	H3K27Ac	WL373	WL377	26102	37690	0.69	22333	44855	0.50	60555

C)

Species	Factor	Rep 1	Rep2	# Peaks	Conserved Peaks
btau	Erg	WL383	WL387	34773	8464
hsap	Erg	WL375	WL379	31175	8337

References:

Castro-Mondragon, J., Jaeger, S., Thieffry, D., Thomas-Chollier, M. and van Helden, J. (2016). RSAT matrix-clustering: dynamic exploration and redundancy reduction of transcription factor binding motif collections. *bioRxiv*.

Consortium, E. P. (2012). An integrated encyclopedia of DNA elements in the human genome. *Nature* **489**, 57-74.

Kawakami, K., Takeda, H., Kawakami, N., Kobayashi, M., Matsuda, N. and Mishina, M. (2004). A transposon-mediated gene trap approach identifies developmentally regulated genes in zebrafish. *Dev Cell* **7**, 133-144.

Landt, S. G., Marinov, G. K., Kundaje, A., Kheradpour, P., Pauli, F., Batzoglou, S., Bernstein, B. E., Bickel, P., Brown, J. B., Cayting, P., et al. (2012). ChIP-seq guidelines and practices of the ENCODE and modENCODE consortia. *Genome Res* **22**, 1813-1831.

Li, H. and Durbin, R. (2009). Fast and accurate short read alignment with Burrows-Wheeler transform. *Bioinformatics* **25**, 1754-1760.

Li, Q., Ritter, D., Yang, N., Dong, Z., Li, H., Chuang, J. H. and Guo, S. (2010). A systematic approach to identify functional motifs within vertebrate developmental enhancers. *Dev Biol* **337**, 484-495.

Mathelier, A., Fornes, O., Arenillas, D. J., Chen, C. Y., Denay, G., Lee, J., Shi, W., Shyr, C., Tan, G., Worsley-Hunt, R., et al. (2016). JASPAR 2016: a major expansion and update of the open-access database of transcription factor binding profiles. *Nucleic Acids Res* **44**, D110-115.

Medina-Rivera, A., Defrance, M., Sand, O., Herrmann, C., Castro-Mondragon, J. A., Delerce, J., Jaeger, S., Blanchet, C., Vincens, P., Caron, C., et al. (2015). RSAT 2015: Regulatory Sequence Analysis Tools. *Nucleic Acids Res* **43**, W50-56.

Sabourin, M., Tuzon, C. T., Fisher, T. S. and Zakian, V. A. (2007). A flexible protein linker improves the function of epitope-tagged proteins in Saccharomyces cerevisiae. *Yeast* **24**, 39-45.

Sacilotto, N., Chouliaras, K. M., Nikitenko, L. L., Lu, Y. W., Fritzsche, M., Wallace, M. D., Nornes, S., Garcia-Moreno, F., Payne, S., Bridges, E., et al. (2016). MEF2 transcription factors are key regulators of sprouting angiogenesis. *Genes Dev* **30**, 2297-2309.

Selvaraj, N., Kedage, V. and Hollenhorst, P. C. (2015). Comparison of MAPK specificity across the ETS transcription factor family identifies a high-affinity ERK interaction required for ERG function in prostate cells. *Cell Commun Signal* **13**, 12.

Smith, R. P., Riesenfeld, S. J., Holloway, A. K., Li, Q., Murphy, K. K., Feliciano, N. M., Orecchia, L., Oksenberg, N., Pollard, K. S. and Ahituv, N. (2013). A compact, in vivo screen of all 6-mers reveals drivers of tissue-specific expression and guides synthetic regulatory element design. *Genome Biol* **14**, R72.

Thomas-Chollier, M., Darbo, E., Herrmann, C., Defrance, M., Thieffry, D. and van Helden, J. (2012). A complete workflow for the analysis of full-size ChIP-seq (and similar) data sets using peak-motifs. *Nat Protoc* **7**, 1551-1568.

Villefranc, J. A., Amigo, J. and Lawson, N. D. (2007). Gateway compatible vectors for analysis of gene function in the zebrafish. *Dev Dyn* **236**, 3077-3087.

Wythe, J. D., Dang, L. T., Devine, W. P., Boudreau, E., Artap, S. T., He, D., Schachterle, W., Stainier, D. Y., Oettgen, P., Black, B. L., et al. (2013). ETS factors regulate Vegf-dependent arterial specification. *Dev Cell* **26**, 45-58.

Zhang, Y., Liu, T., Meyer, C. A., Eeckhoute, J., Johnson, D. S., Bernstein, B. E., Nusbaum, C., Myers, R. M., Brown, M., Li, W., et al. (2008). Model-based analysis of ChIP-Seq (MACS). *Genome Biol* **9**, R137.

Supplemental Figures

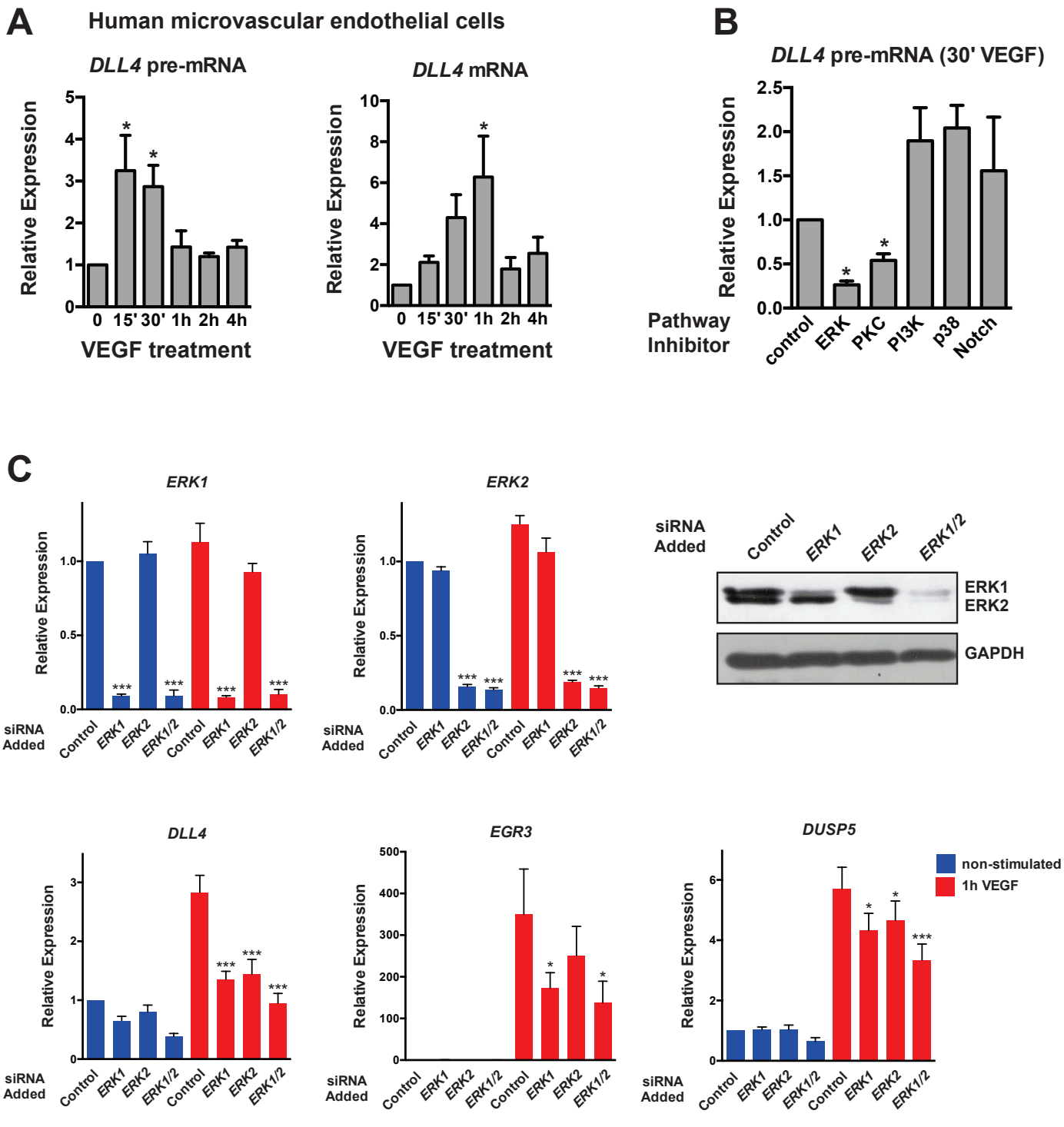

Figure S1: Transcriptional induction of *DLL4* is dynamic and requires MAPK/ERK signaling

A) Induction kinetics of *DLL4* pre-mRNA and mRNA in dermal microvascular ECs as assessed by qRT-PCR (n=3).

B) MAPK-dependence (MEK and PKC inhibitors) of *DLL4* induction in dermal microvascular ECs assessed through the use of small molecule inhibitors of these pathways (n=3).

C) *ERK1* and *ERK2* were knocked down in HUVEC using siRNA. qRT-PCR reveals that the induction of *DLL4, EGR3* and *DUSP5* is ERK1/2-dependent. N = 4-5. A representative western blot (of 3) reveals the extent of ERK1/2 knockdown. GAPDH is shown as a loading control.

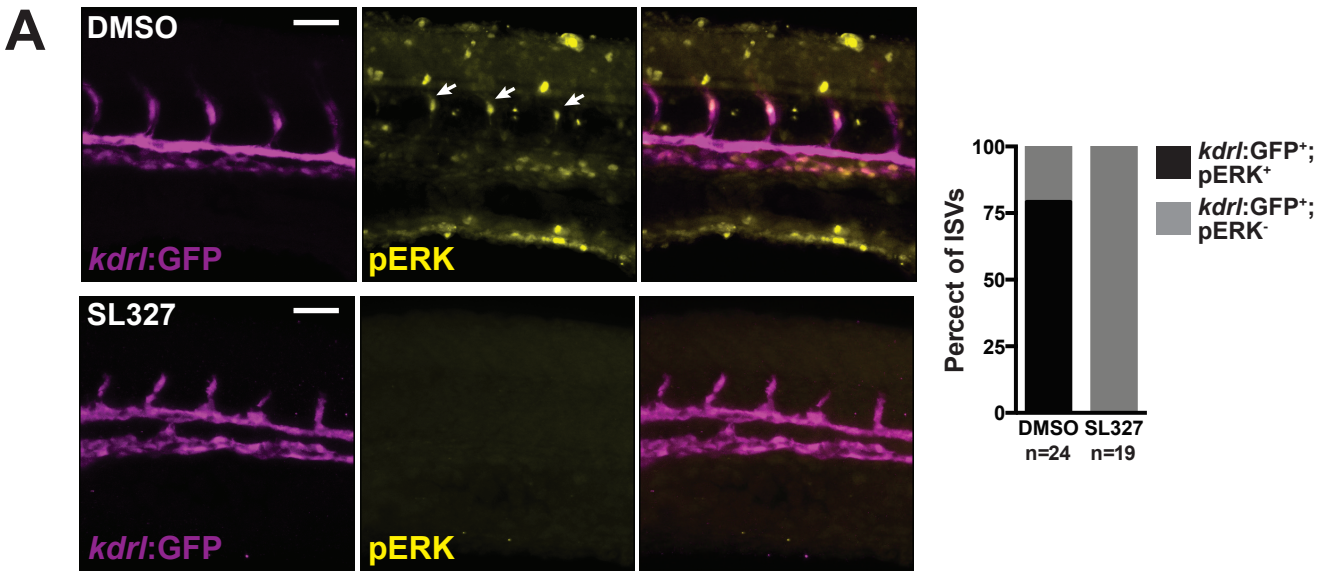

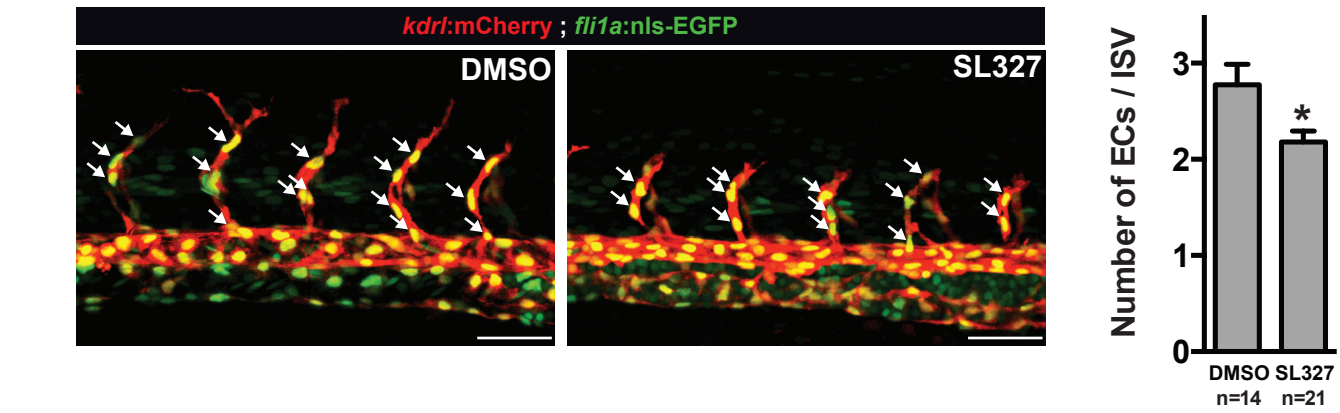

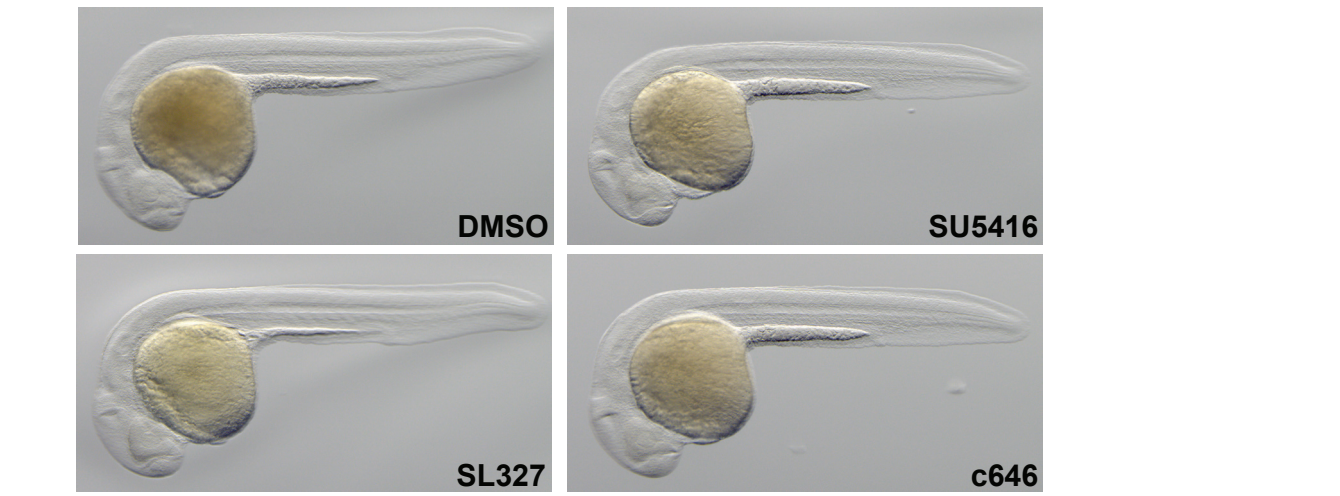

Figure S2: Characterization of sprouting defects in embryos treated with MEK inhibitor (SL327)

A) pERK is enriched in tip cells during ISV formation in zebrafish and this is dependent on MEK signaling as it is negated in MEK-inhibitor (SL327) treated embryos (treated from 18-20 hpf to ~24 hpf). Quantification of the number of ISVs that stained positive for pERK is indicated. 24 hpf. Scale bar = 50 μm.

B) The number of endothelial cells per intersomitic vessel was quantified in *Tg(kdrl*:mCherry;*fli1a*:nls-EGFP) embryos exposed to DMSO or SL327 (30 μM). The number of mCherry/EGFP double-positive cells was counted per intersomitic vessel and averaged per embryo. The number of embryos quantified is indicated.

C) Transmitted light images of DMSO, SL327 (30 μM), SU5416 (5 μM) and c646 (3 μM) treated embryos revealing normal overall development and lack of tissue necrosis or developmental delay.

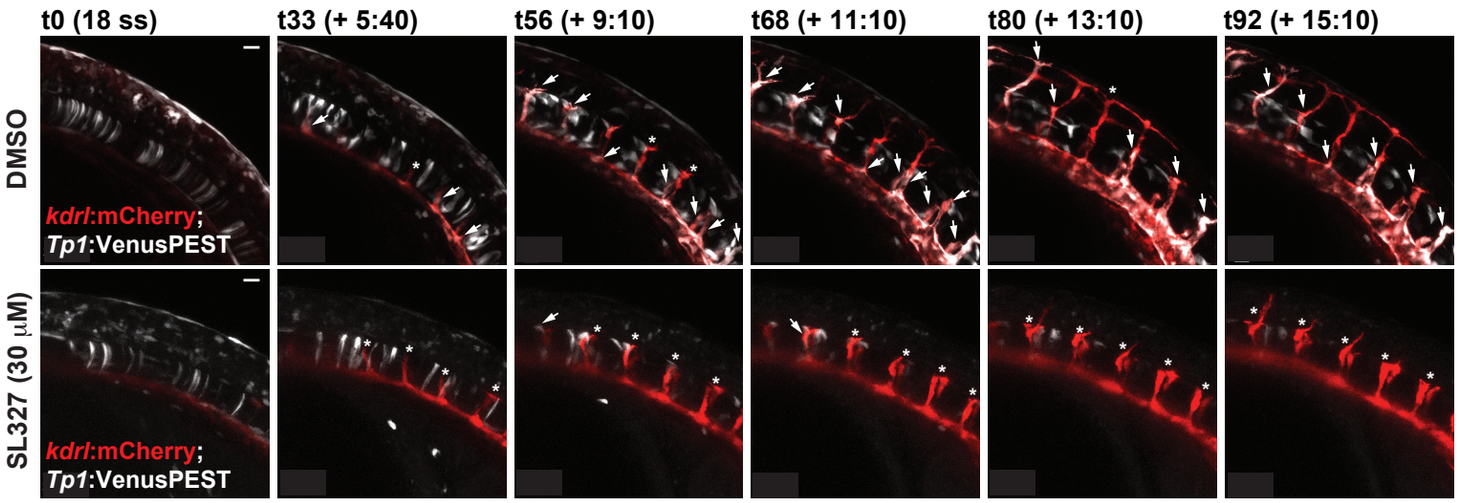

Figure S3: Notch induction in the vasculature is compromised in embryos treated with MEK inhibitor (SL327)

Notch activity is reduced in the vasculature of SL327-treated *Tg*(*kdrl*:mCherry); *Tg*(*Tp1bglob*:Venus-PEST) embryos. Still images from time-lapse microscopy of a representative experiment are shown. Arrows indicate Notch signaling-positive ISVs, while asterisks indicate Notch-negative ISVs. Scale bar = 20 µm. See Videos S1 and S2.

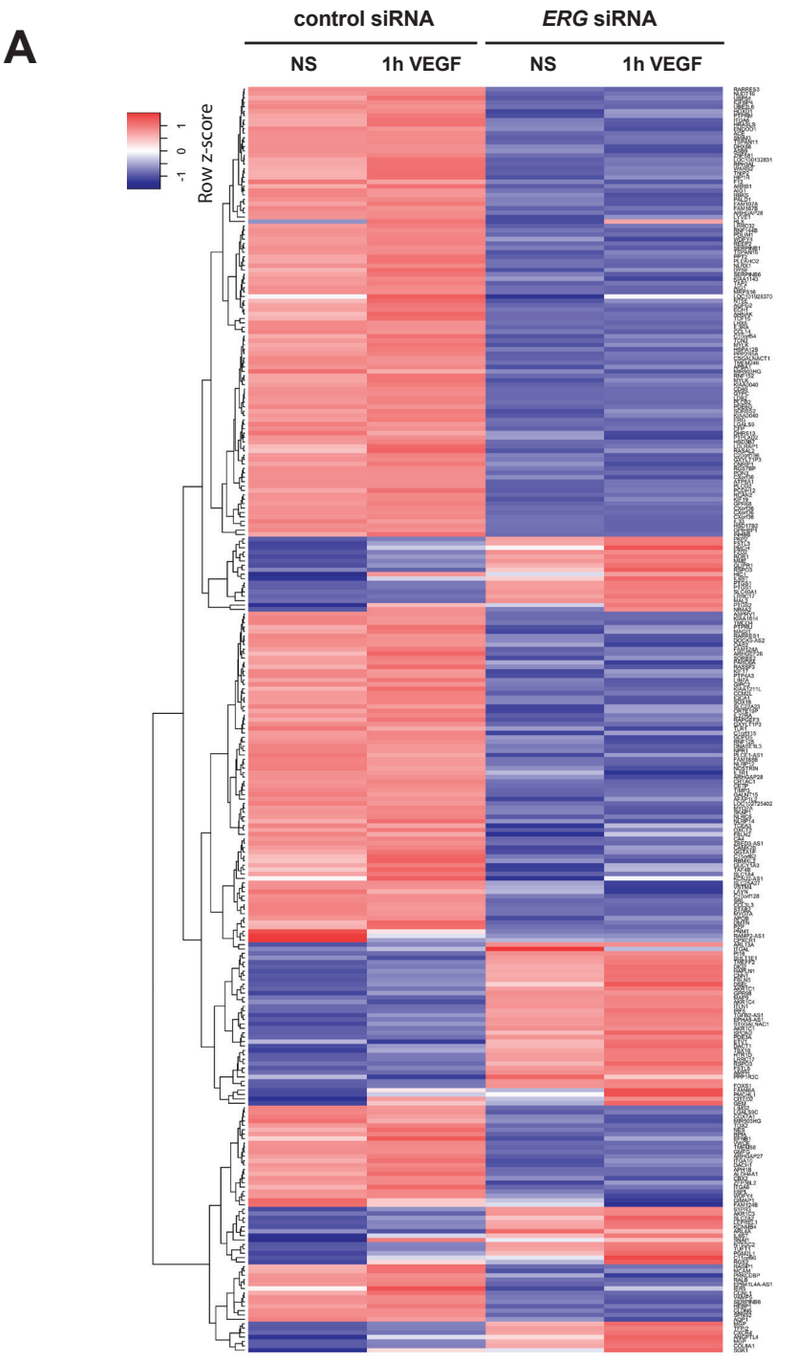

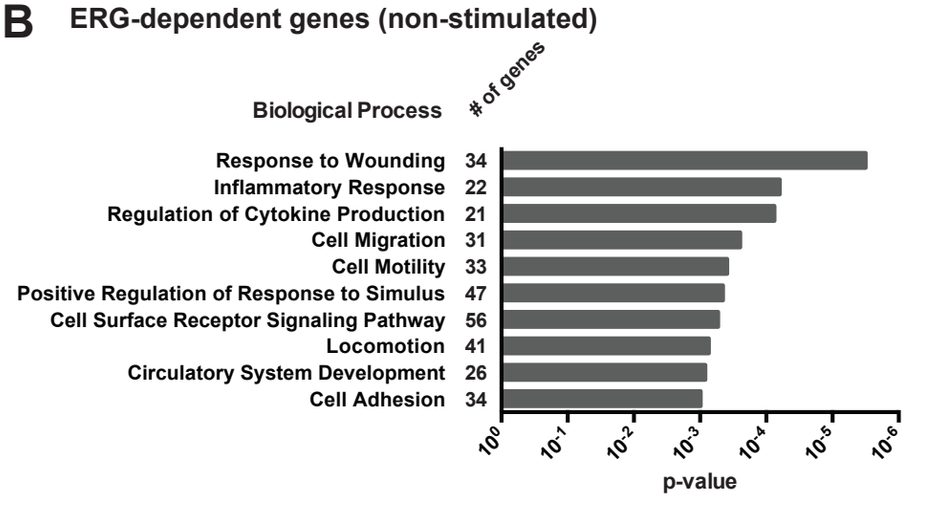

Figure S4: A network of genes are regulated by ERG in endothelial cells
A) Heat map depicting hierarchical clustering of significantly regulated genes in control- and *ERG* siRNA-transfected cells +/- 1h VEGF treatment. NS = not stimulated. Shown are genes that are differentially expressed between 'Control siRNA-NS' and '*ERG* siRNA-NS'.
B) Gene Ontology analysis of dysregulated genes ('Control siRNA-NS' vs. '*ERG* siRNA-NS'). Selected, representative GO terms are displayed with their associated p-value. The number of genes in each GO category is indicated. The GO terms depicted are: Response to wounding (GO:0009611), Inflammatory response (GO:0006954), Regulation of cytokine production (GO:0001817), Cell migration (GO:0016477), Cell motility (GO:0048870), Positive regulation of response to stimulus (GO:0048584), Cell surface receptor signaling pathway (GO:0007166), Locomotion (GO:0040011), Circulatory system development (GO:0072359), Cell adhesion (GO:0007155).

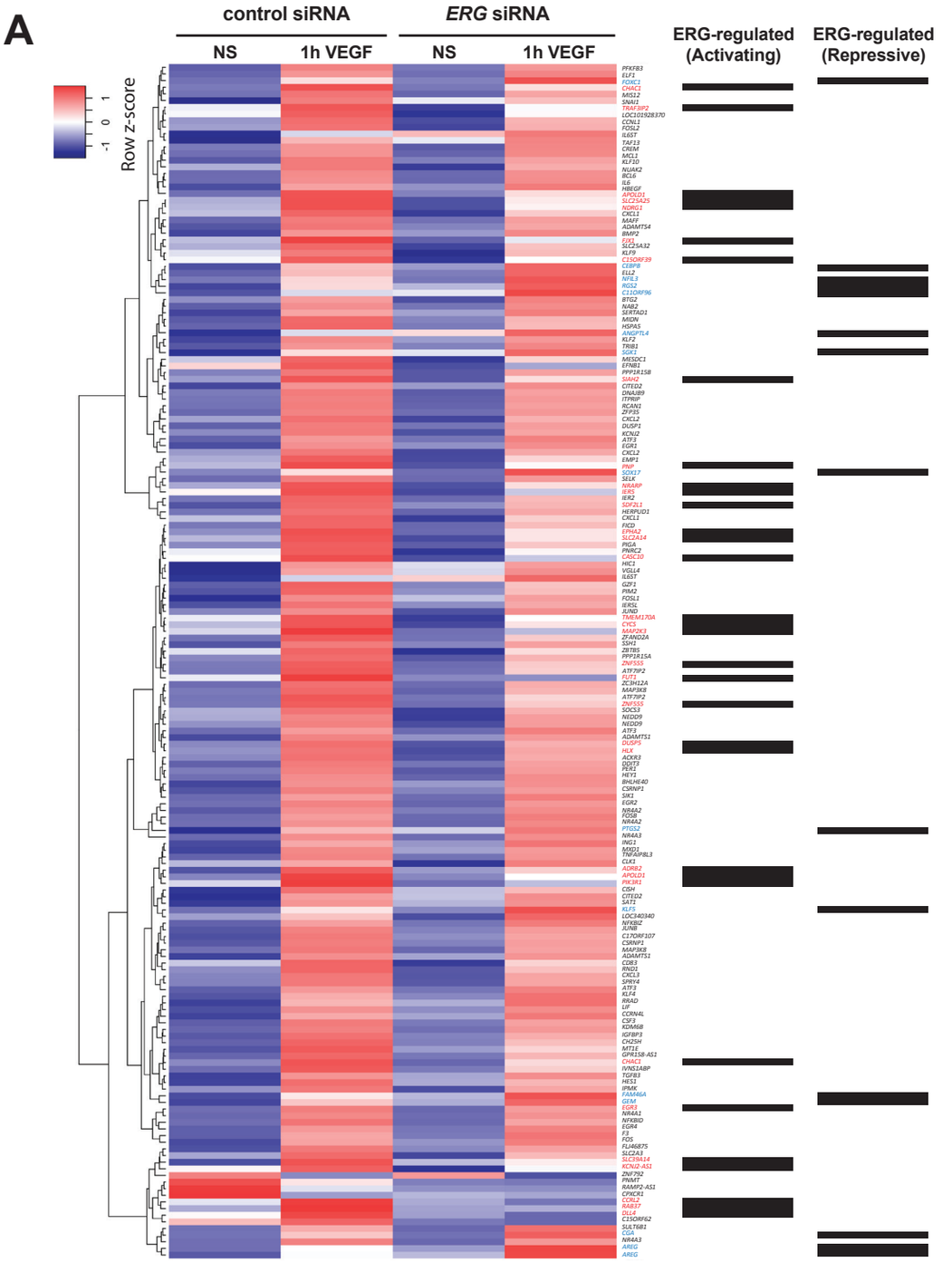

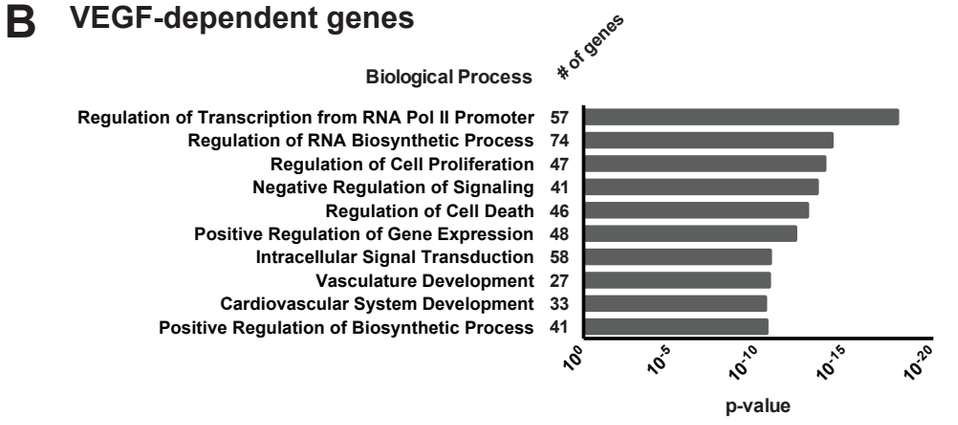

Figure S5: A network of genes are regulated by VEGF and ERG in endothelial cells
A) Heat map of genes that are differentially expressed between 'Control siRNA-NS' and 'Control siRNA-1h VEGF'. The VEGF-inducible genes that are dysregulated upon *ERG* knock-down are highlighted in red (activated) or blue (repressed), and indicated to the right.

B) Gene Ontology analysis of VEGF inducible genes ('Control siRNA-NS' vs. 'Control siRNA-1h VEGF'). Representative GO terms are indicated: Regulation of transcription from RNA Polymerase II promoter (GO:0006357), Regulation of RNA biosynthetic processes (GO:2001141), Regulation of cell proliferation (GO:0042127), Negative regulation of signaling (GO:0023057), Regulation of cell death (GO:0010941), Positive regulation of gene expression (GO:0010628), Intracellular signal transduction (GO:0035556), Vasculature development (GO:0001944), Cardiovascular system development (GO:0072358), Positive regulation of biosynthetic process (GO:0009891).

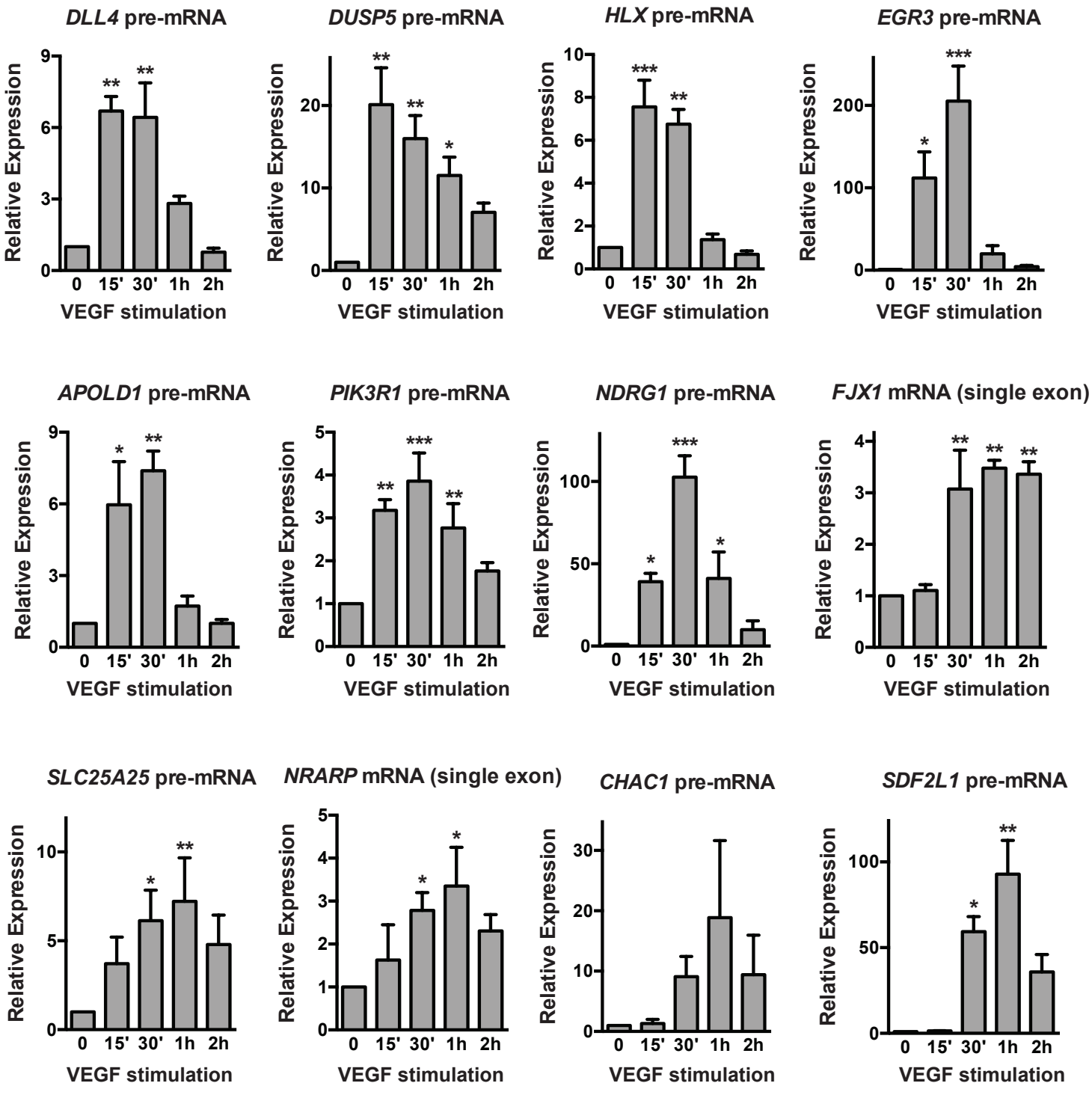

Figure S6: ERG-/VEGF-regulated genes are dynamically expressed
Kinetics of a subset of ERG-/VEGF-regulated genes, as measured by qRT-PCR of pre-mRNA in HUVEC (n=3). Transcriptional induction of these genes is dynamic, with peak transcription between 15'-1h. Note that some of this data is also found in Fig. 1A,E, 7A, but is included here to facilitate direct comparison.

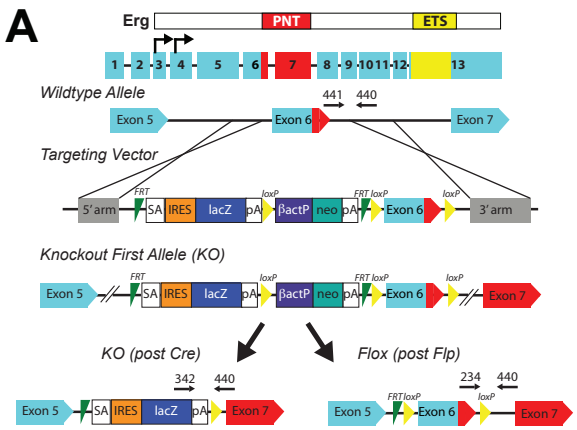

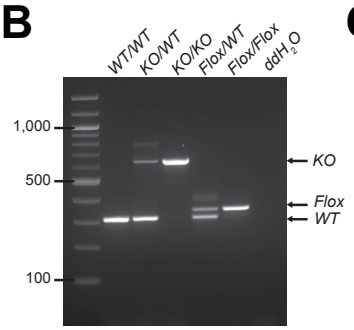

C

Adult (male and female)				
genotype	$Erg^{+/+}$	$Erg^{KO/+}$	$Erg^{KO/KO}$	total
predicted	25%	50%	25%	100%
observed	40%	60%	0%	100%
n	50	74	0	124
E11.5				
predicted	25%	50%	25%	100%
observed	31%	44%	14%	100%
n	6	12	3	21
E10.5				
predicted	25%	50%	25%	100%
observed	26%	44.5%	29.5%	100%
n	57	98	65	220
E10.5				
phenotype	$Erg^{+/+}$	$Erg^{KO/+}$	$Erg^{KO/KO}$	
hemorrhage	0% (0)	3% (3)	43% (28)	
small size	7% (4)	7% (7)	86% (56)	
total	57	98	65	220

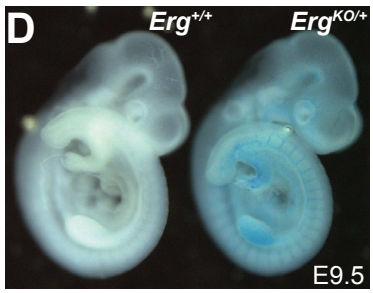

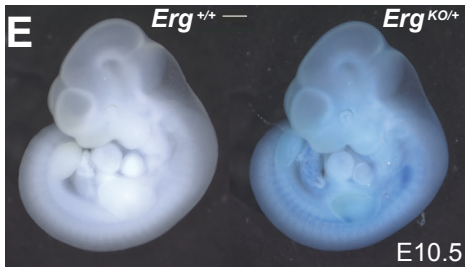

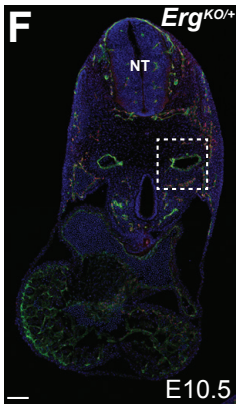

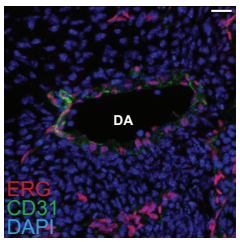

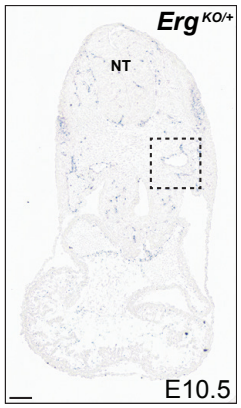

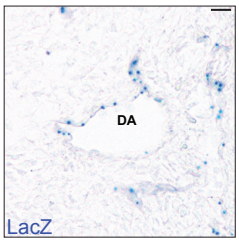

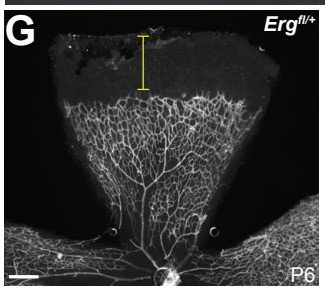

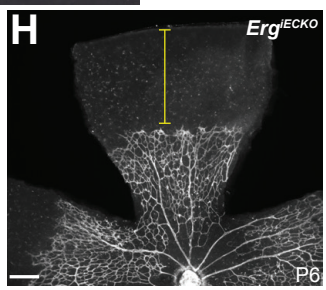

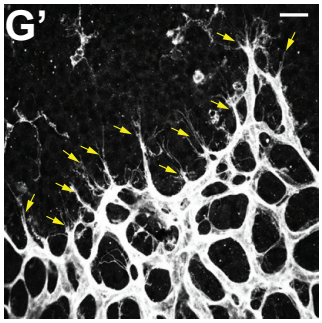

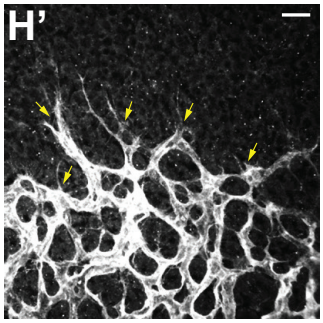

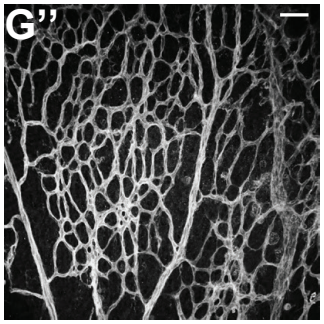

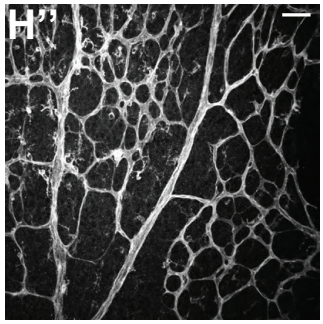

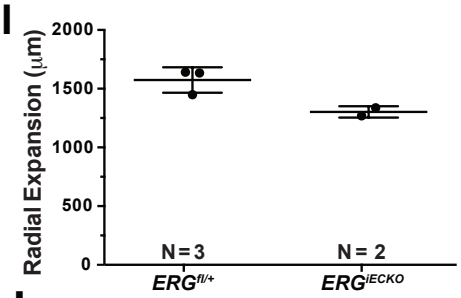

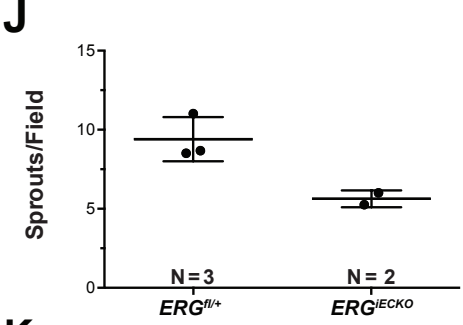

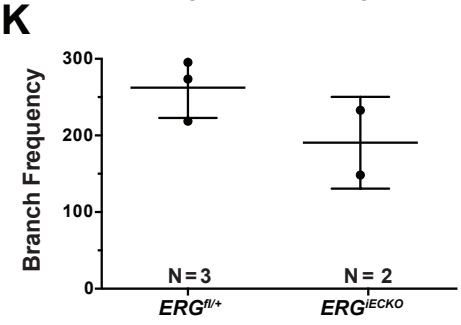

Figure S7: Deletion of *Erg* in mouse embryos results in embryonic lethality, accompanied by defects in angiogenesis, vascular remodeling and vascular integrity

A) Strategy for the generation of an *Erg* knock-out/LacZ knock-in first, conditional ready allele (also known as Erg^{tm1a}). Homologous recombination was used to insert an IRES-LacZ / β-Actin::Neo cassette into intron 5 of *Erg.* Following Cre-mediated recombination, the FRT-flanked β-actin::NEO selection cassette is deleted, leaving an ERG-ires-LacZ gene-trap (also known as Erg^{KO} or Erg^{tm1c}). Following Flp-mediated recombination of Erg^{tm1a}, loxP sites are left flanking exon 6, generating a conditional loss of function allele (also known as Erg^{flox} or Erg^{tm1b}). Genotyping primers are indicated. PNT=pointed domain; ETS=ETS DNA binding domain.

B) Agarose gel electrophoresis of PCR genotyping products to identify *Erg* mutants. 100 bp ladder on the far left lane.

C) Expected and observed ratios of genotypes from the progeny of $Erg^{+/-}$ crosses. Deletion of *Erg* results in embryonic lethality ~E11.5, and increased presence of hemorrhage and smaller embryo size. No defects were observed in heterozygous mutant embryos.

D) Phase images of wholemount, E9.5 $Erg^{+/+}$ and $Erg^{KO/+}$ embryos following lacZ staining.

E) Phase images of wholemount, E10.5 $Erg^{+/+}$ and $Erg^{KO/+}$ embryos following lacZ staining. Scale bar = 500 μm.

F) Immunohistochemistry for ERG (red), CD31 (green), and DAPI (blue) in the left panel, and LacZ staining in the right panel, from serial sections of an $Erg^{KO/+}$ E10.5 embryo, show overlap of Erg and gene-trap *Erg-ires-LacZ* activity. Scale bar = 100 μm. Lower panels are magnified views of the boxed area in the upper panels, scale bar = 20 μm. NT, neural tube; DA, dorsal aorta.

G, H) Representative images of the total retinal vasculature (G, H) and magnified view of the distal, vascular front (G', H') and proximal region (G'', H'') stained with IB4 in $Erg^{fl/+}$ (G, G', G'') and Erg^{iECKO} (H, H', H'') retinas at P6 following tamoxifen administration at P1. Scale bar = 100 μm. The bar in (G, H) indicates avascular area in each retina. Arrows in (G', H') indicate sprouting vessels at the vascular front. Scale bar = 100 μm.

I) Quantification of radial expansion of the $IB4^+$ vasculature within the P6 retina.

J) Vascular sprouting as determined by quantification of $IB4^+$ sprouts in the distal retinal vascular plexus at P6.

K) Vascular density as determined by quantification of $IB4^+$ branches in the proximal retinal vascular plexus at P6.

A

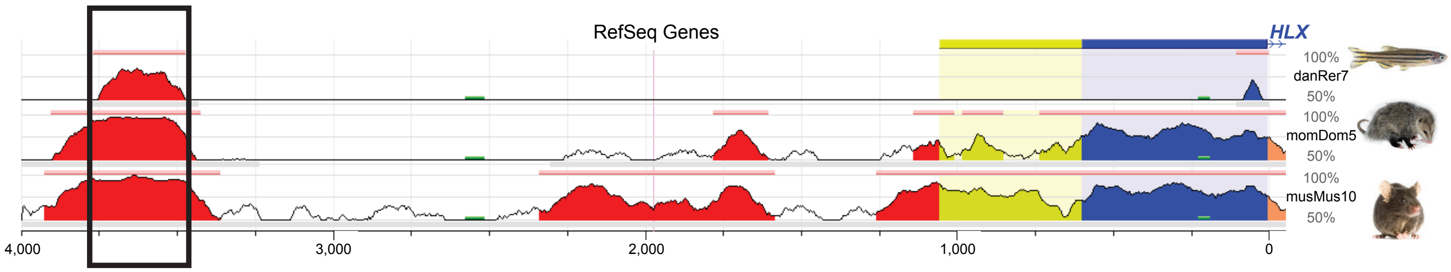

B

```
                                                                         ETS-D
hg19     TAGGGTCTCC-GC----TGCGTAGACC-AAGC-----TCAAGTTAATTCGGT---TTAGCCAGGCCCTTTTCTTTCCTGTTAA-------ATTCTCA-AC
mm10     TAGGCACAGCAGCAACTTGCAAAGTTTTTAGCCACTTTTAAGG-ATGCCAGTGTGTGAACGAAGTTCAAGTAATTTGATTTAATCGGGCCCTTTTCTTTC
danRer7  T--G-TTTTC--------------------GT--CTTT---------CCAG---------CACGCTCTA---TTT-------------------T-----
         *  *     *                   *      *         * *          * *  *        **                   *

                                                                                          HLX-3b FWD
         CCCCATGGCTACCAG-CCCCTGGGGAGCCCTCGCCTCTACCCCCAGGACCTCCCTGCCCG----------GC-TCAGTAGCTCTGGGCCAGTTCATTTCG
         CCTGGTGGTTACAAGGTCCCTTGGGAGTCCACGCCTCTGCCCCCAGGGCCTCCCTGACTAGGTGCACAACGCAACAACAACTCTGGGCTAGTTCATTTCA
         -----TGGC-ACA-GC--AATGTAAAGTT--------------------------GTC-ATGTGCATATGGA-TGA-------------AG----TATC-
              ***  **  *      *    **                           * *             *    *              **    * **

                   ETS-E                                   mef2-a                ETS-G   ETS-H
         CCACAGCCCGGAGCCTCTCGGAAAGCAAAGATTAAAGGGGAAAGTCGCAGCTGTATATTTATATTTTCATTGCTAGAAGGGAATTGATTTCCGTGCATTT
         CCACAGCCCGGGGACGCTCGGAAAGCAAAGATTAAAGGCGAAAGTCGCAGCTGTGTATTTATATTTTCATTGCTAGAAGGGAATTGATTTCCGTGCATTT
         ------------------------------------------GCCTCAGTAGT-TAATTGTGTTTTCGTTTC-AGCGGAGAATAGATTTCC-TCTGTTT
                                                   * * ***  ** ** ** * ***** ** * **  * **** ******* *   ***

                             ets                             gata           srf            ETS-I
         ATTTTGGTAGTTGTAATACATAAGGGCGGATTTGCGTCACCCGAGCAACTTGCCGGTGGAGATAAAGTTGCACAAATATTGAAAGG-GGAAGTGCTAGGA
         ATTTTGGAAGTTGTAATACAGAAGAGCGGATTTGCGTCACCACAGCAACTTGCCGGTGGAGATAAAGTTGCACAAATATTGAAAGG-GGAAGTGCTAGGA
         ATT---------ATAA-GCATAAGGACGGATTTGCGTCACC-GTGCGACTTGCGAGTTGAGATAAAGTTGCACAAATATTGAAAAAGGAAGTGCTAACA
         ***         ***  ** ***  ***************   ** ******  ******************************   *********  *

                                 ETS-J      ets                    mef2-b              mef2-c
         GTCATTATAGAGTTTTT---CT-----CCGGAAGAAATAAGGAT-TTCTGCAGTATCCTAAAATACTAAGGCCGCTTCTATTTGAGACC-AATCTCGCA
         GTCATTATAGAGTTTTT---CT-----CCGGAAGAAATAAGGAT-TTCTGCAGTATCCTAAAATACTAGGACCGCTTCTATTTGAGACC-AATCTCGCA
         GTCATTATAAAGTTCCACCTCTGTGAGTCGGAGGAAATAAGGGTGCTCTGCTGTATCCTAAAATACTAAAGCATCTTCTATTTTTGGCCTAAATCTTGCA
         ********* ****       **      **** ********* *  ***** ****************  *  ********* * *  ***** ***

              ELK1                                                                  ETS-k       sox
         GGCACATCCGCTCATTTAGTCCCGAGTTTGAGCCCATCAAAAAA-CAGGAGATGACCTGAACTCCG-GCGAGCCCAGGGTTTCCTGCTGCTTTCTTGGTT
         GGCATATCCGCTCATTTAG-CCCAAGTTTGAGCCCATCAAAAAAACAGGAGATGACCTGAACTCCGGGCGAGCCCCGGGTTTCCTGCTGCTTTCTTGGTT
         GGAATATCCGCTCATTTAG-CCTGAATCAGAGCTCATCAAAAA--CAGG--ATGACCTG--CATCGA--GAAACTCCTGTTTCCTAATT----------
         ** * ************** **  * *  **** *********  ****  ********  *  **   **         *******  **

                           HLX-3b REV                                                      ETS-L
         CTGAAGAGTGGGGAGTAAGGAGGGCGGGAGTCT-GCGGGCTCAGAACTCGGCGAGGGGCCTGCAGGGGCCAGGCTTGGGCCTGGGG-AAGGGGTAGAGGG
         CTGAAGGGTAGGG-GTAAGGAGGAGGGCAGTGTTCCAAGCTCCCGCCAAAGCGACTGGTCTACAGGGCTTGGGCCTGGAGCAAGAGAGAGTGACCCAAAG
         CCACAGAGCAGAA----AACAC------A--CACACATACACAC---------------ACACACGAGTCG----------------GAGTGTTAGC---
         *   ** *  *      *  *      *      *   * *                 ** *                           ** *

         GGC--------------------G---G--CG----GG--G----G-TC--GCTC-CAA---------------A--GACTT
         TCCTTCCCCTCTTTTCTTTTCTTTTCTTTTCTTTTCTTTTCTTTTCTTTTCTTTTCTTTTCCTCTCCTCTCCTCTCCTCTCC
         ----------------ATTTG--A---T--TG----TG--G----A-TC--ATTT-TTT------------------AATCA
                                                       *     *
```

Figure S8: Comparison of conservation between an upstream human and zebrafish *HLX* enhancer

A) Shown are browser screenshots comparing evolutionary conserved regions (ECR) across multiple, distantly-related vertebrates, with the zebrafish, possum, and mouse genomes aligned to the human genome (chr1:221049800-221053860). Peaks indicate sequence conservation. Red denotes intergenic sequence, yellow indicates the 5' UTR, blue denotes exons, and salmon shows intronic regions. The x-axis denotes position in the base genome and the y-axis represents the percent identity between the base and aligned genomes. The region analyzed in (B) is underlined.

B) ClustalW alignment of a portion of the *HLX-3a* (and *HLX-3b*) enhancer regions from human (hg19), mouse (mm10), and zebrafish (danRer7). Asterisks below the nucleotides indicate sequence conservation across all three species. The human *HLX-3a* region contains 26 ETS consensus sequences (GGA(A/T)) (not shown). The sites are numbered relative to their positive within *HLX-3a*. As H3K27ac flanked *HLX-3a* region did not direct expression in the endothelium (see main text and methods), we focused on the smaller, conserved, region identified by ERG ChIP-seq, *HLX-3b* (denoted by primers). *HLX-3b* contained 6 deeply conserved ETS sites (ETS-H, ets, ETS-I, ETS-J, ELK1, and ETS-K), as well as 3 deeply conserved MEF2 sites, an SRF site, and a GATA site. All ETS sites tested by mutation analysis are indicated in blue and capital letters, while lowercase and gray coloring indicates sites that were not experimentally validated. The human *HLX-3b* enhancer contained 9 total ETS sites.

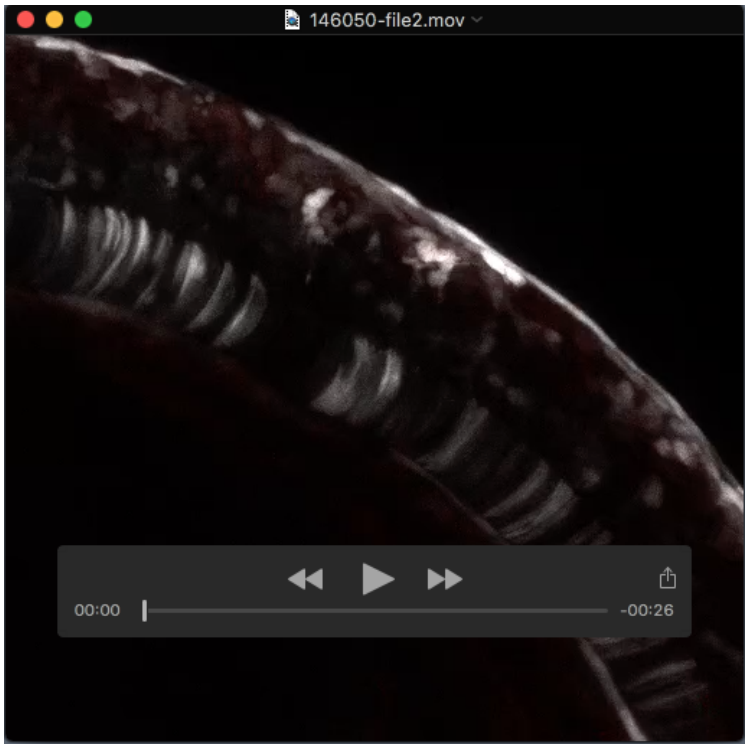

Supplementary Movie 1. Notch signaling is active in the developing vasculature. Representative time-lapse confocal microscopy of a *Tg(kdrl:mCherry)*; *Tg(Tp1:VenusPEST)* embryo treated with DMSO demonstrates Notch activity within the axial and sprouting vasculature (n=6). Embryos were mounted in E3 with tricaine. Treatment began at 18 ss, and continued, at RT, for 15 hours and 10 minutes. See Fig. S3 for still images.

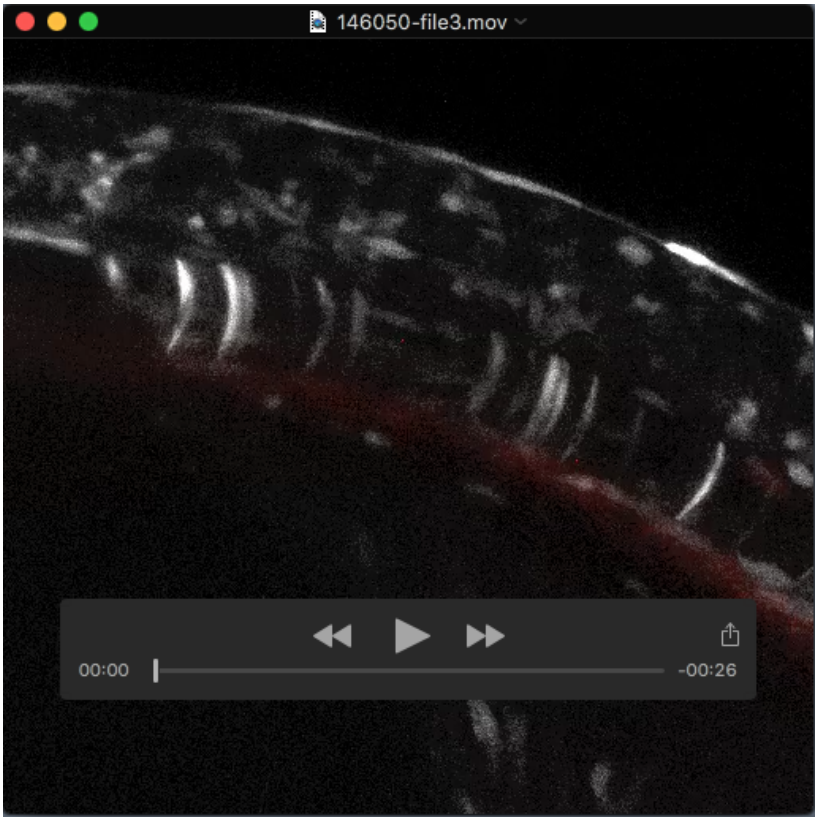

Supplementary Movie 2. Notch signaling is lost in the vasculature upon MAPK inhibition. Representative time-lapse confocal microscopy of a *Tg(kdrl:mCherry)*; *Tg(Tp1:VenusPEST)* embryo treated with SL327 (30 uM) demonstrates reduced Notch activity within the vasculature, and decreased sprout elongation (n=6). Treatment began at 18 ss, and continued, at RT, for 15 hours and 10 minutes. See Fig. S3 for still images.